



TRIBHUVAN UNIVERSITY  
INSTITUTE OF ENGINEERING  
PULCHOWK CAMPUS

THESIS NO: M-146-MSESP-2019/2022

Deviation of Flow Pattern in Pelton Turbine Bucket Due to Angular Eccentricity of the

Jet

by

Rupa Pandey

A THESIS

SUBMITTED TO THE DEPARTMENT OF MECHANICAL AND  
AEROSPACE ENGINEERING IN PARTIAL FULFILLMENT OF THE  
REQUIREMENTS FOR THE DEGREE OF MASTER OF SCIENCE IN  
ENERGY SYSTEM PLANNING AND MANAGEMENT ENGINEERING

DEPARTMENT OF MECHANICAL AND AEROSPACE ENGINEERING

LALITPUR, NEPAL

SEPTEMBER, 2022

## **COPYRIGHT**

The author has agreed that the library, Department of Mechanical and Aerospace Engineering, Pulchowk Campus, Institute of Engineering may make this thesis freely available for readers. Moreover, the author has agreed that permission for extensive copying of this thesis for scholarly purposes may be granted by the professor(s) who supervised the project work recorded herein or, in their absence, by the head of the department wherein the thesis was done. It is understood that due recognition was given to the author of this thesis and the Department of Mechanical and Aerospace Engineering, Pulchowk Campus, Institute of Engineering in any use of the material of this thesis. Copying or publication or other uses of this thesis for financial gain without the approval of the Department of Mechanical and Aerospace Engineering, Pulchowk Campus, Institute of Engineering, and the author's written permission is prohibited.

Request for permission to copy or to make any other use of the material in this report in whole or in part should be addressed to:

Head

Department of Mechanical and Aerospace Engineering

Pulchowk campus, Institute of Engineering

Lalitpur, Nepal

**TRIBHUVAN UNIVERSITY**  
**INSTITUTE OF ENGINEERING**  
**PULCHOWK CAMPUS**

**DEPARTMENT OF MECHANICAL AND AEROSPACE ENGINEERING**

The undersigned certify that they have read, and recommended to the Institute of Engineering for acceptance, a thesis entitled “**Deviation of Flow Pattern in Pelton Turbine Bucket Due to Angular Eccentricity of the Jet**” submitted by Rupa Pandey, in partial fulfillment of the requirements for the degree of Master of Science in Energy System Planning And Management Engineering.

---

Supervisor, Dr. Mahesh Chandra Luintel

Professor

Department of Mechanical and Aerospace Engineering

---

External Examiner, Er. Dipesh Thapa

Sr. Mechanical Engineer

TAC Hydro Consultancy Pvt.Ltd.

---

Committee Chairperson, Dr. Surya Prasad Adhikari

Head, Associate Professor

Department of Mechanical and Aerospace Engineering

Date: September 21, 2022

## ABSTRACT

One of the primary operating issues for the hydropower sector is the severe degradation of the hydro-mechanical components of hydropower projects (apart from storage-type plants). The eroded pieces are regularly replaced with fresh ones (or repaired ones) and are fixed by welding. The templates created from sheets and utilized for bucket profile control during repair and maintenance have the drawback of not being able to record the angular deviation of the bucket profile. Additionally, secondary flows and bucket warping may be brought on by unequal loading, an eccentric jet, and changes in mechanical qualities. A relative angular eccentricity between the jet and bucket results from both of the aforementioned cases. This study aims to investigate how the angular eccentricity between the jet and bucket affects the flow behavior. Numerical flow analysis is done in this work to examine the impact of eccentricity on the Pelton turbine's bucket using the commercial Computational Fluid Dynamics (CFD) Fluent code ANSYS. To mesh, ANSYS ICEM was utilized, and the Volume of Fluid (VOF) method's implicit scheme formulation was employed to represent the transient state of the jet until a steady state was reached. For focal situations of jet-bucket interaction, the results of theoretical calculations, experimental observations, and numerical modeling were compared. There is a -11.5% error in the jet velocity and a 32.75% error in the thickness of the water sheet as compared to theoretical estimates. The study of flow simulation over a bucket was conducted to analyze flow in the eccentric situation by dividing the bucket into two parts, the upper half and the bottom half, at three distinct angular deviations (specifically 2.5, 5, and 7.5 degree). A flow model is used to represent the velocity profile, pressure profile, and water volume percentage at various locations between the needle tip and bucket exit. With angular deviation, velocity profiles and pressure profiles have changed, and it has been shown that as eccentricity increases, the thickness of the water sheet in the bucket also does. Calculations were made for the overpressure coefficient produced in the bucket at an eccentric angle. The results were 0.1544, 0.247, 0.1235, 0.1204, 0.1853, and 0.3087 for the top and lower halves of 2.5, 5, and 7.5 degrees respectively. This suggests that eccentric installation increases bucket loading. Additionally, a thicker water sheet means that a bucket will hold more mass than it would under ideal conditions. Along with imbalanced forces, which are generally considered for studying mechanical vibrations, this additional weight of water in the bucket is a source of mechanical vibrations as well.

## ACKNOWLEDGMENTS

I would like to express my sincere gratitude to my supervisor Prof. Dr. Mahesh Chandra Luitel who was extremely helpful, consistently supportive, and constantly guided in bringing out the best results. Whatever I have done is only due to such guidance, care, and motivation.

I am grateful to Er. Ashesh Babu Timilsina for his constant support and guidance throughout the thesis work. I would like to express my sincere gratitude to Prof. Dr. Tri Ratna Bajracharya for allowing me to use their design and data in theoretical calculation. I would like to thank the Department of Mechanical and Aerospace Engineering committee for their support of the thesis work and the high-end comment during the mid-term defense. My appreciation extended to Dr. Nawraj Bhattarai the coordinator of MS-ESPM for providing a good pathway for thesis work. I would also like to thank Er. Tejendra Rahadi Magar (Anil), Er. Anil Sapkota and Er. Hari Pandey for their valuable suggestions and time. I would like to thank my parents, family, and friends for their support and encouragement throughout my thesis work.

## TABLE OF CONTENTS

<b>COPYRIGHT .....</b>	<b>2</b>
<b>APPROVAL PAGE .....</b>	<b>3</b>
<b>ABSTRACT .....</b>	<b>4</b>
<b>ACKNOWLEDGMENTS .....</b>	<b>5</b>
<b>TABLE OF CONTENTS.....</b>	<b>6</b>
<b>LIST OF TABLES .....</b>	<b>10</b>
<b>LIST OF FIGURES .....</b>	<b>11</b>
<b>LIST OF SYMBOLS .....</b>	<b>13</b>
<b>LIST OF ABBREVIATIONS .....</b>	<b>14</b>
<b>CHAPTER ONE: INTRODUCTION .....</b>	<b>15</b>
1.1 Background .....	15
1.2 Problem Statement .....	20
1.3 Rationales of Research.....	21
1.4 Research Objectives .....	21
1.4.1 Main Objective.....	21
1.4.2 Specific Objectives.....	21
1.5 Assumptions and Limitations.....	21
<b>CHAPTER TWO: LITERATURE REVIEW .....</b>	<b>22</b>
2.1 Working Principle .....	22
2.2 Energy Conversion in Pelton Turbine.....	23
2.3 Jet Impingement on a Flat Plate .....	24
2.4 Water-Jet-Bucket Interaction .....	25
2.5 Coincidence and Symmetry Conditions.....	26
2.5.1 Deflection of the Flow at the Bucket Main Splitter .....	26
2.5.2 Thickness of Water Sheet in the Bucket .....	28
2.5.3 Exit Condition and Over Pressure.....	28
2.6 Computational Fluid Dynamics .....	29
2.6.1 Governing Equations.....	30

2.6.2 Pre-Processor.....	30
2.6.3 Solver .....	30
2.6.4 Post-Processor .....	31
2.6.5 Commercial CFD Codes .....	31
2.6.6 Turbulence Modeling in CFD .....	31
2.7 Work done in the Department of Mechanical and Aerospace Engineering.....	32
<b>CHAPTER THREE: RESEARCH METHODOLOGY .....</b>	<b>34</b>
3.1 Control Volume of the Study .....	35
3.2 CFD Solution Procedure.....	36
3.2.1 Pre-processing .....	38
3.2.2 Solver Settings .....	39
3.3 Measurements in Field Setting Research .....	40
<b>CHAPTER FOUR: RESULTS AND DISCUSSION .....</b>	<b>42</b>
4.1 Observation in Field Study.....	42
4.2 Numerical Modeling of Flow for Zero Angular Deviation.....	43
4.2.1 Volume Fraction (Water Flow) for Centric Placement.....	43
4.2.2 Velocity Distribution.....	45
4.2.3 Pressure Distribution .....	46
4.2.4 Water Sheet Thickness .....	48
4.3 Theoretical Calculations for Zero Angular Deviation .....	49
4.3.1 Water Sheet Thickness .....	49
4.3.2 Overpressure coefficient calculation for centric condition .....	50
4.3.3 Comparison of Numerical and Theoretical Calculation.....	51
4.4 Numerical Modeling of Angular Deviation .....	52
4.4.1 Flow Modeling .....	52
4.4.2 Velocity Profile at Needle Tip .....	53
4.4.3 Pressure Profile at Needle Tip.....	56

4.4.4 Velocity Profile at Splitter Tip.....	58
4.4.5 Pressure Profile at Splitter Tip.....	61
4.4.6 Velocity Profile at Middle of Bucket.....	63
4.4.7 Pressure in Middle of Bucket.....	66
4.4.8 Velocity Profile at Exit Side of Bucket.....	68
4.4.9 Pressure Profile at Exit Side of Bucket.....	71
4.4.10 Water Volume Fraction at Needle Tip.....	73
4.4.11 Water Volume Fraction at Splitter Tip.....	76
4.4.12 Water Volume Fraction at Middle of bucket.....	78
4.4.13 Water Volume Fraction at Exit Side of Bucket.....	81
4.4.14 Calculation of Overpressure and Flow Condition at Bucket Exit.....	83
4.5 Comparison of Flow Parameters Charts.....	85
4.5.1 Velocity Profile at Needle Tip.....	85
4.5.2 Pressure Profile at Needle Tip.....	87
4.5.3 Velocity Profile at Splitter Tip.....	88
4.5.4 Pressure Profile at Splitter Tip.....	89
4.5.5 Velocity Profile at Middle of Bucket.....	90
4.5.6 Pressure at Middle of Bucket.....	92
4.5.7 Velocity Profile at Exit Side of Bucket.....	93
4.5.8 Pressure Profile at Exit Side of Bucket.....	94
4.5.9 Water Volume Fraction at Needle Tip.....	96
4.5.10 Water Volume Fraction at Splitter Tip.....	97
4.5.11 Water Volume Fraction at Middle of bucket.....	98
4.5.12 Water Volume Fraction at Exit Side of Bucket.....	100
4.5.13 Deviation vs Overpressure Coefficient.....	102
<b>CHAPTER FIVE: CONCLUSIONS AND RECOMMENDATIONS.....</b>	<b>103</b>
5.1 Conclusions.....	103



5.2 Recommendations .....	104
<b>REFERENCES .....</b>	<b>105</b>
<b>PUBLICATION .....</b>	<b>108</b>
<b>APPENDIX .....</b>	<b>109</b>

## LIST OF TABLES

Table 1.1: Major Hydropower Projects with Pelton Turbine.....	17
Table 2.1: List of works done in the department of mechanical and aerospace engineering in advancing numerical modelling of Pelton turbine and assembly .....	32
Table 4.1: Eccentricity Reading of Pelton Turbine.....	42
Table 4.2: Eccentricity and Bearing Temperature .....	43
Table 4.3: Velocity profile of centric case at a different deviation.....	45
Table 4.4: Pressure profile of centric case at a different position.....	46
Table 4.5: Water volume fraction profile of centric case at different positions .....	48
Table 4.6: Experimental reading and error calculation.....	49
Table 4.7: Flow model for deviated angles .....	52
Table 4.8: Velocity profile of different angular deviations at needle tip .....	53
Table 4.9: Pressure profile of different angular deviations at needle tip .....	56
Table 4.10: Velocity profile of different angular deviation at splitter tip.....	58
Table 4.11: Pressure profile of different angular deviation at splitter tip .....	61
Table 4.12: Velocity profile of different deviations at middle of bucket.....	63
Table 4.13: Pressure profile of different angular deviations in middle of bucket.....	66
Table 4.14: Velocity profile of different angular deviations at exit side of bucket .....	68
Table 4.15: Pressure profile of different angular deviations at exit side of bucket .....	71
Table 4.16: Water volume fraction of different angular deviations at needle tip .....	73
Table 4.17: Water volume fraction of different angular deviation at splitter tip .....	76
Table 4.18: Water volume fraction of different angular deviation at Middle of bucket .....	78
Table 4.19: Water volume fraction of different angular deviations at exit side of bucket .....	81
Table 4.20: Overpressure coefficient value at different angular deviation.....	85

## LIST OF FIGURES

Figure 1.1: Turbine Selection Nomogram .....	16
Figure 1.2: Twisting of Bucket due to uneven jet loading.....	19
Figure 1.3: Evolution of the vibration signatures in a Pelton turbine. The stress distribution for the runner excited without and with jet misalignment has been represented .....	19
Figure 1.4: Design templates used during the repair of Runner .....	20
Figure 2.1: Typical Installation of horizontal axis Pelton turbine .....	22
Figure 2.2: Energy conversion diagram .....	23
Figure 2.3: Round jet impact on a flat plate and water sheet spreading .....	25
Figure 2.4: Jet piece abcd and specific bucket positions .....	26
Figure 2.5: Flow deflection at the main splitter .....	27
Figure 2.6: Flow conditions determination at the bucket exit.....	29
Figure 3.1: Methodology for Research Work .....	34
Figure 3.2: Control Volume for this Study .....	35
Figure 3.3: General Layout of Horizontal Axis Pelton Unit.....	36
Figure 3.4: Bucket Twist.....	36
Figure 3.5: Process Flow of CFD Simulation .....	36
Figure 3.6: Refine Mesh Area.....	37
Figure 3.7: Half Mesh of Bucket-Jet.....	38
Figure 3.8: Full Mesh of Bucket Jet.....	39
Figure 3.9: Basic Workflow .....	40
Figure 3.10: Measurement Plant to Understand Effect of Eccentricity on Bearing Temperature .....	40
Figure 3.11: Eccentricity Measurement Using Dial Gauge .....	41
Figure 4.1: Volume Fraction of Water after steady state flow.....	43
Figure 4.2: (a),(b) Actual flow-through model .....	45
Figure 4.3: Upper half velocity of different angular deviation .....	85
Figure 4.4 Lower half velocity of different angular deviation.....	86
Figure 4.5: Upper half pressure variation of different angular deviation .....	87
Figure 4.6: Lower half pressure variation of different angular deviation.....	87
Figure 4.7: Upper half velocity variation of different angular deviation .....	88
Figure 4.8: Lower half velocity variation of different angular deviation .....	88

Figure 4.9: Upper half pressure variation of different angular deviation .....	89
Figure 4.10: Lower half pressure variation of different angular deviation .....	90
Figure 4.11: Upper half velocity variation of different angular deviation .....	90
Figure 4.12: Lower half velocity variation of different angular deviation.....	91
Figure 4.13: Upper half pressure variation of different angular deviation .....	92
Figure 4.14: Lower half pressure variation of different angular deviation .....	92
Figure 4.15: Upper half velocity variation of different angular deviation .....	93
Figure 4.16: Lower half velocity variation of different angular deviation .....	93
Figure 4.17: Upper half pressure variation of different angular deviation .....	94
Figure 4.18: Lower half pressure variation of different angular deviation .....	95
Figure 4.19: Upper half water volume fraction of different angular deviation.....	96
Figure 4.20: Lower half water volume fraction of different angular deviation .....	96
Figure 4.21: Upper half water volume fraction of different angular deviation.....	97
Figure 4.22: Lower half water volume fraction of different angular deviation .....	97
Figure 4.23: Upper half water volume fraction of different angular deviation.....	98
Figure 4.24: Lower half water volume fraction of different angular deviation .....	99
Figure 4.25: Upper half water volume fraction of different angular deviation.....	100
Figure 4.26: Lower half water volume fraction of different angular deviation .....	101
Figure 4.27: Overpressure coefficient at different angular deviation .....	102

## LIST OF SYMBOLS

kg	Kilogram
kW	Kilowatt
MW	Megawatt
m	Meter
s	Second
mm	Millimeter
C	Jet speed
$C_2$	Exit flow velocity
H	Net pressure head
$f_{jet}$	jet impact force
$k_m$	Peripheral speed coefficient
$e_{shock}$	Shock-specific work
$\eta_{shock}$	Shock efficiency
S	Trajectory length
B	Width of the bucket
$h_2$	Height of water sheet at exit
$p_b$	Overpressure
$r_b$	Radius of curvature
$C_p$	Coefficient of overpressure

## **LIST OF ABBREVIATIONS**

3D	Three Dimensional
CAD	Computer-Aided Design
CFD	Computational Fluid Dynamics
HPP	Hydro Power Plant
IPPAN	Independent Power Producers Association of Nepal
NEA	Nepal Electricity Authority
FY	Fiscal Year
UTHL	Upper Tamakoshi Hydropower Limited
CHCL	Chilime Hydropower Company Limited
IPPs	Independent Power Producers

## CHAPTER ONE: INTRODUCTION

### 1.1 Background

In Nepal, there are about 6,000 rivers and rivulets. Due to its unique geography and abundant water supply, Nepal has a wealth of hydropower potential. There is an overall economically viable production capacity of 83,000 megawatts (MW) and a production capacity of roughly 43,000 MW. Compared to the similar amount of 6,529 GWh in FY 2019/20, the total energy usage in FY 2020/21 was 7,319 GWh, a small rise. The annual energy output from hydropower plants has surpassed the target projected by 95.25 percent (NEA, 2021).

Furthermore, the Himalayan region as a whole offers significant potential for the development of hydropower. However, due to the issue of silt erosion, hydropower production faces numerous technical difficulties. Tropical temperature, immature geology, and heavy seasonal rainfall are a few examples of the physical and climatic factors that contribute to problems with sedimentation and erosion. Therefore, during the monsoon and the time of major flooding, the rivers in this area move a significant amount of silt. A key element in increasing the efficiency of hydraulic turbines may be how hydropower projects are managed. Because of this, the security, dependability, and longevity of hydropower projects are now top priorities. Large amounts of silt, typically in the form of quartz-based rock shards or hard, abrasive minerals, are found in the Himalayan Rivers. The presence of brittle rocks in mountains, great relief, and extremely strong monsoon rainfall are the primary causes of sediment particles in rivers. Determining the safety, dependability, and lifespan of infrastructures like the electromechanical parts of hydropower projects has thus become one of the most crucial issues. (Pachhain, 2020)

Building hydropower facilities across rivers that are heavily packed with sediment is extremely difficult due to the flow of sediment particles. Particularly at high- and medium-head hydroelectric power facilities, the hydro turbines experience erosion due to the abrasive impact of hard particles like quartz and feldspar. (Sangal et al., 2018) (Poudel et al., 2012). According to a forced perspective on the erosion phenomenon in the Pelton bucket, the outer part of the bucket is more vulnerable to erosion because there, the separation forces acting on the sediment particles are the strongest. (Kumar et

al., 2019). Due to the smallest radius of curvature in the bottom portion of the bucket, the Pelton bucket suffers the highest erosion (Rai et al., 2021)

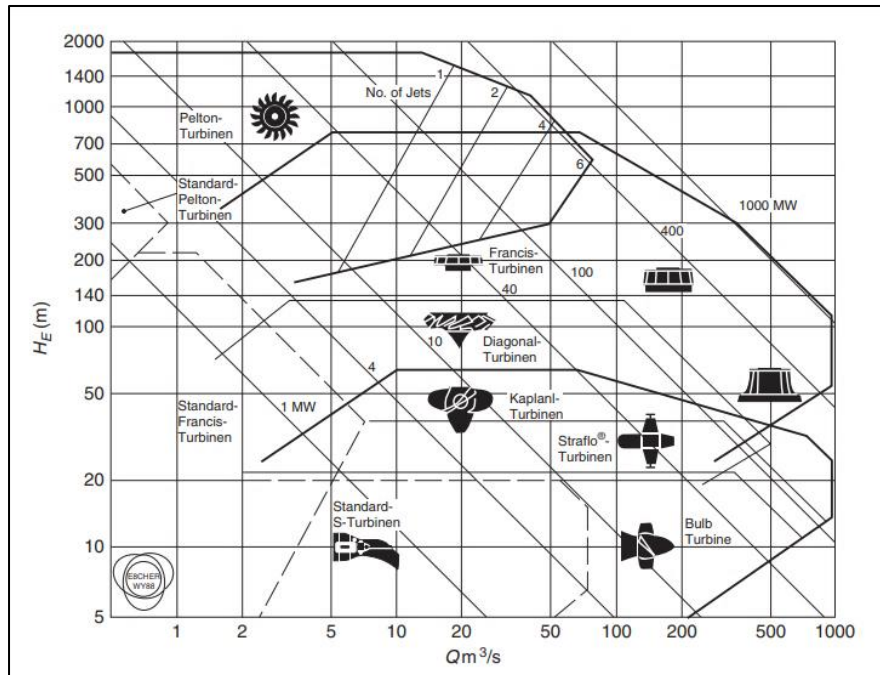


Figure 1.1: Turbine Selection Nomogram

The head and flow parameters determine which hydro turbine should be used at a particular location. The application ranges of several types of hydraulic turbines are depicted in Figure 1.1. The Pelton turbine is used in high head sites, as seen in the picture.

In unstable mountainous areas, hydropower plants must contend with significant hydro-abrasive erosion of hydraulic components, which reduces efficiency, causes frequent power-generating disruptions, and requires downtime for repair or replacement. A Pelton turbine is prone to erosion because parts like nozzles and buckets have high flow rates (Rai et al., 2021).

Hydro-abrasive erosion of hydraulic turbines is an economically important issue due to maintenance costs and production losses, in particular at high- and medium-head run-off-river hydropower plants (HPP) on sediment-laden rivers (Felix et al., 2016).

Table 1.1 presents the list of major hydropower projects in which Pelton turbines are installed in Nepal.



Table 1.1: Major Hydropower Projects with Pelton Turbine

	S.N	Name of the Project	Total Capacity (in MW)	Unit Capacity (in MW)	Status	Reference
Owned by NEA	1	Kulekhani I	60	30.5	Running	NEA, 2017
	2	Ilam (Puwakhola)	6.2	3.1	Running	NEA, 2017
	3	Sundarijal	0.64	0.32	Running	NEA, 2017
Owned by IPPs	1	Khimtikhola	60	12	Running	IPPAN, 2018
	2	Chilime	22	11	Running	IPPAN, 2018
	3	Chhyangdi	2	1	Running	IPPAN, 2018
	3	Upper Tamakoshi	456	76	Running	IPPAN, 2018
	4	Sanjen	42.5	15	Under Construction	IPPAN, 2018
Total Operating (Running)			606.84			

The project stated in the above table are state-owned, owned by the Nepal Electricity Authority (NEA), and some by Independent Power Producers (IPPs) which operate under the umbrella organization Independent Power Producers Association of Nepal (IPPAN). From the NEA information companies like Upper Tamakoshi Hydropower Limited (UTHL), and Chilime Hydropower Company Limited (CHCL) are sister companies. In total available energy, NEA's generation contributed 31.66%, whereas those imported from India and domestic IPPs accounted for 31.83% and 36.51% respectively. Table 1.1 show that the 606.84 MW of power generated from the power plant having Pelton turbine to the national grid.

Hence, it can be seen that 16.45 % of the total power is contributed by the Pelton turbine. In Nepal, most of the micro and mini ( $\leq 1000$  kW) employ the Pelton turbine for its cost-effectiveness and flat efficiency curve which shows the Pelton turbine's importance in Nepal.

Pelton turbine buckets are mounted on the periphery of the runner. Either double hemispherical or double ellipsoidal-shaped buckets are mounted. Bajracharya et al (2008) is an initial comprehensive study on sediment erosion in the Pelton turbine available online. This was the first time that a study specifically focused on understanding erosion in Pelton turbine nozzles has been published. Computational fluid dynamics (CFD) has developed and advanced to the point where erosion patterns may now be anticipated through simulation. In particular, the usual installation of Runner and distributor parts is analyzed for the hydro-abrasive erosion analysis in the Pelton turbine by CFD simulation.

The erosion is followed by a decrease in the runner's efficiency and the introduction of mechanical vibration. Therefore, to maintain a reasonable level of vibration and overall generating efficiency, the runners must be replaced regularly. When reinstalling a Pelton turbine, there is a chance that needle tip and bucket splitter will be eccentric or out of alignment. Studies on the eccentric flow behavior of the needle eccentricity, eccentric bucket-jet interaction, and the erosion behavior of the Pelton turbine needle, bucket, and mechanical behavior (mechanical vibration) of the Pelton Turbine are thoroughly conducted. However, a warp is created in the bucket as a result of the eccentric jet-bucket contact, changing the flow and water content of the bucket. Due to uneven loading, eccentric jet, and change in mechanical properties, secondary flows and warping of the bucket can be caused (see Figures 1.2 and 1.3). This study intends to study the change in flow behavior due to bucket warp (or Twist).

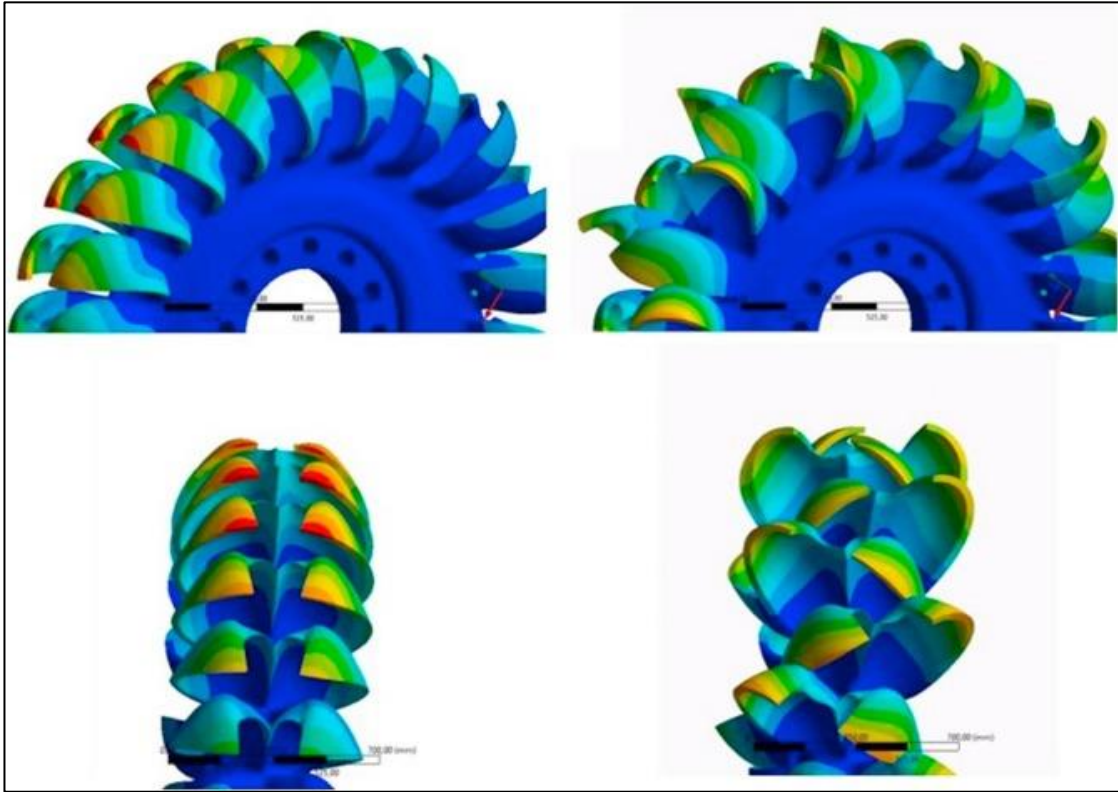


Figure 1.2: Twisting of Bucket due to uneven jet loading((Egusquiza et al., 2018)

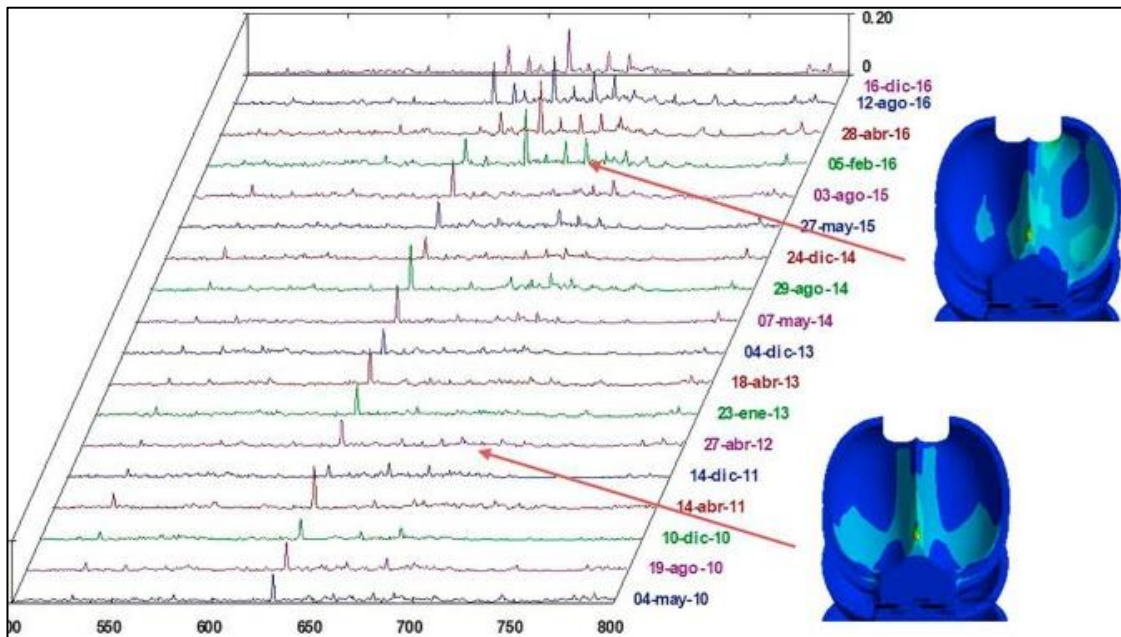


Figure 1.3: Evolution of the vibration signatures (Frequency vs Amplitude) in a Pelton turbine.

The stress distribution for the runner excited without and with jet misalignment has been represented in Figure 1.3 (Egusquiza et al., 2018)

This misalignment may also be caused during the repair and maintenance of the Pelton turbine.



Figure 1.4: Design templates used during the repair of Runner (Panthee et al., 2015)

Figure 1.4 depicts the templates used for profile control of the bucket during repair and maintenance. One limitation of such template is that it is unable to capture the angular deviation of the bucket profile.

## 1.2 Problem Statement

Erosion of turbine runner is reported as the most challenging and researched topic in the hydropower sector. After the erosion, the efficiency of the runner decreases as well as mechanical vibration is introduced. Hence, replacement of runners should be done continual basis to keep overall generation efficiency and vibration at the recommended level. In the case of the Pelton turbine, during reinstallation, there are chances of mismatch or eccentricity between the needle tip and bucket splitter. It is reported by an experienced Pelton turbine operator that this causes an abnormal increase in the thrust bearing temperature and causes mechanical vibration along with reduced efficiency. Having known the effect of eccentricity on bearing temperature and vibrations, alteration of flow due to warping of bucket surface is least studied. In this study, by numerical modeling of the angular deviation of the jet-bucket interaction, change in flow behavior due or eccentric jet-bucket interaction shall be studied. It is believed that the findings of this research would be a good help to operators to understand alteration of flow and efficiency loss due to bucket twisting.

### **1.3 Rationales of Research**

The main rationale of this research is to enhance the current capacity to model flow in the Pelton turbine bucket. The main innovative aspect of the study is that investigation of change in flow behavior due to angular eccentricity of jet-bucket interaction of Pelton turbine is done. The turbine used in this study is the turbine developed by Bajracharya 2008(Bajracharya et al., 2008). The turbine has a nozzle diameter of 20 mm, and a 16 bucket, 2 kW, 1450 RPM Pelton turbine runner with a mean diameter of 175 mm.

### **1.4 Research Objectives**

#### **1.4.1 Main Objective**

To study the effect of the angular eccentricity of jet-bucket interaction of Pelton turbine on the hydraulic performance of the bucket.

#### **1.4.2 Specific Objectives**

The specific objectives of these studies are:

1. To perform flow analysis (hydraulic analysis) for jet deviation in Pelton turbine splitter and compare it with theoretical analysis and experimental observation for model verification.
2. To model flow and hydraulic analysis in case of the angular eccentricity of jet-bucket interaction of Pelton turbine
3. To compare velocity profile, pressure profile, water sheet thickness in of angular eccentricity of jet and compute exit flow conditions.

### **1.5 Assumptions and Limitations**

The assumptions and limitations of this study are:

1. The occurrence of cavitation in the flow domain was neglected.
2. Water is assumed as an incompressible fluid. This assumption will allow us to use the pressure-based solver on Fluent (for planar analysis).
3. The cause for bucket warp (angular eccentricity of jet-bucket) may be the change in mechanical properties of the repaired bucket or eccentric jet hitting of the bucket. In such cases, the splitter tip may possess some eccentricity with the bucket tip. In this study for simplicity, it shall be assumed that bucket twisting is about the splitter tip.

## CHAPTER TWO: LITERATURE REVIEW

In any hydropower plant, the hydraulic energy is harnessed as the available potential energy which exists in the form of the height variation between the water level and the position of water turbines in the hydropower plant. This height difference is defined by the terminology hydraulic head (Zhang, 2016b).

### 2.1 Working Principle

Pelton turbine is the impulse type water turbine commonly employed in high head sites. The rotor of this turbine consists of a circular disc with several vanes (also represented as buckets) placed around the periphery. The nozzles are positioned in a way that each water jet from the nozzle impinges directly along a tangent to the circle (Dixon & Hall, 2010) causing the runner to rotate about its central axis. Figure 2.1 is a typical installation of a horizontal axis Pelton turbine which shall aid to understand the working principle.

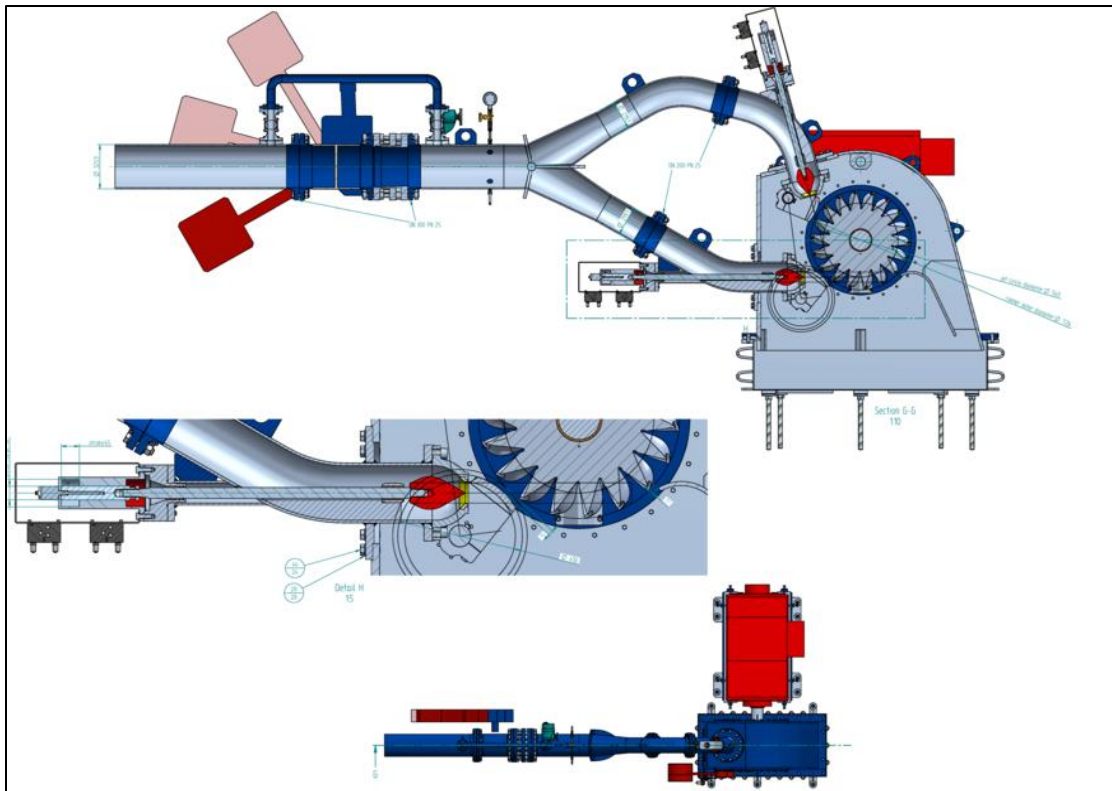


Figure 2.1: Typical Installation of horizontal axis Pelton turbine

Figure 2.1 gives a schematic of the installation of a Pelton turbine. As seen from the diagram, the water from the penstock is directed towards the runner by a nozzle with an internally fitted spear. The wheel spear changes the linear position of the needle altering

the net area for the flow of water which thus serves the purpose of governing (Rajput, 1999).

## 2.2 Energy Conversion in Pelton Turbine

A general schematic of a horizontal axis Pelton turbine is shown in Figure 2.1. By applying nozzles to convert water flow into the form of high-speed jets at the height of the turbine wheel, potential energy is first transformed into kinetic energy, which is then converted into useful mechanical energy. Depending on the flow potential of the site, multiple (Up to 6) nozzles may be used. Thus, the mechanical energy of the shaft fully comes from the momentum exchange high-speed water jet and the buckets. The energy conversion diagram in a Pelton turbine is shown in Figure 2.2. The diagram shows how the high-pressure, low-velocity flow changes into a high-velocity jet in an area with atmospheric pressure as a result of the flow over the nozzle.

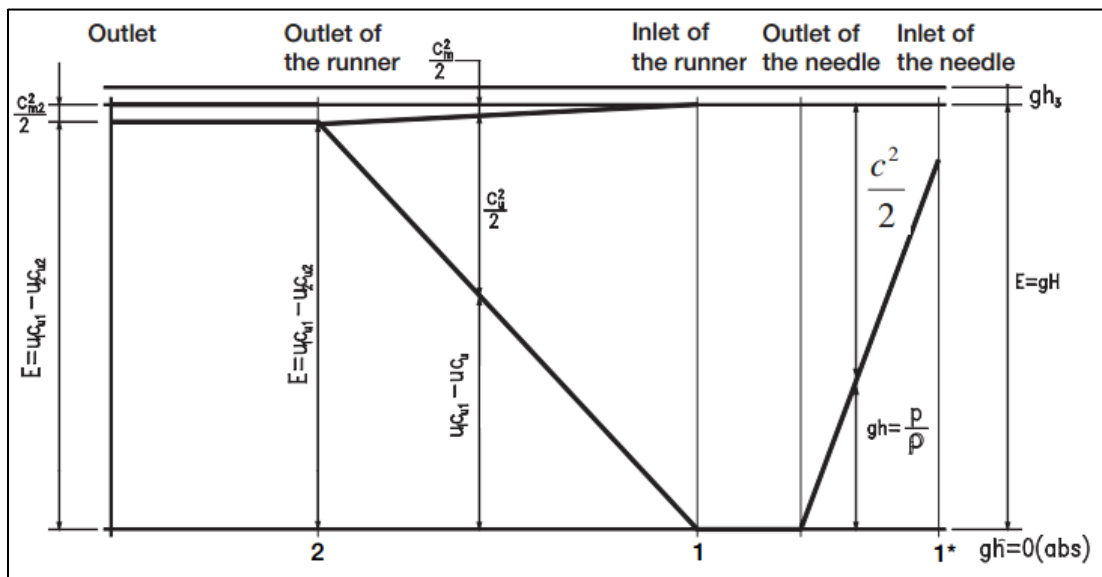


Figure 2.2: Energy conversion diagram (Adopted from(Kjølle, 2001))

The Bernoulli equation for incompressible, steady, and flow without friction along the streamline is given by

$$\frac{p_2 - p_1}{\rho} + \frac{1}{2}(c_2^2 - c_1^2) + g(z_2 - z_1) = 0 \quad \text{Equation 2.1}$$

Concerning Figure 2.2, evaluating from point 1\* to 1 and solving for the jet velocity at 1, by neglecting losses in the injector due to friction, the speed of the jet is calculated to be

$$c_1 = k^* \sqrt{2gH} \quad \text{Equation 2.2}$$

Where  $H$  is the net pressure head at the nozzle and  $g$  is the local value of acceleration due to gravity.

### 2.3 Jet Impingement on a Flat Plate

Impingement of a round jet at an angle  $\theta$  on a flat plate can represent a fundamental jet mechanics concept (Figure 2.3). The water sheet spreading across the plate surface is calculated using the equations of conservation of mass, momentum, and energy. The speed for spreading water-sheet is inferred to be equal to jet speed using the energy conservation equation, jet frictionless deflection, and frictionless water sheet spreading assumptions. While flow distribution at the perimeter circle and radial extent is determined using the law of momentum. And to determine the integrated mass flow along those perimeter circles, which is a reflected jet, the conservation law of mass is applied. Hasson and Peck's (1964) computation of the flow distribution was the first to be accurate. Equation 2.3 is used to calculate the water-sheet height distribution along the periphery of any arbitrary circle.

$$\frac{h.2r}{R^2} = \frac{\sin 3\theta}{(1 - \cos\theta \cos\phi)^2} \quad \text{Equation 2.3}$$

The stagnation point of the round and center of the arbitrary circle coincides together on the flat plate which is eccentric to the jet axis it's distance as given by

$$\frac{s}{R} = \cos\theta \quad \text{Equation 2.4}$$

The law of momentum provides the interaction force between jet speed 'C' and flat plate. As frictionless flow is assumed there is no component of force in the plane of the plate resulting in interaction force perpendicular to a flat plate.



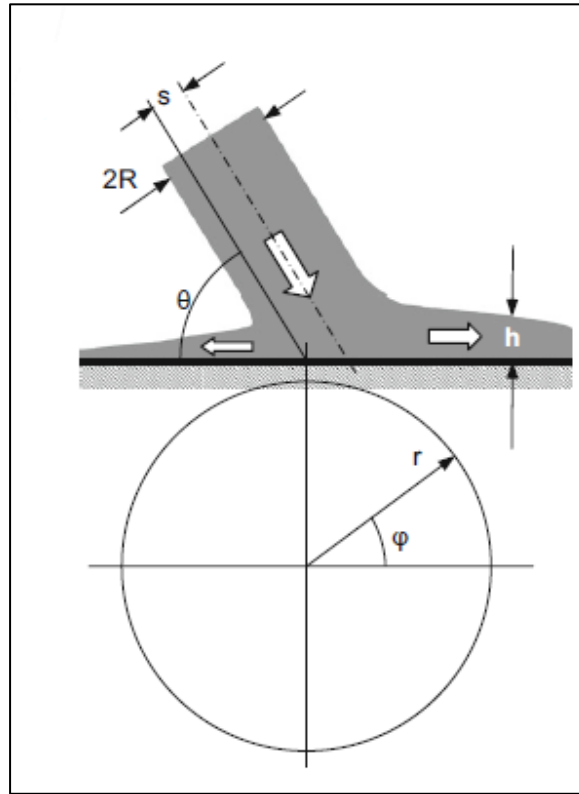


Figure 2.3: Round jet impact on a flat plate and water sheet spreading (Zhang, 2016b)

$$F_{jet} = \pi R^2 \cdot \rho C^2 \cdot \sin\theta \quad \text{Equation 2.5}$$

The aforementioned jet force is referred to as jet impact force.

#### 2.4 Water-Jet-Bucket Interaction

As the buckets of the turbine are continuously bombarded with periodic jet impingement, the bucket profile design and its optimization are crucial. For that, the interacting jet piece should be determined. The  $\alpha_a$  marks the position of corresponding bucket and is derived as

$$\cos\alpha_a = \frac{R_m - d_o/2}{R_c} = \frac{D_m - d_o}{D_c} \quad \text{Equation 2.6}$$

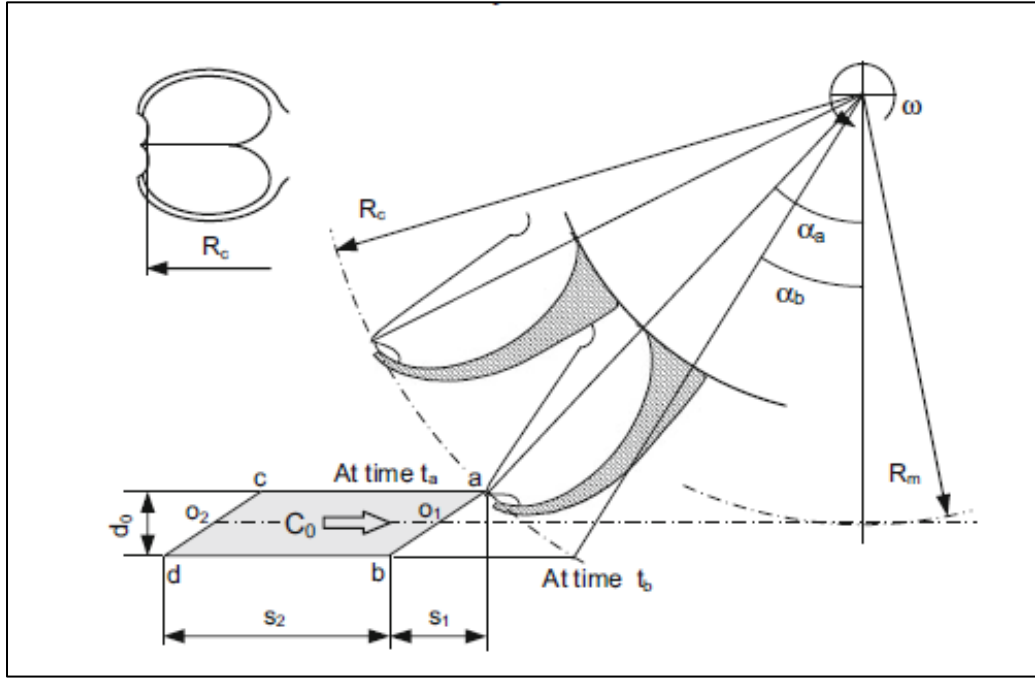


Figure 2.4: Jet piece abcd and specific bucket positions(Zhang, 2016b)

If a definite jet piece contacts the bucket, then the bucket sweeps at angular range  $\Delta\alpha = \alpha_d - \alpha_a$ . The angular range is significant when the turbine has two or more injectors. The offset angle should be higher than  $\Delta\alpha$  to avoid jet interference between two injectors.

## 2.5 Coincidence and Symmetry Conditions

For practical applications, the peripheral speed coefficient 'k<sub>m</sub>' of Pelton turbines is selected at the range of 0.45-0.48 where maximum efficiency is expected. The peripheral speed coefficient k<sub>m</sub> is:

$$k_m = \frac{2\pi}{N} \frac{2\lambda - 1}{\tan\alpha_{01} - \tan(\alpha_{01} - \frac{4\lambda\pi}{N})} \quad \text{Equation 2.7}$$

If  $\lambda$  is equal to 1, this explains that the two interacting buckets are under full jet impingement simultaneously. The factor ( $\lambda$ ) is denoted by multi-bucket factor.  $\lambda$  is a function of both the specific and peripheral speed coefficient for the wheel of Pelton turbine.

### 2.5.1 Deflection of the Flow at the Bucket Main Splitter

An angle  $2\varepsilon$  which is around  $25^\circ$  to  $40^\circ$  is used for the bucket main splitter configuration of Pelton turbines as shown in Figure 2.5. Generally, the jet impinges at an angle that is

non-perpendicular to jet axis and also to relative flow velocity. With simplifications for further study, only the cases with the bucket main splitter present perpendicular to axis of jet are undertaken. An unwanted shock would be developed by the sudden flow deflection on an angle  $\epsilon$ . The force of shock load is applied on the moving bucket which could add up to shaft power.

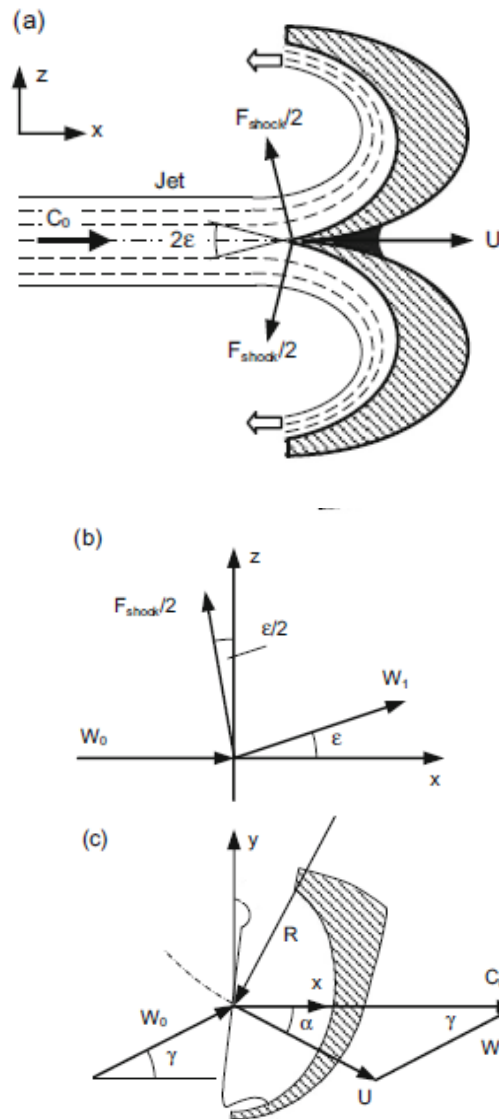


Figure 2.5: Flow deflection at the main splitter(Zhang, 2016b)

The shock load force can be obtained by equation 2.8.

$$e_{shock} = \frac{P_{shock}}{\rho \dot{Q}_w} = W_0 U \cos \alpha \cdot \cos \gamma (1 - \cos \epsilon) \quad \text{Equation 2.8}$$

If there is specific kinetic energy for jet as  $C_0^2/2$ , partial efficiency can be obtained for the shock load force.

$$\eta_{shock} = \frac{e_{shock}}{\frac{1}{2}C_0^2} = 2 \frac{W_0}{C_0} \frac{U}{C_0} \cos\alpha \cdot \cos\gamma \cdot (1 - \cos\epsilon) \quad \text{Equation 2.9}$$

2.9

### 2.5.2 Thickness of Water Sheet in the Bucket

The water-sheet width in the bucket can be considered to increase linearly with the distance traveled by the flow as:

$$d = d_0 + \frac{d_2 - d_0}{S} s \quad \text{Equation 2.11}$$

Where  $d_2$  is water-sheet widths at the bucket exit and  $S$  is the trajectory length of the flow. The width of the water sheet is equivalent to jet diameter  $d_0$  at the entry of the bucket. Whereas for the bucket exit, an assumption of 85% of bucket  $B$  width at a nominal flow rate. But the viscous friction can slow down the relative velocity by 10% which can increase the height of the water sheet correspondingly. Thus, actual water-sheet height should be considered for ensuring sound exit flows from buckets with a correctly set exit angle.

### 2.5.3 Exit Condition and Over Pressure

A pressure increase is observed along the water sheet and bucket surface because of the curved streamlines body in bucket flow. This pressure increase is estimated with the help of the local radius of curvature of the bucket. The overpressure coefficient of the related overpressure is written as equation 2.14 which can determine the orders of magnitude for  $C_p$ -values in bucket flow.

$$C_p = \frac{P_b}{\frac{1}{2}\rho C_0^2} = 2(1 - k_m)^2 \frac{h}{r_b} \quad \text{Equation 2.12}$$

For example, the bucket is designed for a nominal flow rate which can be determined by the diameter of the jet. It can be noted from Fig 2.6 that for the sound and free exit of water flows the bucket without interruptions, the flow velocity for exiting ' $C_2$ ' has a lateral  $x$ -component. For a limited time interval, the water flow particles must pass through the side distance of  $h_a$ , which is determined by the summation of the water-sheet

height and thickness of the bucket wall. Therefore, the exit flow condition is formulated as

$$C_{2x}\Delta t > h_a$$

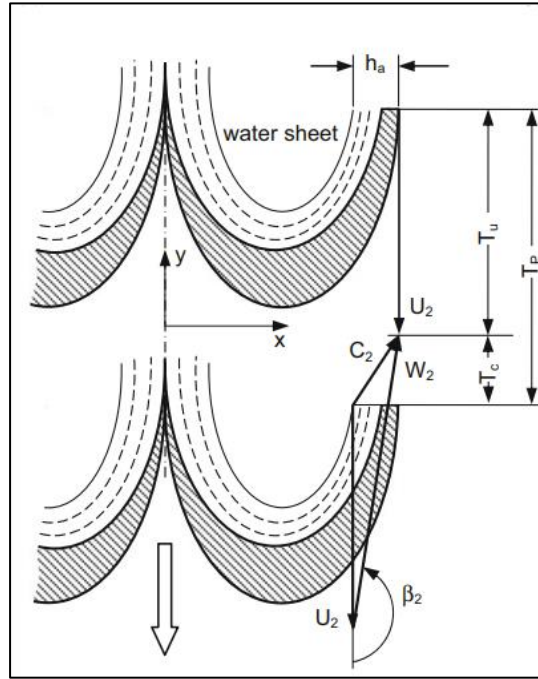


Figure 2.6: Flow conditions determination at the bucket exit(Zhang, 2016b)

## 2.6 Computational Fluid Dynamics

Computational Fluid Dynamics (CFD) is used extensively in solid particle erosion research. A complete CFD-based erosion prediction model comprises several steps which include the particle-fluid interaction, flow modeling, particle-wall interaction, particle-particle interaction, and particle erosion modeling (Frawley *et al.*, 2009) and (Pandya, 2013). The literature of this section is mostly based on (Anderson, 1995a, 1995b; ANSYS Inc, 2013; Versteeg & Malalasekera, 1995).

CFD uses a high computing environment to simulate flow-related problems and provide solutions. While simulating a problem, one should provide the mathematical framework and associated programming tools to solve the high-order polynomials. The data is produced and analyzed within the solving environment. The fluid flows are explained based on the conservation laws including mass, momentum, and energy. CFD solves complex partial differential equations and provides solutions with the help of high-computational computers. Using CFD, we can obtain the qualitative prediction of fluid

flow depending on our boundary conditions and fluid transfer environment. CFD analysis is performed in three major steps: (1) a pre-processor, (2) a solver, and (3) a post-processor. ANSYS CFX and ANSYS Fluent are the widely used commercial CFD workspace available for free for education purposes.

### **2.6.1 Governing Equations**

ANSYS Fluent solves conservation of mass and conservation of momentum for all flows and special conservation equations are solved depending upon the case. In this case, the following shall be the governing equations:

- Conservation of Mass
- Conservation of Momentum
- Conservation of Energy
- Turbulence model: Realizable kappa-epsilon model
- Particle motion equations for the Euler-Lagrange approach

### **2.6.2 Pre-Processor**

In Pre-Processor, the flow problem is inputted into the CFD program with the help of a user-friendly interface and the associated information is provided to develop the desired model for the solver to provide the solution. The detailed steps are given below:

- At first, the desired geometry is defined in the computation workspace.
- The geometry is subdivided into smaller blocks by employing the grid generation feature where several sub-domains are created that might be grids or cells.
- Now, multi-physics models are selected depending upon the user problem. This might include chemical or physical fundamental studies.
- The provided fluid properties with the wall boundaries are well defined.

### **2.6.3 Solver**

The solver can be performed with either of the following available numerical techniques: finite element, finite difference, or spectral methods. Here are the following steps during the solver process:

- Using simple functions for approximating unknown variables of flow.
- Substitute the approximated values in governing equations and discretization followed by further mathematical manipulations.
- Finally, the solution for algebraic problems.

The aforementioned numerical techniques differ in the way how flow variables are determined and how they are discretized for problem-solving. Here, the project utilizes the finite volume method.

#### **2.6.4 Post-Processor**

Owing to the development of high-computations work stations, many have high-quality graphics ability, and are equipped with handy data visualization tools. Some of those interfaces are

- Vector Plots
- Surface Plots
- Particle Tracking

#### **2.6.5 Commercial CFD Codes**

From the literature survey, it is seen that ANSYS CFX, ANSYS Fluent, and STAR CCM+ are commonly used commercial solvers to numerically solve flow and erosion in Pelton turbine needles. ANSYS Fluent is chosen for this study as a CFD solver for this study for experience with the code. Most of sections 2.5.5 and 2.5.6 are based upon the theory guide of ANSYS Fluent.

#### **2.6.6 Turbulence Modeling in CFD**

Smooth, orderly laminar flow is strictly limited to finite values of critical parameters like Reynolds Number, Grashoff Number, etc. Beyond some critical values, the flow becomes unstable and new flow regimes are created which are dominated by a fluctuating and disorderly motion, often known as turbulence. It is very difficult to completely analyze turbulence due to the complex motion of fluid and the unpredictable nature of the flow.

The Reynolds number describes the ratio between the inertia and viscous forces in the fluid. If there is a high Reynolds number, then the flow becomes turbulent. In laminar

flow, a small perturbation is dampened by viscous forces, which is not the case with turbulent flows.

## 2.7 Work done in the Department of Mechanical and Aerospace Engineering

Table 2.1: List of works done in the department of mechanical and aerospace engineering in advancing numerical modelling of Pelton turbine and assembly

List of Works done in the Department of Mechanical and Aerospace Engineering in Advancing Numerical Modelling of Pelton Turbine and Assembly				
S.N.	Name Of Student	Year	Type	Description
1.	Ashesh Babu Timilsina	2019	Numerical and Experimental	Title: Sand Particle Led Erosion in Pelton Turbine Injector(Timilsina, 2019)
2.	Anil Pachhain	2020	Numerical	Title: Numerical modeling of deterioration of efficiency of Pelton turbine due to bucket erosion(Pachhain, 2020)
3.	Sourav Dhungana	2020	Numerical	Title: Flow analysis in an eccentric bucket of Micro Pelton turbine: Multiphase modeling with transient state condition(Dhungana, 2020)
4.	Sameep Shrestha et al.	2021	Numerical and Experimental	Title: Effect of Pelton Turbine Needle Eccentricity on Jet Quality and Injector Erosion( Sameep Shrestha et al, 2021)
5.	Narendra Kumar Mandal	2021	Field Setting Research	Title: Pelton Runner Erosion Due To Cavitation: A Case Study Of Storage Hydropower Plant, Kulekhani First Hydropower



				Station(Narendra Kumar Mandal, 2021)
6.	Anil Sapkota	2021	Numerical	Title: Numerical Modelling of Sand Particle Led Erosion in Reverse Engineered Pelton Turbine Bucket(Anil Sapkota, 2021)

This study is an addition to this series of research by contributing alteration of flow behavior in Bucket flow due to twisted buckets.

### CHAPTER THREE: RESEARCH METHODOLOGY

As shown in figure 3.1, the study will commence with the development of the CAD model for modeling the flow domain and the result of the analysis will be incorporated into the flow simulation model. The eccentricity of the bucket will be analyzed and the results will be compared to that obtained from CFD simulation. The water sheet thickness of the bucket of the Pelton turbine in design condition is obtained from the simulation results compared with the theoretical value.

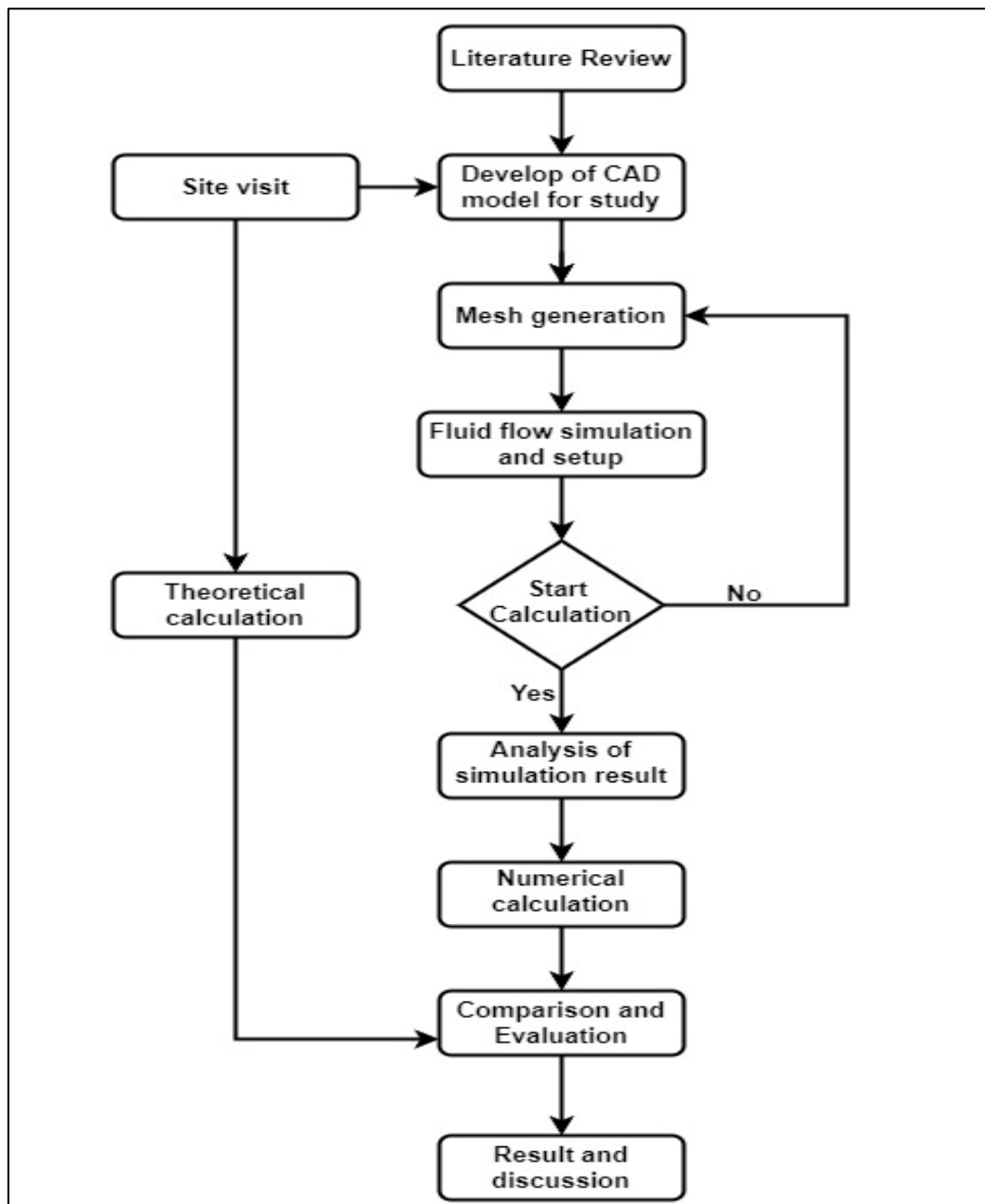


Figure 3.1: Methodology for Research Work

### 3.1 Control Volume of the Study

Figures 3.2 and 3.3 depict the control volume and general layout of the horizontal axis machine.

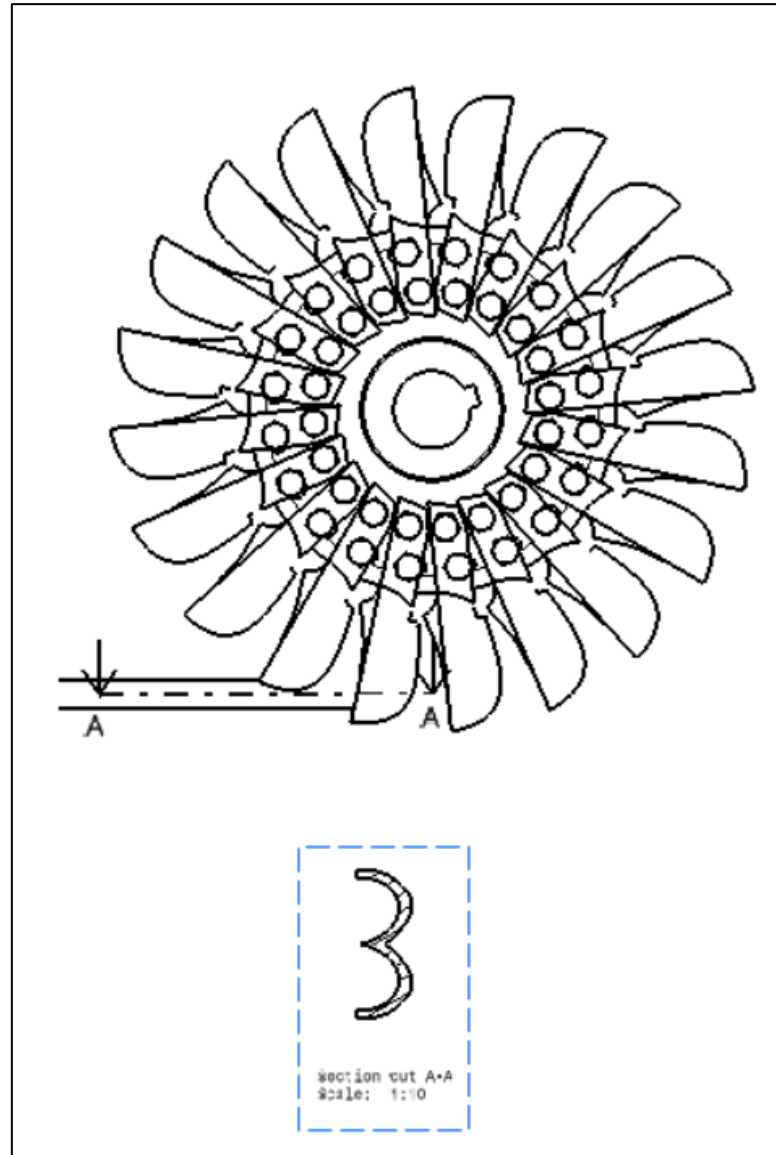


Figure 3.2: Control Volume for this Study

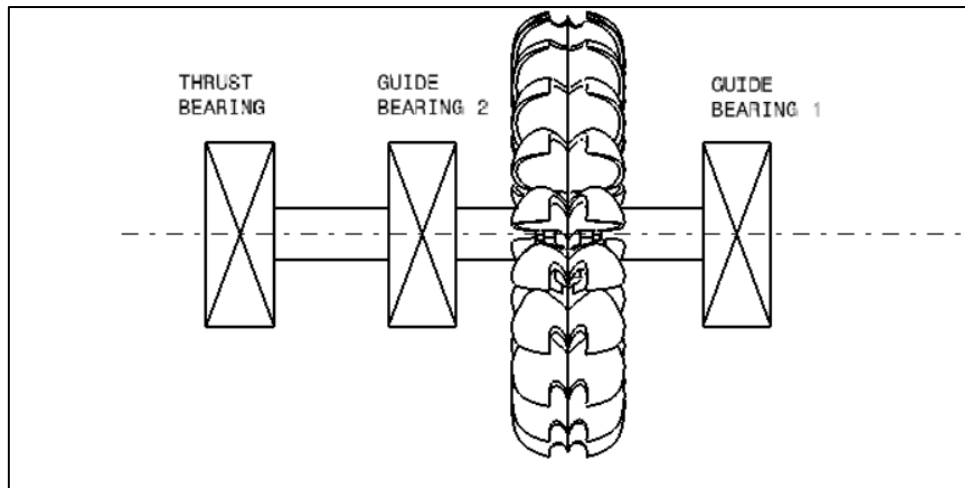


Figure 3.3: General Layout of Horizontal Axis Pelton Unit

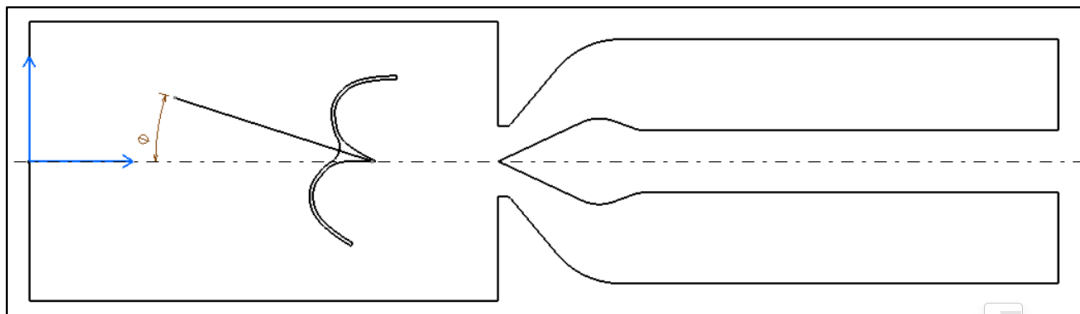


Figure 3.4: Bucket Twist

### 3.2 CFD Solution Procedure

The method adopted for any CFD simulation process is summarized in figure 3.5.

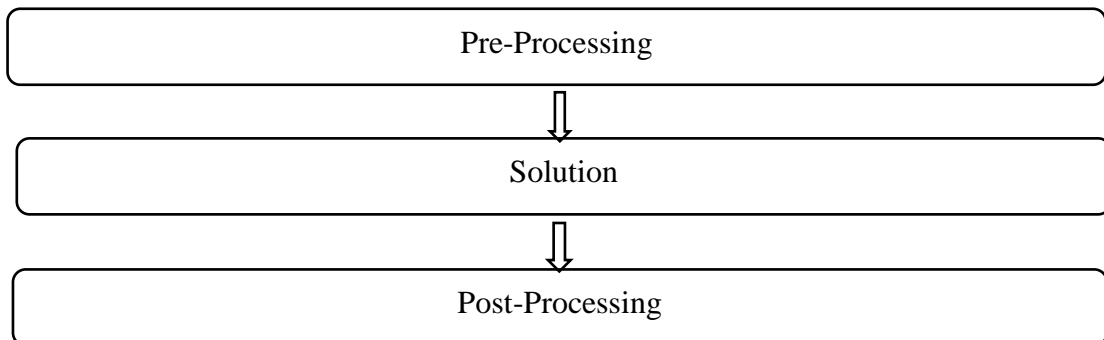


Figure 3.5: Process Flow of CFD Simulation

The above Figure 3.5 shows the three major phase technique of CFD simulation.

1. The first one is Pre-processing, the analyst develops a finite element mesh in this phase to divide the subject geometry into subdomains for mathematical analysis and applies material properties and boundary conditions.

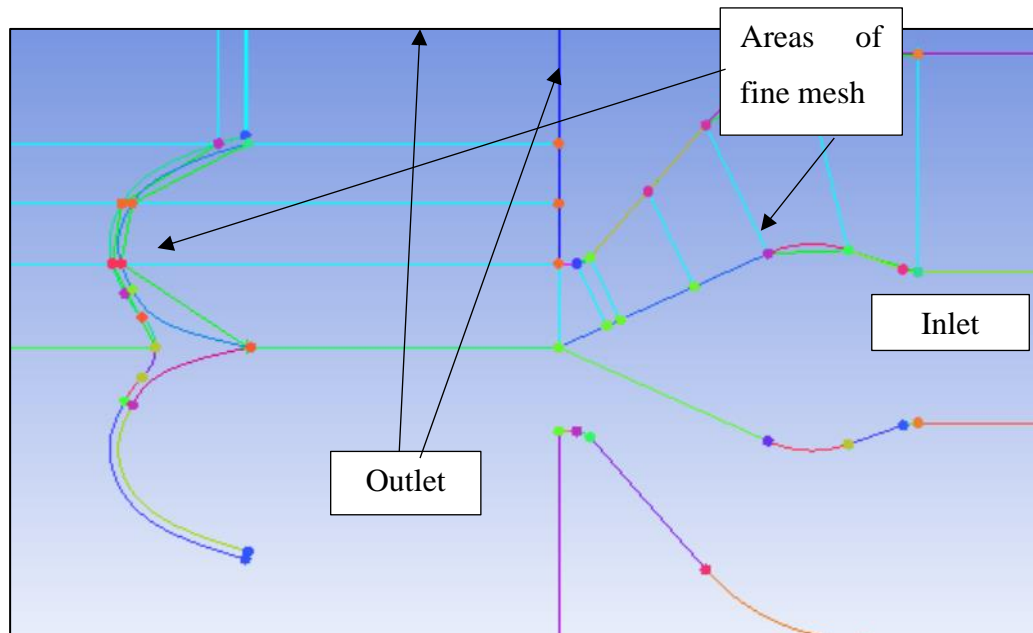


Figure 3.6: Refine Mesh Area

Boundary conditions information will be used as per ((Bajracharya et al., 2008)) and also by experiments study done during the site visit. With ANSYS Fluent, the eccentric shape of the bucket will be studied from different parameters and the twisting effect will be captured. The results will be obtained for different angles and different lengths from the simulation in the ANSYS fluent and compared with the experimental data.

2. The second one is the solution, from the model the program derives the governing matrix equations and solves for the primary quantities.

Here we will use ANSYS Fluent 2020 for the solution. Fluent is a finite volume-based program that has two solvers i.e., pressure-based and density based. As our problem doesn't incorporate changes in density, we will use the pressure-based solver. By adopting finite volume most commercial codes are now developed. The finite volume method is easier (or more natural) to implement for unstructured meshes and is more stable. Most importantly, FLUENT can be epitomized using UDFs. UDFs are flawless if we want to do dim alternation to the standard models.

3. And the last one is post-processing, the validity of the solution can be analyzed by the analyst by checking and examining the values of primary quantities (such as displacements and stresses) and deriving and examining additional quantities (such as specialized stresses and error indicators). An inbuilt program in ANSYS Workbench CFD Post shall be used for post-processing the CFD results.

### 3.2.1 Pre-processing

In this case, to model the flow domain, 3D CAD software, CATIA will be used for its ability to better model the surface topology. Better modeling of surface topology is expected to ease us during the mesh generation. As two-dimensional and three-dimensional flow simulation will be done and our domain is eccentric, a part of the domain will be modeled which will then be used to generate the whole domain. The meshing of the domain will be done by using ICEM CFD 2020. To capture the viscous layer effects (boundary layer) in fluid flow, the fine mesh will be used near the spear, inside the bucket, and in the wall of course. Thus, O-grid will be the efficient choice in this study, with the fine mesh being used on either side of the flow.

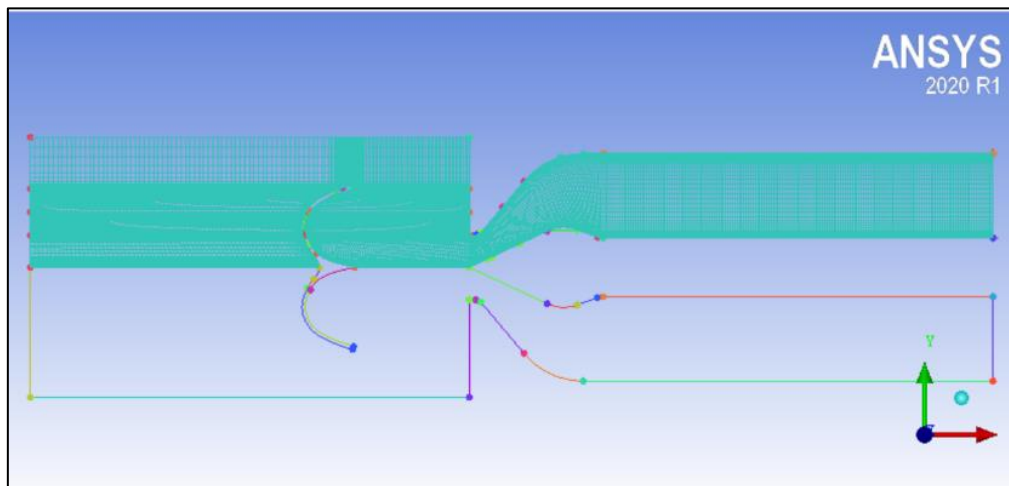


Figure 3.7: Half Mesh of Bucket-Jet

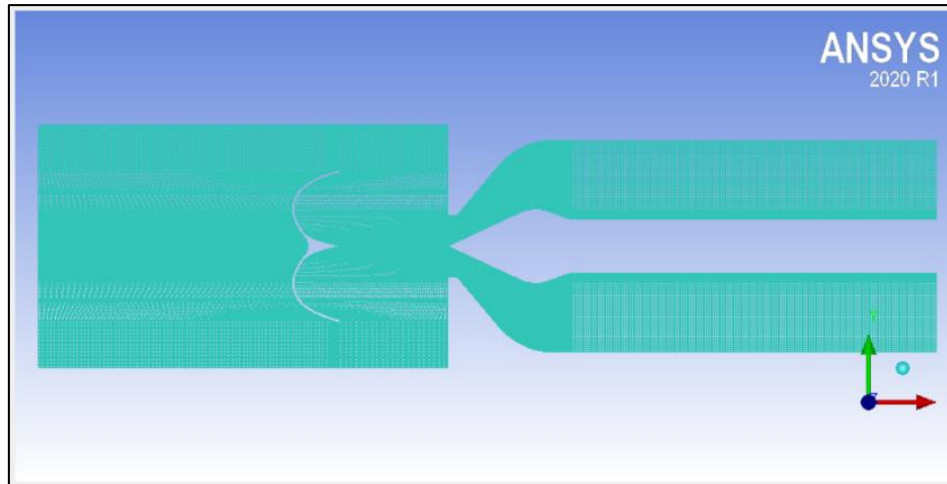


Figure 3.8: Full Mesh of Bucket Jet

### 3.2.2 Solver Settings

Two-Phase Transient State Modeling:

Gravity was defined in negative y-axis (i.e  $-9.8 \text{ m/s}^2$  ). turbulence model used was a realizable k-epsilon model based on past practice and as recommended by the ANSYS Fluent theory guide for multiphase flow simulation for jet flows. The VOF model was employed with primary fluid assigned to air and secondary fluid was set to water with the surface tension coefficient set to  $0.072 \text{ N/m}$ , and the surface tension model was continuum surface force. The second order discretization scheme was chosen and as recommended by ANSYS Fluent theory guide, default transient scheme, second order backward Euler was chosen. To trace the interface of water and air, the geo-reconstruct scheme was employed. Residuals are important for they measure convergence, for all governing equations  $10^{-3}$ . As regards boundary conditions, the inlet was defined as a pressure inlet condition with the numerical value set to 3 bar, the outlet was set to one atmosphere. For multiphase simulation, at the inlet, the value of the water phase was set to 1 and the value of air was set to 0. For the rest of the nodes across the domain, the velocity was initialized to  $1.5 \text{ m/s}$ , pressure to 3 bar, and air volume fraction as 1.

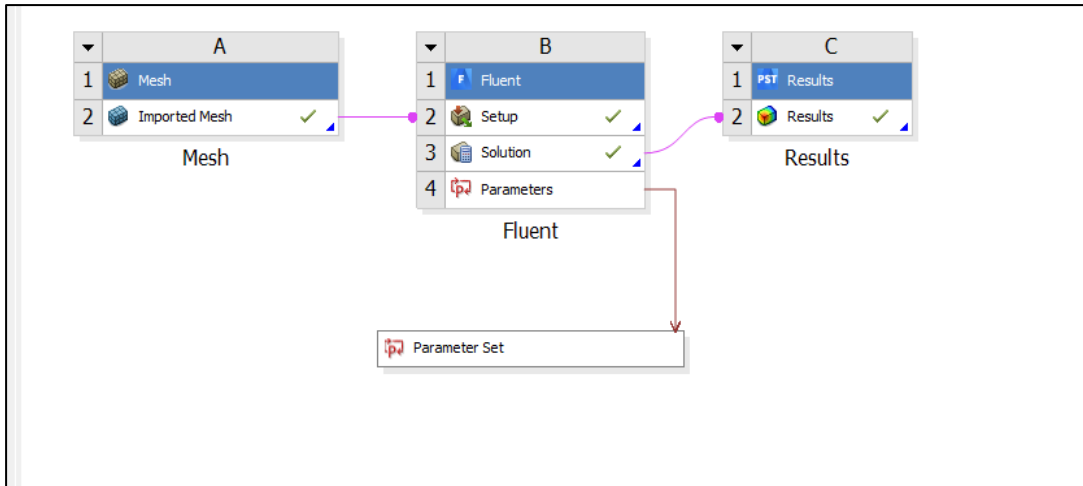


Figure 3.9: Basic Workflow

### 3.3 Measurements in Field Setting Research

Figure 3.10 shows the bearing position on the shaft where the Pelton turbine aligned and also shows the measurement eccentricity and temperature with help of dial gauge.

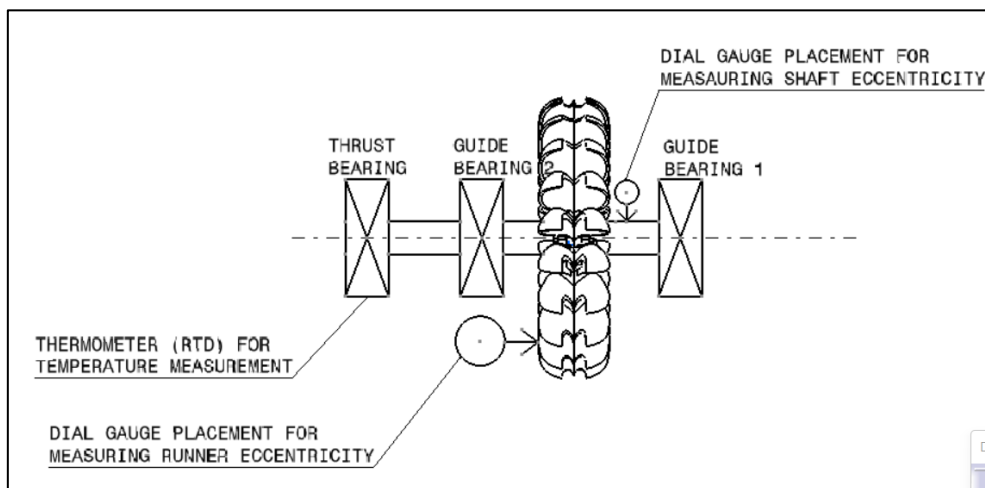


Figure 3.10: Measurement Plant to Understand Effect of Eccentricity on Bearing Temperature

One of the pronounced effects of bucket eccentricity is an unbalanced loading of the bucket causing torque that warps the bucket. This warping creates axial forces which have to be resisted by the thrust bearing. These axial forces cause axial vibration of the runner and subsequent rise in bearing temperature. For measurement purposes, two dial gauges were set, one in the runner disc and another in the shaft for measuring disc



eccentricity and shaft eccentricity. Readings from previously set bearing were taken to note temperature rise.



Figure 3.11: Eccentricity Measurement Using Dial Gauge

## CHAPTER FOUR: RESULTS AND DISCUSSION

### 4.1 Observation in Field Study

During the site visit, several eccentricity values (absolute) of 4 mm, 5 mm (maximum), and 0 mm (minimum) were observed which were not constant as a runner was rotated. Figure 4.1 and 4.2 below shows the recorded value of eccentricity for the refurbished turbine. Moreover, due to eccentricity the thrust bearing temperature was changed and spiked by 20 degrees than the desired limit. The normal operating temperature of the bearing was 60 degree Celsius which rose to 80 degrees Celsius upon the eccentric running of the Runner. It decreases the load carrying area of the pad and reduces the oil film thickness, which causes the breakdown of the bearing or malfunction resulting in loss of efficiency. Table 4.1 and 4.2 summarizes the readings noted.

Table 4.1: Eccentricity Reading of Pelton Turbine

S.N.	Rotation in Degree(°)	Eccentricity (Dial Gauge Reading) in mm
1.	45	2.6
2.	90	4.1
3.	135	5
4.	180	3.1
5.	225	2.4
6.	270	2.3
7.	315	1.7
8.	360	0
Average		2.65

Table 4.2: Eccentricity and Bearing Temperature

S.N.	Average Eccentricity (in mm)	Bearing Temperature (°C)
1.	0	60
2.	2.65	80

## 4.2 Numerical Modeling of Flow for Zero Angular Deviation

### 4.2.1 Volume Fraction (Water Flow) for Centric Placement

The Figure 4.1 show the flow for centric placement.

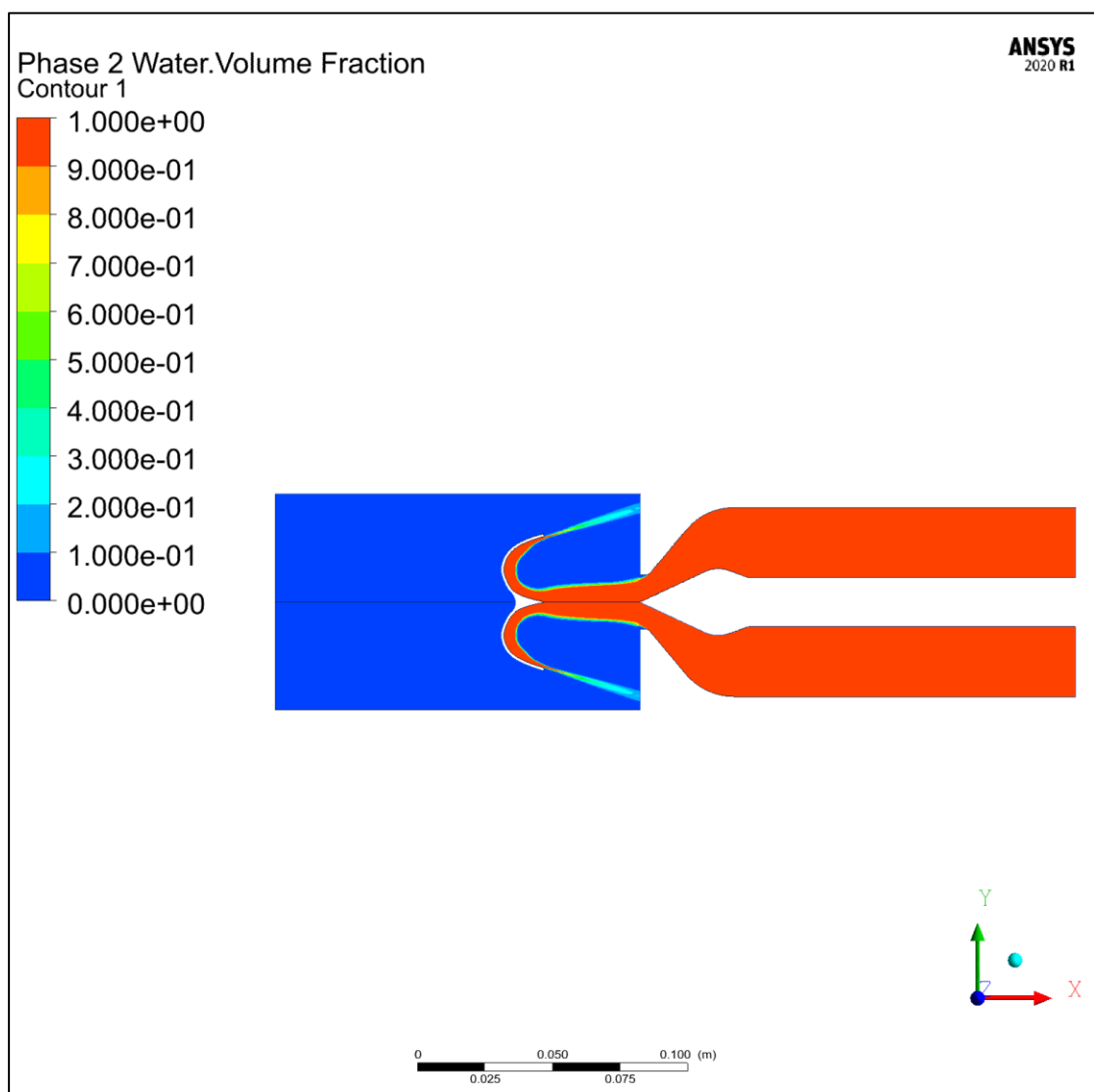
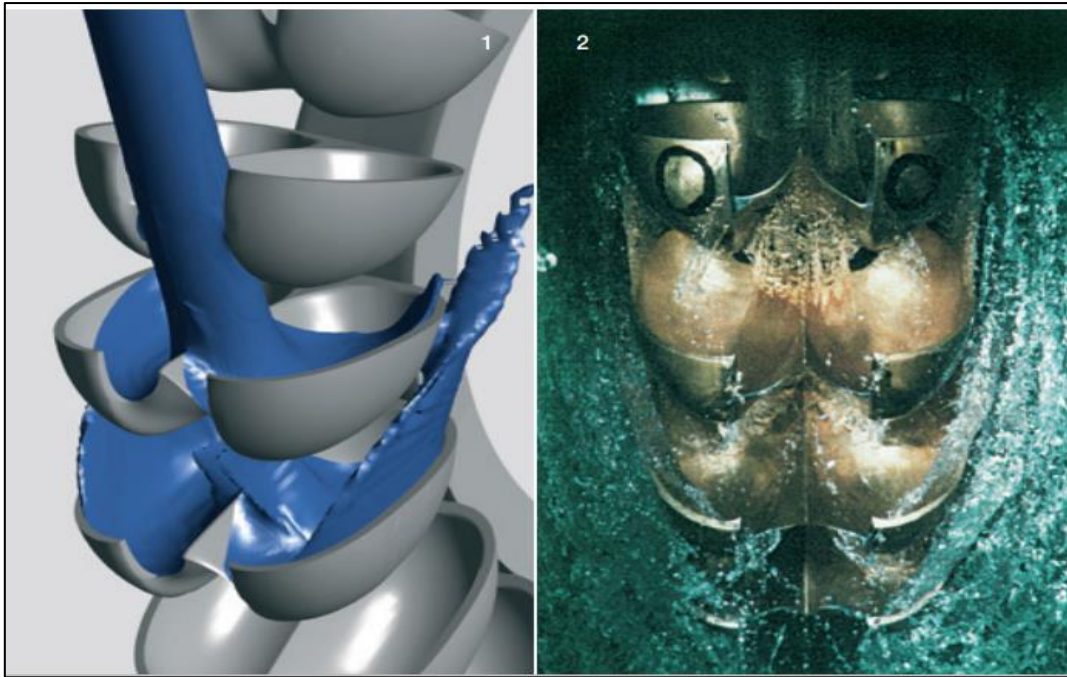


Figure 4.1: Volume Fraction of Water after steady state flow

Figure 4.1 is the distribution of water flow in the bucket after the achievement of the steady-state flow. It can be seen that as depicted in texts of Zhang, the water sheet gradually gets thin as it comes close to the bucket exit and after the flow exits it gets dispersed. The water sheet thickness first increases as the height of flow spread in the bucket increases and gradually get decreases at the exit condition the water sheet thickness is more or less equal to the bucket thickness which meets the previous study results.



(a)



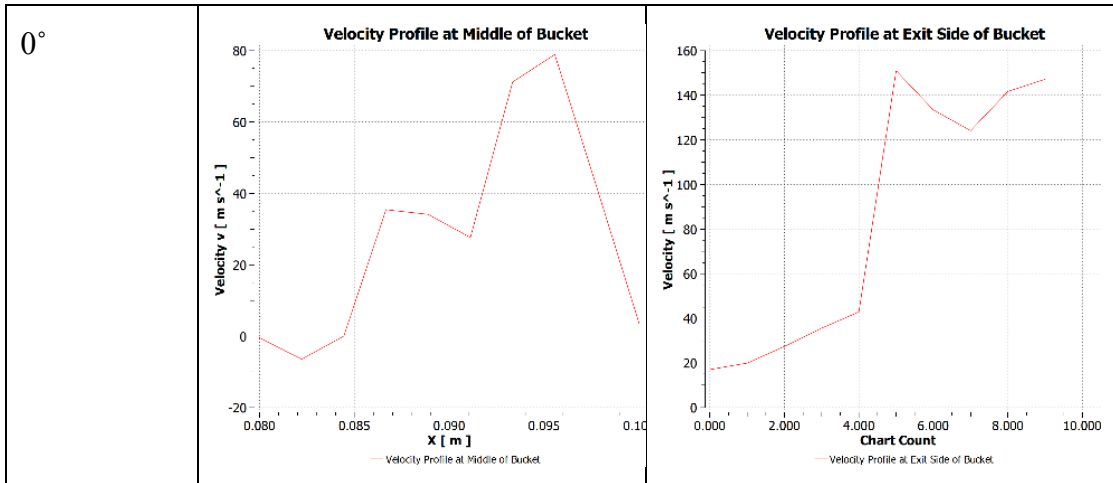
(b)

Figure 4.2: (a),(b) Actual flow-through model(VOITH Workshop, St. Poelten, 2019)

#### 4.2.2 Velocity Distribution

Table 4.3: Velocity profile of centric case at a different deviation

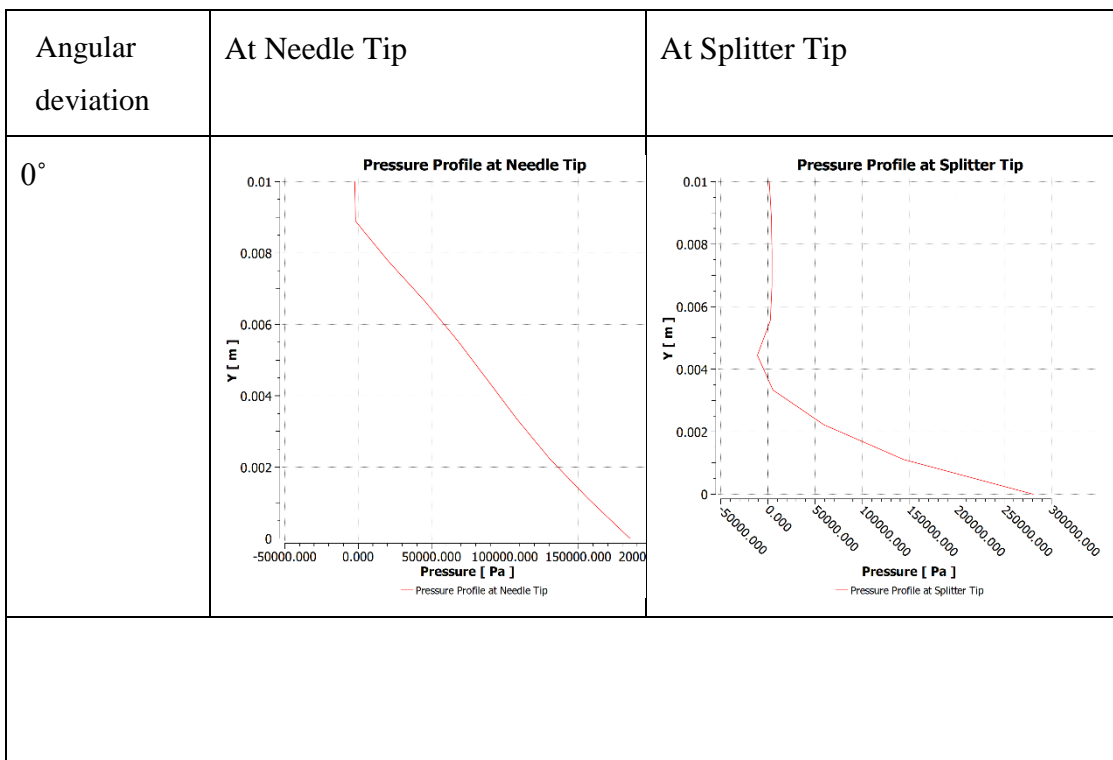
Angular deviation	At Needle Tip	At Splitter Tip
0°	<p>The graph shows a velocity profile at the needle tip. The y-axis represents the vertical distance <math>y</math> in meters, ranging from 0 to 0.01. The x-axis represents the velocity <math>u</math> in <math>\text{m s}^{-1}</math>, ranging from -25,000 to -5,000. The velocity profile is shown as a red dashed line, starting at approximately -20,000 <math>\text{m s}^{-1}</math> at <math>y=0</math>, increasing to about -15,000 <math>\text{m s}^{-1}</math> at <math>y=0.002</math>, and then rising to approximately -5,000 <math>\text{m s}^{-1}</math> at <math>y=0.01</math>.</p>	<p>The graph shows a velocity profile at the splitter tip. The y-axis represents the vertical distance <math>y</math> in meters, ranging from 0 to 0.01. The x-axis represents the velocity <math>u</math> in <math>\text{m s}^{-1}</math>, ranging from -120,000 to -20,000. The velocity profile is shown as a red dashed line, starting at approximately -120,000 <math>\text{m s}^{-1}</math> at <math>y=0</math>, increasing to about -40,000 <math>\text{m s}^{-1}</math> at <math>y=0.002</math>, and then rising to approximately -20,000 <math>\text{m s}^{-1}</math> at <math>y=0.01</math>.</p>
Angular deviation	In Middle of Bucket	At Exit Side of Bucket

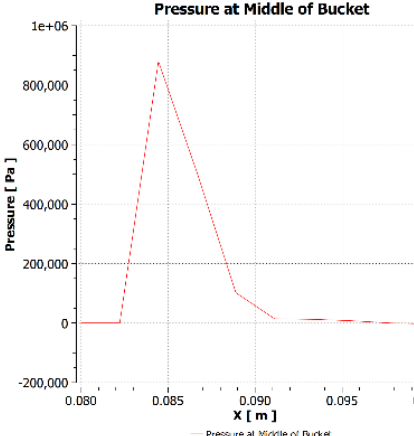
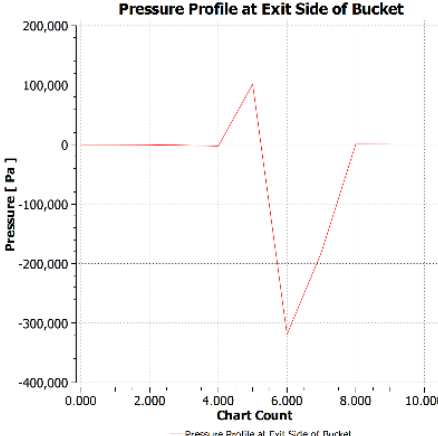


As shown in Table 4.3, the velocity obtained at needle tip is zero as the jet move towards the splitter tip its velocity gradually get increases which show the simulation of the model is right. The velocity profile at splitter tip seen that the velocity obtained is 20m/s. The maximum velocity is around 80m/s obtain in middle of bucket. As the flow exit from the bucket, the velocity is not zero which shows the jet fly away from the bucket and dispersed freely from the buckets.

### 4.2.3 Pressure Distribution

Table 4.4: Pressure profile of centric case at a different position



Angular deviation	In Middle of Bucket	At Exit Side of Bucket
0°	 <p>The graph titled "Pressure at Middle of Bucket" shows Pressure [Pa] on the y-axis (ranging from -200,000 to 1e+06) versus X [m] on the x-axis (ranging from 0.080 to 0.100). The pressure is zero until approximately X = 0.083, then rises sharply to a peak of about 850,000 Pa at X = 0.085, and then gradually decreases back to zero by X = 0.095.</p>	 <p>The graph titled "Pressure Profile at Exit Side of Bucket" shows Pressure [Pa] on the y-axis (ranging from -400,000 to 200,000) versus Chart Count on the x-axis (ranging from 0.000 to 10.000). The pressure is zero until Chart Count = 4.000, then rises to a peak of about 100,000 Pa at Chart Count = 5.000, drops to a minimum of about -300,000 Pa at Chart Count = 6.000, and then rises back to zero by Chart Count = 8.000.</p>

As shown in Table 4.4, the pressure at needle tip is 200 kPa and at splitter tip is 300 kPa. From the pressure profile at middle of bucket pressure is zero which verifies the maximum velocity at middle of bucket. Pressure at the exit is initially seen as zero which means that the velocity at some extent at the exit has near to the maximum value after passing some distance pressure increases and then decreases respectively.

#### 4.2.4 Water Sheet Thickness

Table 4.5: Water volume fraction profile of centric case at different positions

Angular deviation	At Needle Tip	At Splitter Tip
0°		
Angular deviation	In Middle of Bucket	At Exit Side of Bucket
0°		

Table 4.5 show the water volume fraction at a different position. Water sheet thickness at needle tip has a maximum value which gradually decreases as the height of the flow increases and at the exit condition water sheet height is equal to the bucket thickness. (Zhang, 2016b)



### 4.3 Theoretical Calculations for Zero Angular Deviation

Table 4.6: Experimental reading and error calculation

Calculation of Jet Velocity (Experiment)			
S.N.	Item	Value	Units
1	Runner PCD	0.175	M
2	Measured Runner RPM	1430	RPM
3	The linear speed of Bucket	13.10	m/s
4	Assuming maximum eff. Condition, Jet Velocity	26.21	
Error analysis			
Velocity from Computations as measured at the location of runner bucket, the point where Jet and Bucket Interact			
1	X- Velocity (Absolute)	21.99	m/s
	Error in Computation	-16.08%	
1	Resultant Velocity (Absolute)	23.219	m/s
	Error in Computation	-11.5%	

The error as calculated in Table 4.6 is accounted for the fact that, though the design has been done for maximum efficiency conditions, the jet constant, which is calculated to be 0.5 for maximum efficiency conditions may not achieve during manufacturing. In addition, there are errors present in Numerical simulation which are systematic.

#### 4.3.1 Water Sheet Thickness

For Centric condition

Bucket width (B) =48.661 mm (from geometry)

Water sheet width ( $d_2$ ) at exit =  $d_{2,N} = 0.85B = 0.85*3d_0 \approx 2.5d_0$  (from equation 2.11)

$$=0.85*48.661$$

$$= 41.361\text{mm}$$

(Jet diameter = water sheet width) at entry

At exit, Jet diameter  $d_0 = \frac{d_2}{2.5} = 16.54475 \text{ mm}$

Trajectory length(S) = 42.08mm (from geometry)

The water sheet width of the bucket can be calculated as (from equation 2.12)

$$d = d_0 + \frac{d_2 - d_0}{S} = 16.54475 + \frac{41.361 + 16.54475}{42.08} * 16.54475$$
$$= 26.408 \text{ mm}$$

#### 4.3.2 Overpressure coefficient calculation for centric condition

The overpressure coefficient in terms of 'h' can be calculated as (from equation 2.14)

$$c_p = \frac{P_b}{\frac{1}{2} \rho C_0^2} = 2(1 - k_m)^2 \frac{h}{r_b}$$

The radius of curvature of the surface profile can be represented as

$$r_b = 0.55d_0$$

The overpressure coefficient in terms of 'water sheet width' can be calculated as (from equation 2.14)

$$c_p = (1 - k_m)^2 \frac{\pi d_0^2}{4 r_b d}$$

Overpressure coefficient at  $0^\circ$  (with  $k_m=0.47$ )(Zhang, 2016b)

$$c_p = (1 - 0.47)^2 \frac{\pi d_0^2}{4 * 0.55 * d_0 * d}$$

$$c_p = (1 - 0.47)^2 \frac{\pi * 16.54475^2}{4 * 0.55 * 26.408}$$

$$= 0.2513$$

#### Error Calculation

The water-sheet height h along the sheet width d, can be assumed to be uniform and thus constant. The height of the water sheet at the bucket exit can be expressed as

$$h_{2,N} \approx 0.05 * B$$

$$= 0.05 * 48.661 \text{ mm}$$

$$=2.43305 \text{ mm}$$

From numerical results we can get the range for water sheet thickness (From X-axis) for volume fraction of water equal to 1 which is 3.23 mm (for centric placement).

$$\begin{aligned} \text{error} &= \frac{\text{Numerical value} - \text{Theoretical value}}{\text{Theoretical value}} \\ &= \frac{3.23 - 2.43305}{2.43305} \\ &= 32.755\% \end{aligned}$$

As we compare the theoretical and numerical value 32.75% error encountered in the thickness of the water sheet as compared to theoretical estimates. The error occur due to the mesh sizing, design of the bucket, viscous water sheet and theoretical assumption, stationary bucket position. A thicker water sheet means that a bucket will hold more mass than it would under ideal conditions. Along with imbalanced forces, which are generally considered for studying mechanical vibrations, this additional weight of water in the bucket is a source of mechanical vibrations as well.

### **4.3.3 Comparison of Numerical and Theoretical Calculation**

#### **Velocity Comparison**

For verification of the current adopted numerical modeling, a comparison of velocity profile with experimentally measured value was done. There is a -11.5% error in the jet velocity, which was calculated from experimental and computational value. The average velocity from numerical result 22.2 m/s is similar to the previous simulation 23.219 m/s, which show the solver setting for the simulation is right and verified the model for the further study of different angular deviation cases.

#### **Sheet Thickness**

Water sheet thickness obtained from the theoretical calculation is 2.43305mm and from the numerical result is 3.23 mm. The variation occur due to the mesh sizing, design of the bucket, viscous water sheet and theoretical assumption, stationary bucket position. The water sheet thickness at needle tip is 5.56 mm, at splitter tip is 2.22 mm, mid of the bucket 3.23 mm and at the exit side is 1 mm. the value of the water sheet thickness at different position show the water sheet thickness varies as the height of the flow

direction changes. The obtained value for the centric condition meet the statement as the height increases the water sheet thickness increases (Zhang, 2016a).

### Overpressure Coefficient

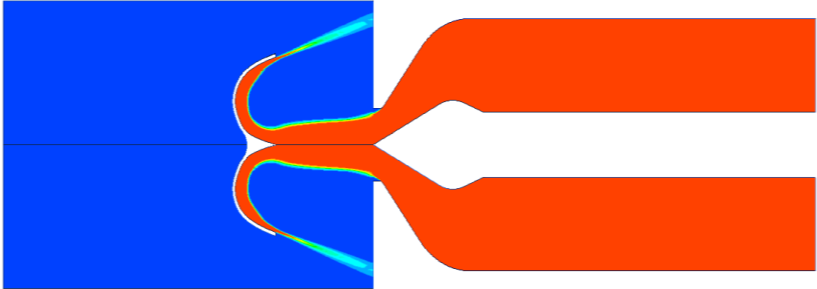
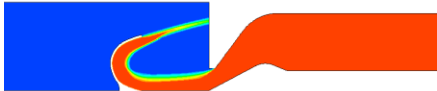
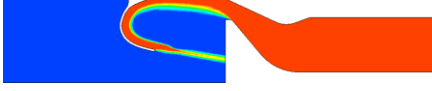
The obtained value of overpressure coefficient is 0.2513 which is slightly closer to the value mention in the Zhang book. The calculated value shows that the parameter considered during centric condition is applicable for the further study of the different cases.

## 4.4 Numerical Modeling of Angular Deviation

### 4.4.1 Flow Modeling

The Table 4.7 of flow model of different angular deviation show the sable relation between the jet and the stationary bucket.

Table 4.7: Flow model for deviated angles

S. N.	Deviati on	For centric condition	
1.	0°		
		Upper half	Lower Half
2.	2.5°		

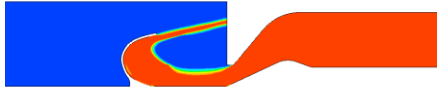
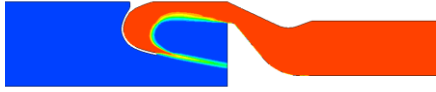
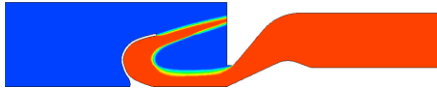
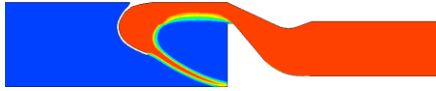
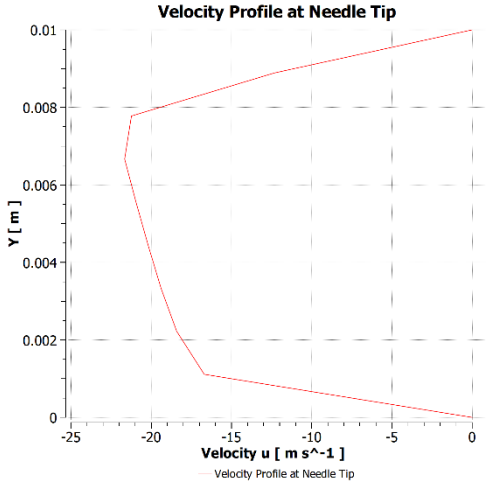
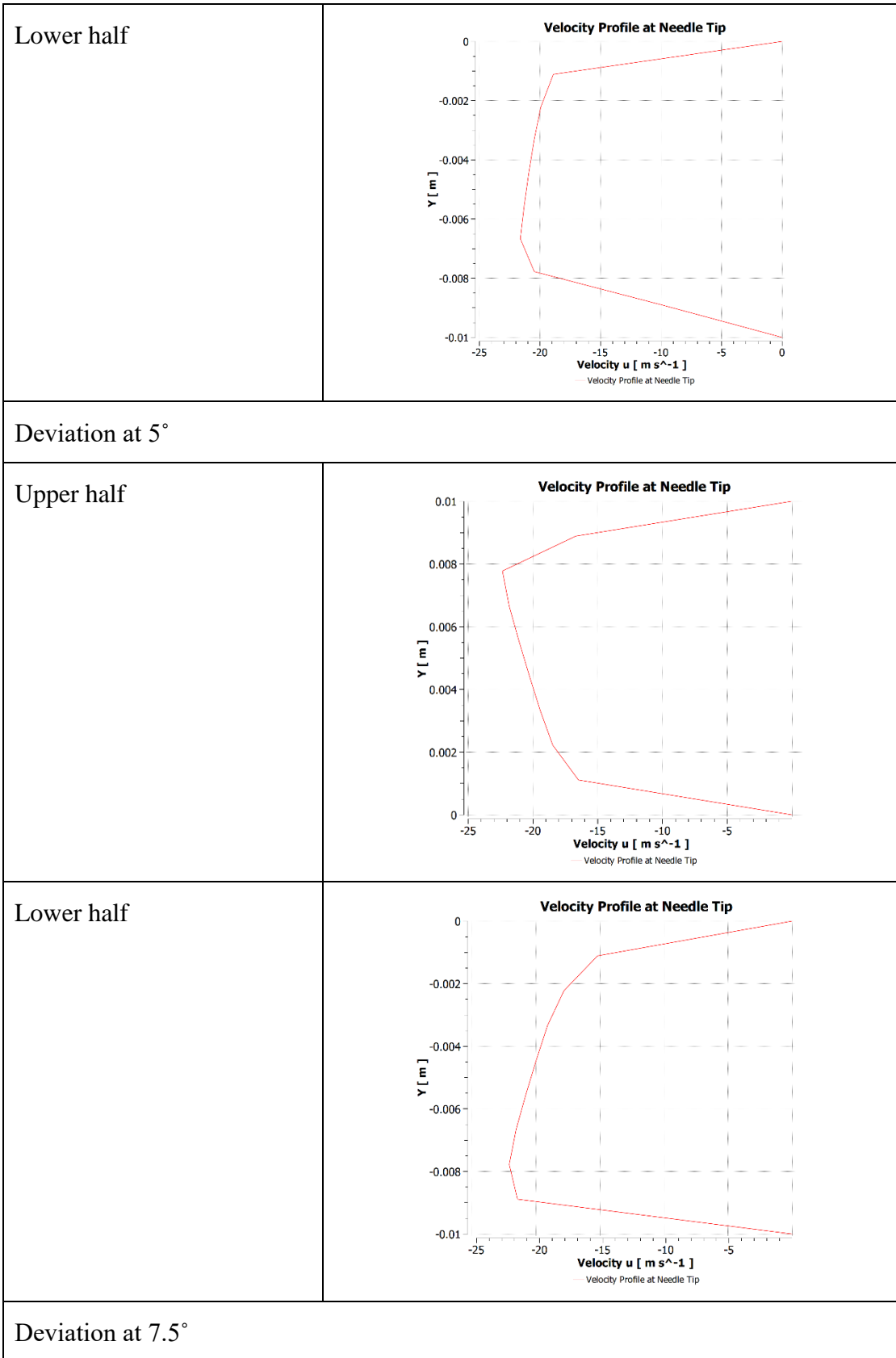
3.	5°		
4.	7.5°		

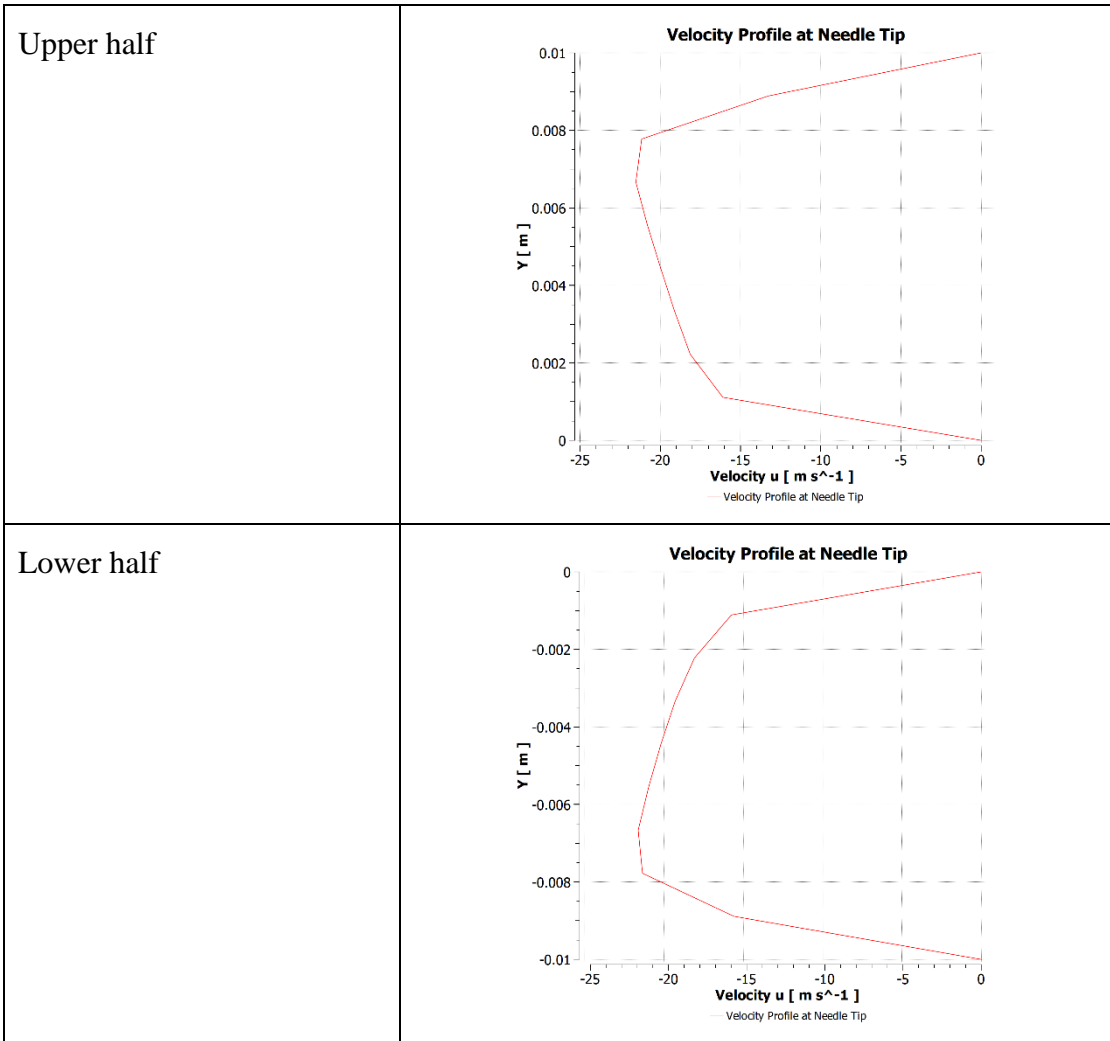
Table 4.7 is the distribution of water flow in the bucket in different cases. It can be seen that as the angle of deformation increases the water sheet thickness increases. In the upper half, the water sheet thickness is greater than in the lower half.

#### 4.4.2 Velocity Profile at Needle Tip

Table 4.8: Velocity profile of different angular deviations at needle tip

Deviation at 2.5°	
Upper half	

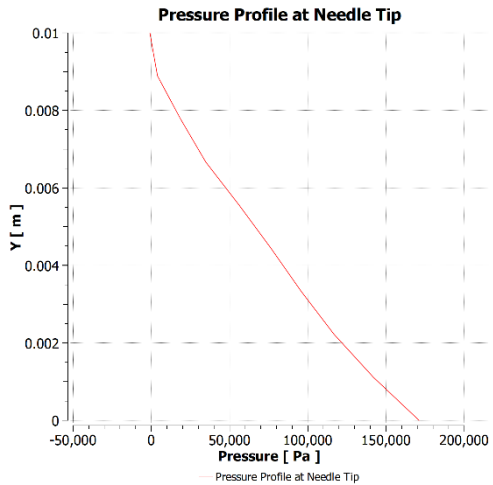
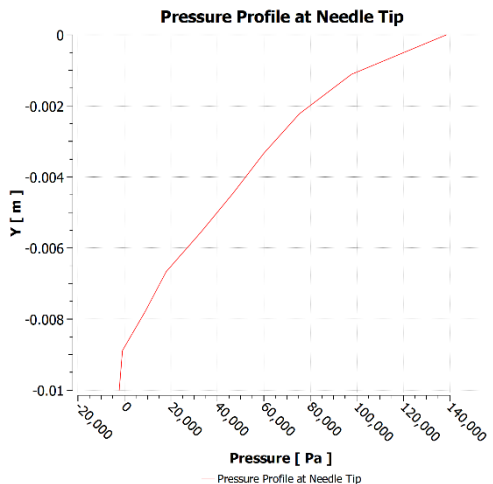




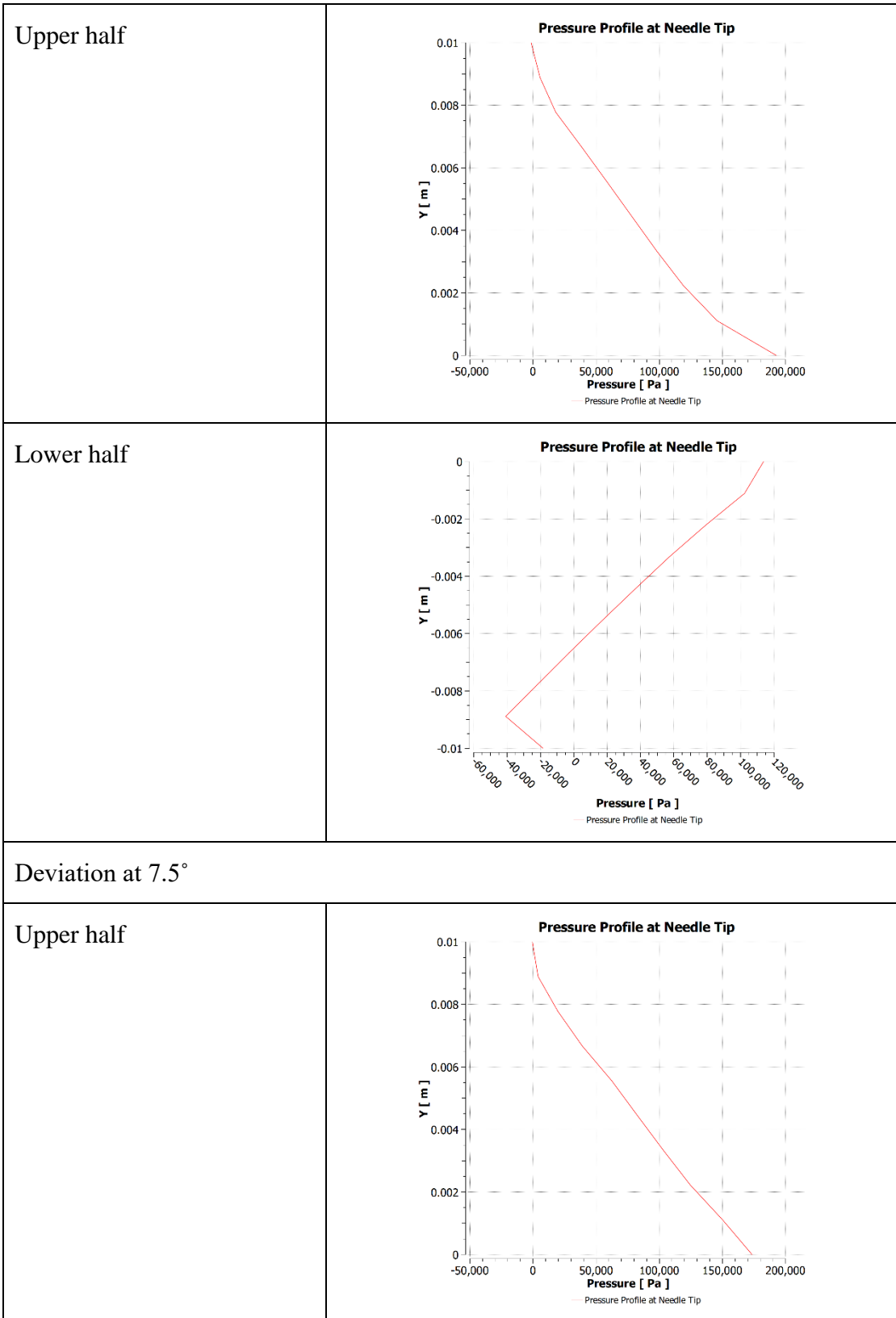
From Table 4.8 it is seen that the velocity profile at different angular deviations at needle tip has zero velocity which is similarly to the centric case. This shows that the simulations of the different cases are right.

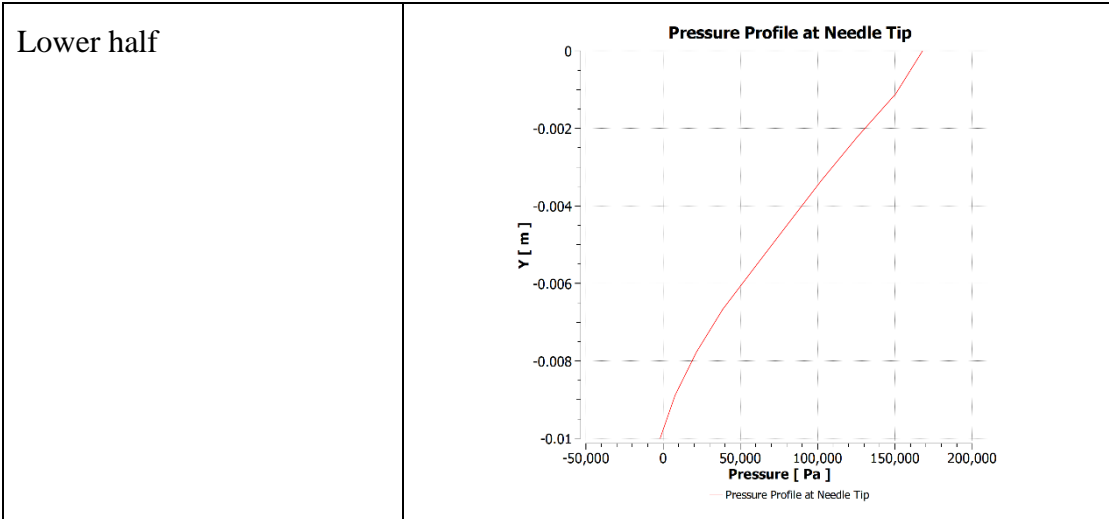
### 4.4.3 Pressure Profile at Needle Tip

Table 4.9: Pressure profile of different angular deviations at needle tip

Deviation at 2.5°	
Upper half	 <p>Pressure Profile at Needle Tip</p> <p>Y [m]</p> <p>Pressure [ Pa ]</p> <p>— Pressure Profile at Needle Tip</p>
Lower half	 <p>Pressure Profile at Needle Tip</p> <p>Y [m]</p> <p>Pressure [ Pa ]</p> <p>— Pressure Profile at Needle Tip</p>
Deviation at 5°	



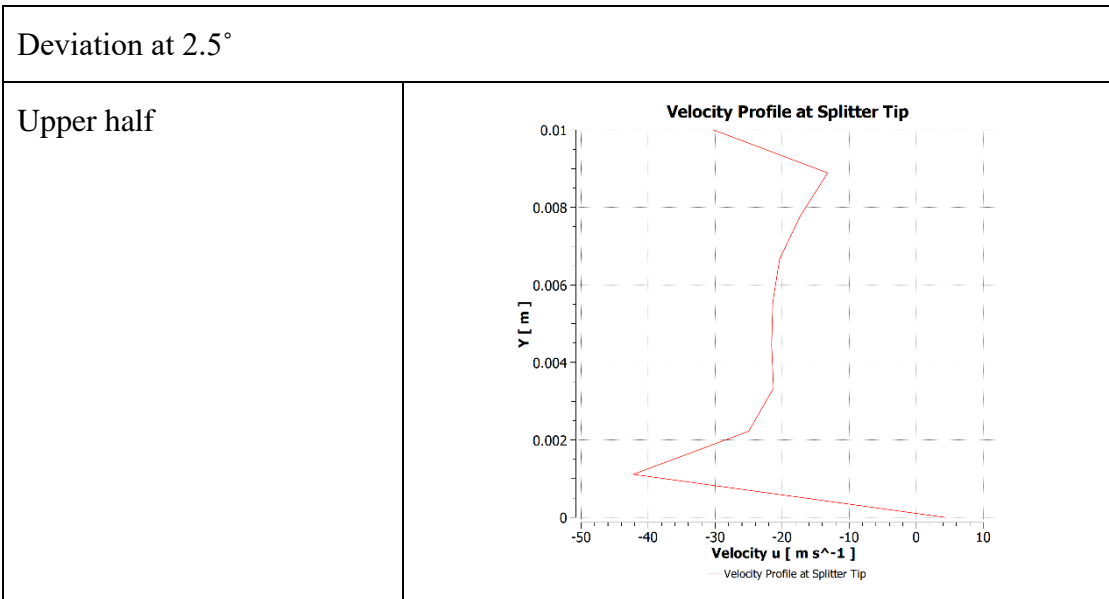




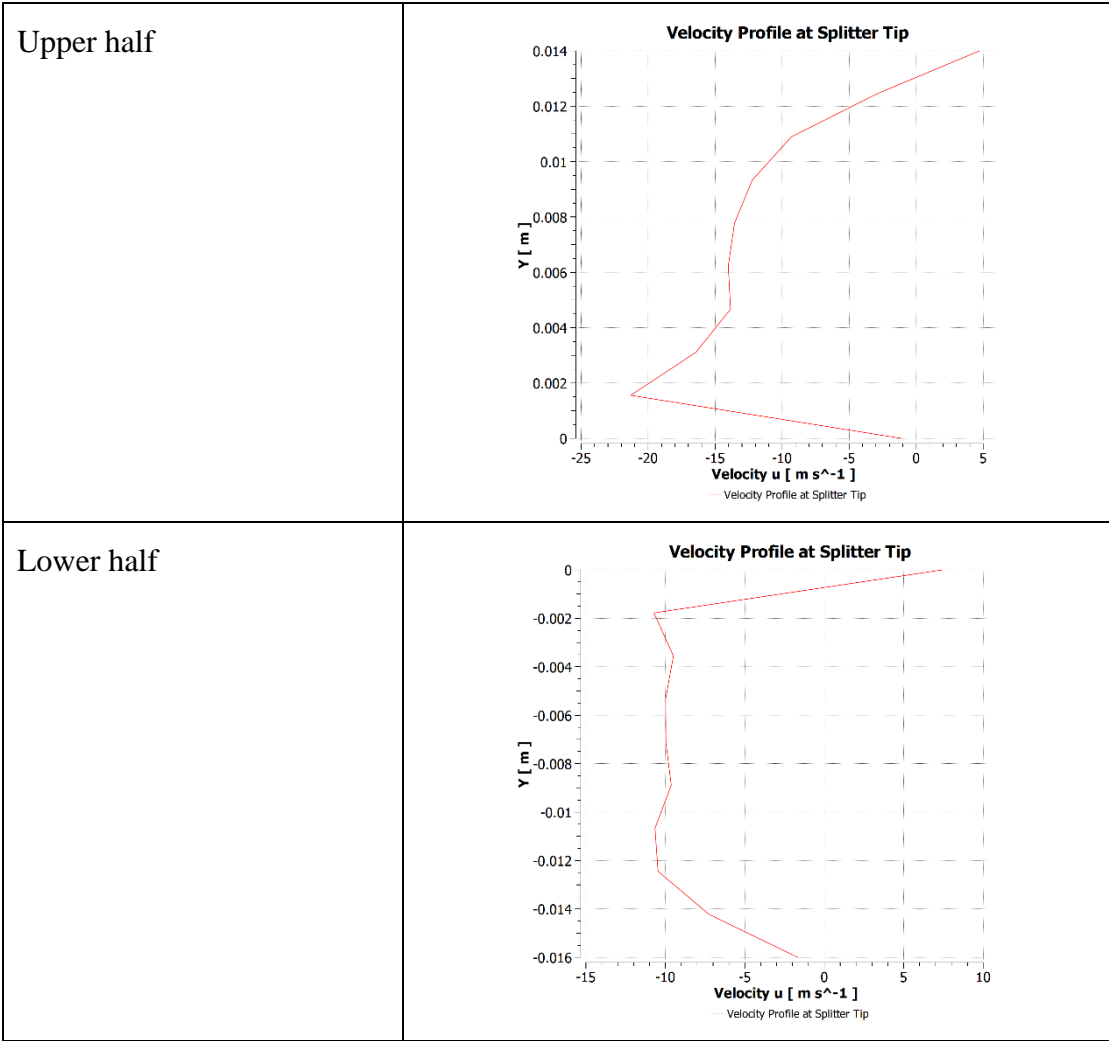
From the 4.9 the maximum pressure profile is obtained at needle tip which validates the velocity profile at needle tip according to the past study i.e at maximum pressure velocity is minimum.

#### 4.4.4 Velocity Profile at Splitter Tip

Table 4.10: Velocity profile of different angular deviation at splitter tip



Lower half	
Deviation at 5°	
Upper half	
Lower half	
Deviation at 7.5°	

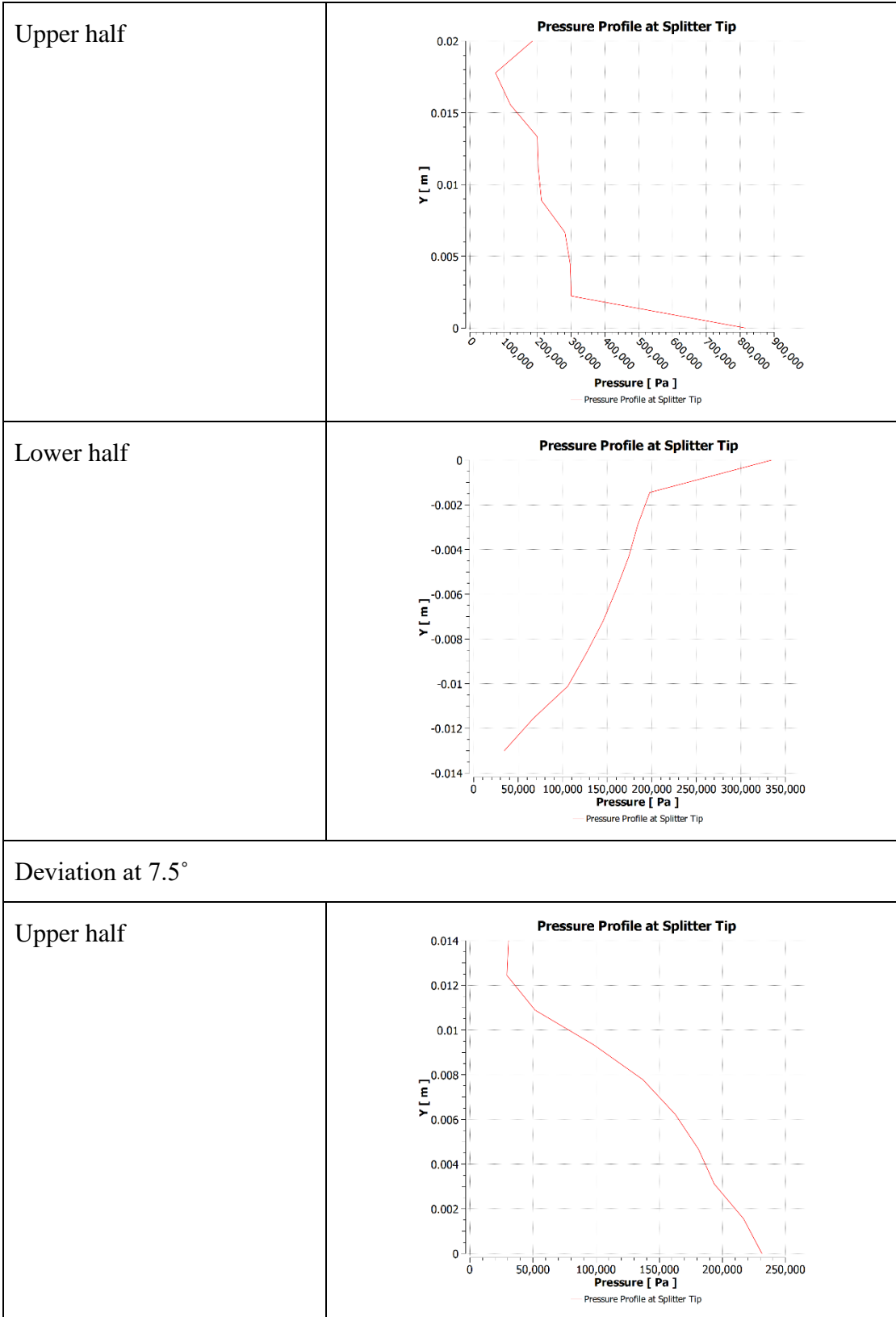


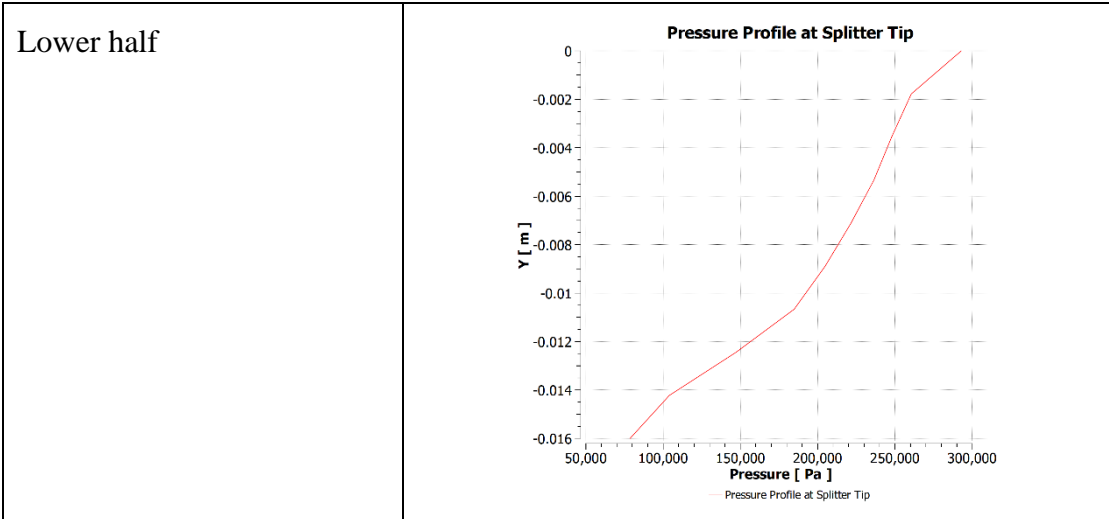
As shown in Table 4.10 the velocity at splitter tip step by step increases as the height of the water sheet increases. The maximum velocity at the splitter is shown in the upper half of the 5-degree angle of deviation.

#### 4.4.5 Pressure Profile at Splitter Tip

Table 4.11: Pressure profile of different angular deviation at splitter tip

Deviation at 2.5°															
Upper half	<p><b>Pressure Profile at Splitter Tip</b></p> <table border="1"> <caption>Approximate data for Upper half, 2.5° deviation</caption> <thead> <tr> <th>Y [m]</th> <th>Pressure [Pa]</th> </tr> </thead> <tbody> <tr><td>0.000</td><td>0</td></tr> <tr><td>0.002</td><td>100,000</td></tr> <tr><td>0.004</td><td>50,000</td></tr> <tr><td>0.006</td><td>25,000</td></tr> <tr><td>0.008</td><td>10,000</td></tr> <tr><td>0.010</td><td>0</td></tr> </tbody> </table>	Y [m]	Pressure [Pa]	0.000	0	0.002	100,000	0.004	50,000	0.006	25,000	0.008	10,000	0.010	0
Y [m]	Pressure [Pa]														
0.000	0														
0.002	100,000														
0.004	50,000														
0.006	25,000														
0.008	10,000														
0.010	0														
Lower half	<p><b>Pressure Profile at Splitter Tip</b></p> <table border="1"> <caption>Approximate data for Lower half, 2.5° deviation</caption> <thead> <tr> <th>Y [m]</th> <th>Pressure [Pa]</th> </tr> </thead> <tbody> <tr><td>0.000</td><td>0</td></tr> <tr><td>-0.002</td><td>100,000</td></tr> <tr><td>-0.004</td><td>200,000</td></tr> <tr><td>-0.006</td><td>300,000</td></tr> <tr><td>-0.008</td><td>400,000</td></tr> <tr><td>-0.010</td><td>450,000</td></tr> </tbody> </table>	Y [m]	Pressure [Pa]	0.000	0	-0.002	100,000	-0.004	200,000	-0.006	300,000	-0.008	400,000	-0.010	450,000
Y [m]	Pressure [Pa]														
0.000	0														
-0.002	100,000														
-0.004	200,000														
-0.006	300,000														
-0.008	400,000														
-0.010	450,000														
Deviation at 5°															

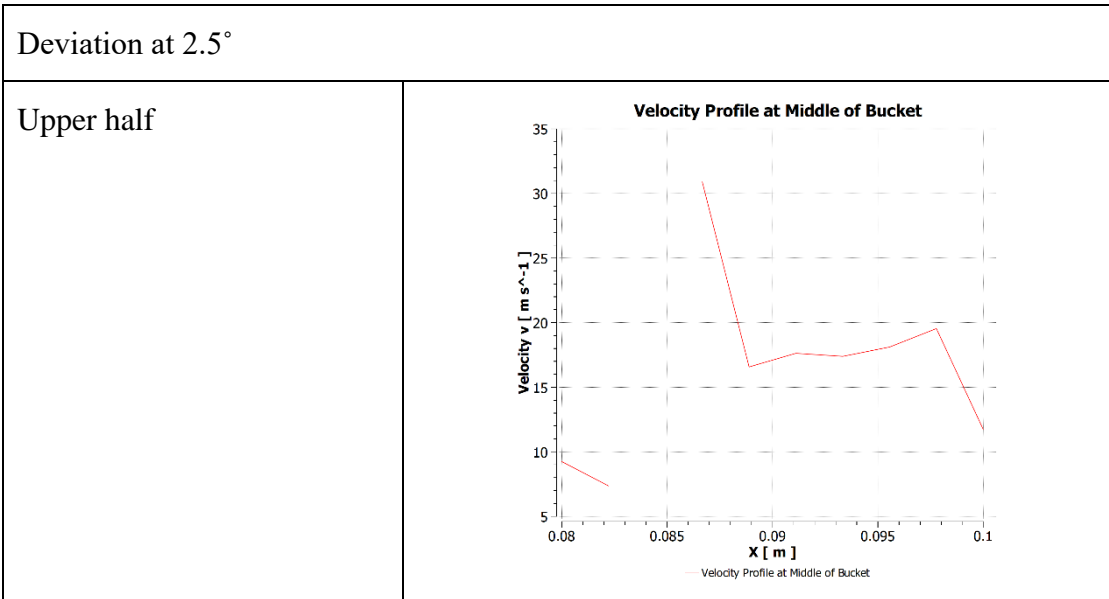




From Table 4.11 the larger pressure variation is seen at a different position. The variation in the pressure at 5 degrees upper half and the lower half has a greater value difference. Whereas the in-between upper half and lower half pressure variation of 2.5 degrees and 7.5degree has more or less similar values.

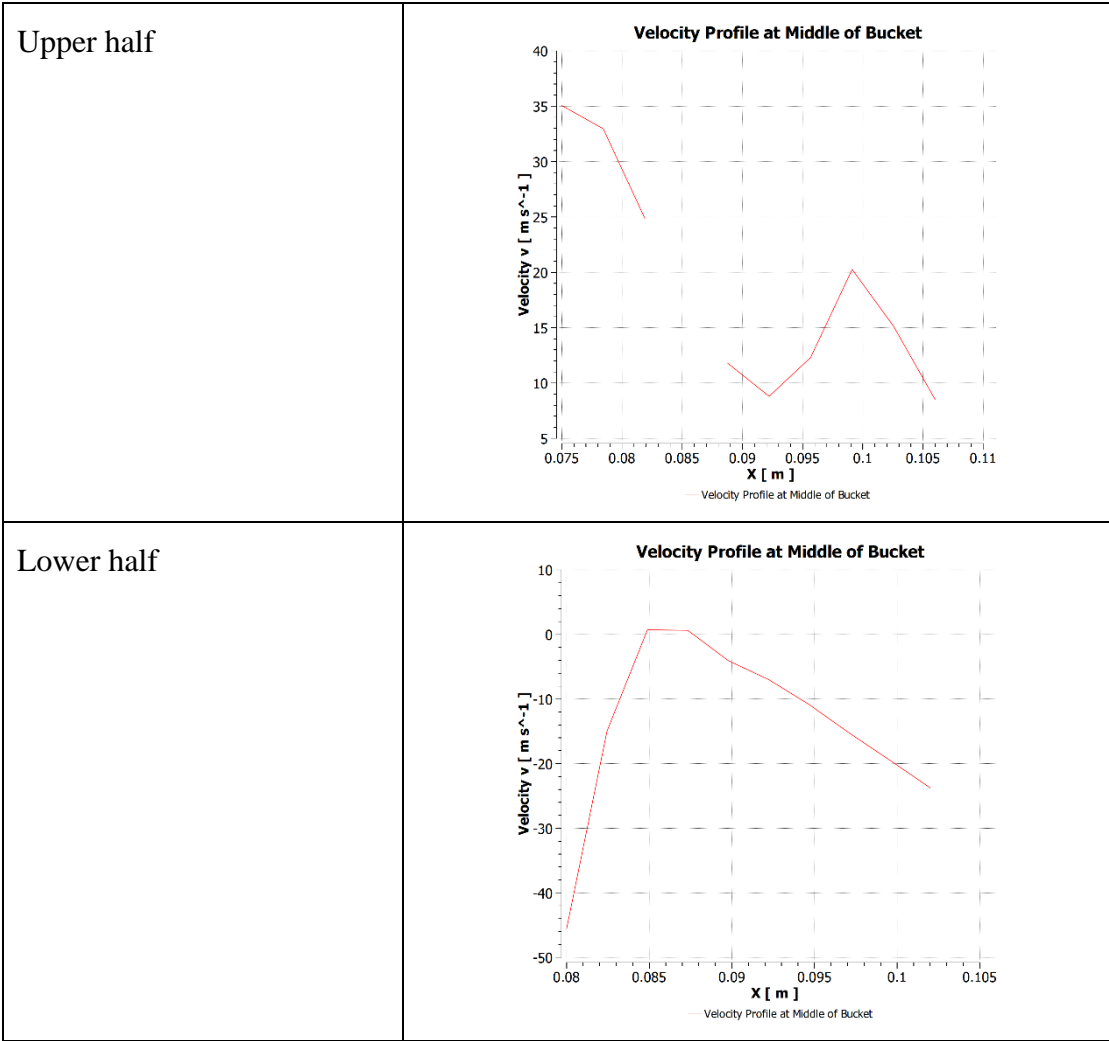
**4.4.6 Velocity Profile at Middle of Bucket**

Table 4.12: Velocity profile of different deviations at middle of bucket



<p>Lower half</p>	<p>Velocity Profile at Middle of Bucket</p>
<p>Deviation at 5°</p>	
<p>Upper half</p>	<p>Velocity Profile at Middle of Bucket</p>
<p>Lower half</p>	<p>Velocity Profile at Middle of Bucket</p>
<p>Deviation at 7.5°</p>	



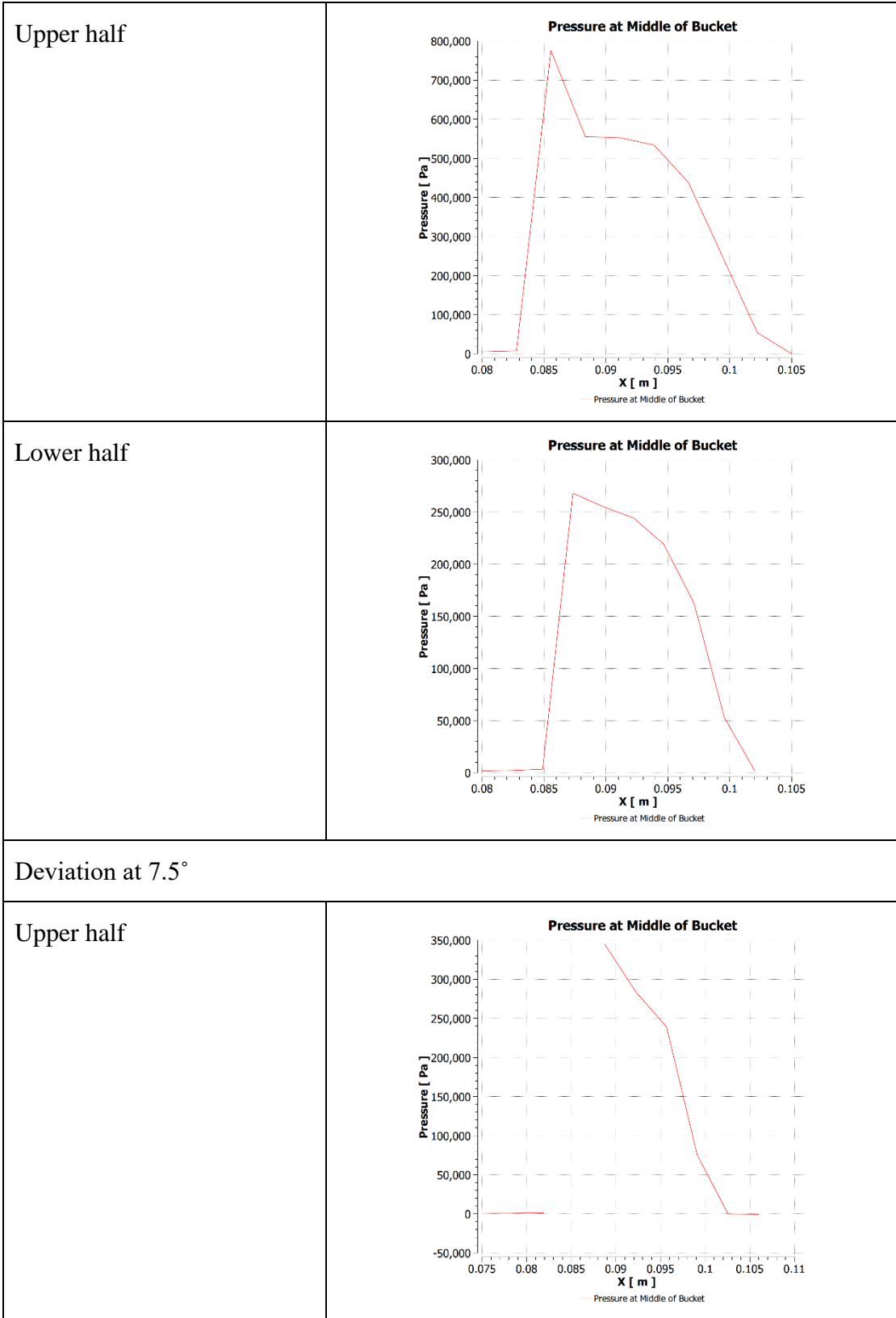


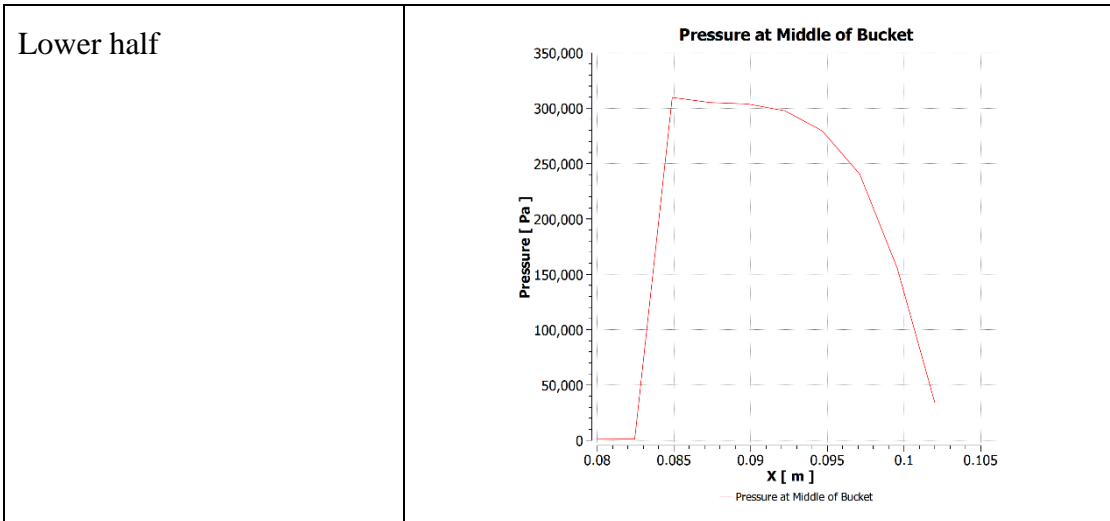
As shown in Table 4.12 the maximum velocity among all the angular deviation profiles at different positions in middle of bucket has been recorded.

#### 4.4.7 Pressure in Middle of Bucket

Table 4.13: Pressure profile of different angular deviations in middle of bucket

Deviation at 2.5°																			
Upper half	<p>Pressure at Middle of Bucket</p> <table border="1"> <caption>Data for Upper half, 2.5° deviation</caption> <thead> <tr> <th>x [m]</th> <th>Pressure [Pa]</th> </tr> </thead> <tbody> <tr><td>0.080</td><td>0</td></tr> <tr><td>0.085</td><td>0</td></tr> <tr><td>0.087</td><td>380,000</td></tr> <tr><td>0.088</td><td>220,000</td></tr> <tr><td>0.090</td><td>100,000</td></tr> <tr><td>0.092</td><td>20,000</td></tr> <tr><td>0.095</td><td>0</td></tr> <tr><td>0.100</td><td>0</td></tr> </tbody> </table>	x [m]	Pressure [Pa]	0.080	0	0.085	0	0.087	380,000	0.088	220,000	0.090	100,000	0.092	20,000	0.095	0	0.100	0
x [m]	Pressure [Pa]																		
0.080	0																		
0.085	0																		
0.087	380,000																		
0.088	220,000																		
0.090	100,000																		
0.092	20,000																		
0.095	0																		
0.100	0																		
Lower half	<p>Pressure at Middle of Bucket</p> <table border="1"> <caption>Data for Lower half, 2.5° deviation</caption> <thead> <tr> <th>x [m]</th> <th>Pressure [Pa]</th> </tr> </thead> <tbody> <tr><td>0.080</td><td>0</td></tr> <tr><td>0.084</td><td>0</td></tr> <tr><td>0.086</td><td>800,000</td></tr> <tr><td>0.088</td><td>350,000</td></tr> <tr><td>0.090</td><td>50,000</td></tr> <tr><td>0.092</td><td>0</td></tr> <tr><td>0.096</td><td>0</td></tr> </tbody> </table>	x [m]	Pressure [Pa]	0.080	0	0.084	0	0.086	800,000	0.088	350,000	0.090	50,000	0.092	0	0.096	0		
x [m]	Pressure [Pa]																		
0.080	0																		
0.084	0																		
0.086	800,000																		
0.088	350,000																		
0.090	50,000																		
0.092	0																		
0.096	0																		
Deviation at 5°																			

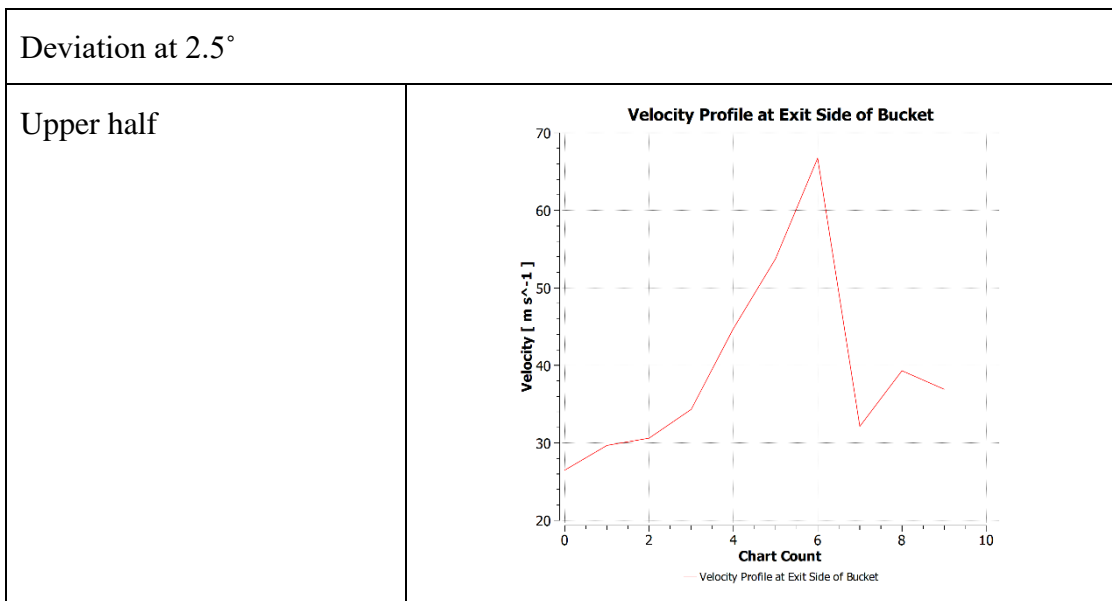




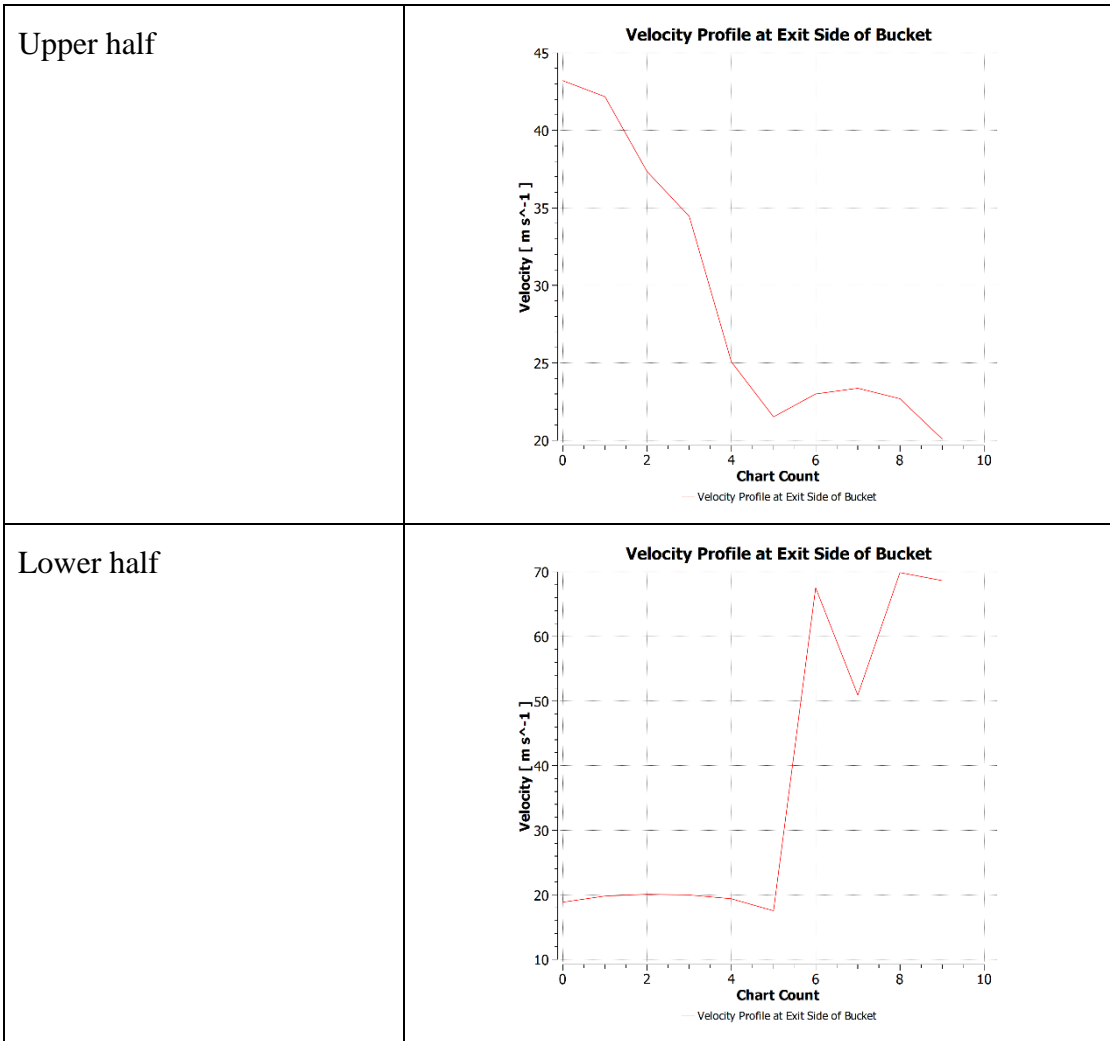
From Table 4.13 pressure at the upper half of the 5-degree angular deviation show the maximum value while other cases show more or less similar value.

#### 4.4.8 Velocity Profile at Exit Side of Bucket

Table 4.14: Velocity profile of different angular deviations at exit side of bucket



<p>Lower half</p>	<p>Velocity Profile at Exit Side of Bucket</p> <table border="1"> <thead> <tr> <th>Chart Count</th> <th>Velocity [ m s<sup>-1</sup> ]</th> </tr> </thead> <tbody> <tr><td>0</td><td>35</td></tr> <tr><td>1</td><td>45</td></tr> <tr><td>2</td><td>25</td></tr> <tr><td>3</td><td>25</td></tr> <tr><td>4</td><td>25</td></tr> <tr><td>5</td><td>23</td></tr> <tr><td>6</td><td>22</td></tr> <tr><td>7</td><td>22</td></tr> <tr><td>8</td><td>32</td></tr> <tr><td>9</td><td>33</td></tr> <tr><td>10</td><td>34</td></tr> </tbody> </table>	Chart Count	Velocity [ m s <sup>-1</sup> ]	0	35	1	45	2	25	3	25	4	25	5	23	6	22	7	22	8	32	9	33	10	34
Chart Count	Velocity [ m s <sup>-1</sup> ]																								
0	35																								
1	45																								
2	25																								
3	25																								
4	25																								
5	23																								
6	22																								
7	22																								
8	32																								
9	33																								
10	34																								
<p>Deviation at 5°</p>																									
<p>Upper half</p>	<p>Velocity Profile at Exit Side of Bucket</p> <table border="1"> <thead> <tr> <th>Chart Count</th> <th>Velocity [ m s<sup>-1</sup> ]</th> </tr> </thead> <tbody> <tr><td>0</td><td>30</td></tr> <tr><td>1</td><td>25</td></tr> <tr><td>2</td><td>30</td></tr> <tr><td>3</td><td>35</td></tr> <tr><td>4</td><td>35</td></tr> <tr><td>5</td><td>35</td></tr> <tr><td>6</td><td>33</td></tr> <tr><td>7</td><td>35</td></tr> <tr><td>8</td><td>55</td></tr> <tr><td>9</td><td>130</td></tr> <tr><td>10</td><td>130</td></tr> </tbody> </table>	Chart Count	Velocity [ m s <sup>-1</sup> ]	0	30	1	25	2	30	3	35	4	35	5	35	6	33	7	35	8	55	9	130	10	130
Chart Count	Velocity [ m s <sup>-1</sup> ]																								
0	30																								
1	25																								
2	30																								
3	35																								
4	35																								
5	35																								
6	33																								
7	35																								
8	55																								
9	130																								
10	130																								
<p>Lower half</p>	<p>Velocity Profile at Exit Side of Bucket</p> <table border="1"> <thead> <tr> <th>Chart Count</th> <th>Velocity [ m s<sup>-1</sup> ]</th> </tr> </thead> <tbody> <tr><td>0</td><td>20</td></tr> <tr><td>1</td><td>20</td></tr> <tr><td>2</td><td>22</td></tr> <tr><td>3</td><td>25</td></tr> <tr><td>4</td><td>25</td></tr> <tr><td>5</td><td>125</td></tr> <tr><td>6</td><td>50</td></tr> <tr><td>7</td><td>115</td></tr> <tr><td>8</td><td>115</td></tr> <tr><td>9</td><td>110</td></tr> <tr><td>10</td><td>110</td></tr> </tbody> </table>	Chart Count	Velocity [ m s <sup>-1</sup> ]	0	20	1	20	2	22	3	25	4	25	5	125	6	50	7	115	8	115	9	110	10	110
Chart Count	Velocity [ m s <sup>-1</sup> ]																								
0	20																								
1	20																								
2	22																								
3	25																								
4	25																								
5	125																								
6	50																								
7	115																								
8	115																								
9	110																								
10	110																								
<p>Deviation at 7.5°</p>																									



As shown in Table 4.14 the recorded velocity profile at different deviation angle values lies in the same range but the upper half profile of 7.5 degrees shows the maximum value among all the cases on the exit side.

#### 4.4.9 Pressure Profile at Exit Side of Bucket

Table 4.15: Pressure profile of different angular deviations at exit side of bucket

Deviation at 2.5°																									
Upper half	<p><b>Pressure Profile at Exit Side of Bucket</b></p> <table border="1"> <caption>Data for Upper half, 2.5° deviation</caption> <thead> <tr> <th>Chart Count</th> <th>Pressure [Pa]</th> </tr> </thead> <tbody> <tr><td>0</td><td>0</td></tr> <tr><td>1</td><td>-5,000</td></tr> <tr><td>2</td><td>0</td></tr> <tr><td>3</td><td>42,000</td></tr> <tr><td>4</td><td>16,000</td></tr> <tr><td>5</td><td>13,000</td></tr> <tr><td>6</td><td>8,000</td></tr> <tr><td>7</td><td>2,000</td></tr> <tr><td>8</td><td>1,000</td></tr> <tr><td>9</td><td>1,000</td></tr> <tr><td>10</td><td>1,000</td></tr> </tbody> </table>	Chart Count	Pressure [Pa]	0	0	1	-5,000	2	0	3	42,000	4	16,000	5	13,000	6	8,000	7	2,000	8	1,000	9	1,000	10	1,000
Chart Count	Pressure [Pa]																								
0	0																								
1	-5,000																								
2	0																								
3	42,000																								
4	16,000																								
5	13,000																								
6	8,000																								
7	2,000																								
8	1,000																								
9	1,000																								
10	1,000																								
Lower half	<p><b>Pressure Profile at Exit Side of Bucket</b></p> <table border="1"> <caption>Data for Lower half, 2.5° deviation</caption> <thead> <tr> <th>Chart Count</th> <th>Pressure [Pa]</th> </tr> </thead> <tbody> <tr><td>0</td><td>0</td></tr> <tr><td>1</td><td>0</td></tr> <tr><td>2</td><td>0</td></tr> <tr><td>3</td><td>2,000</td></tr> <tr><td>4</td><td>12,000</td></tr> <tr><td>5</td><td>25,000</td></tr> <tr><td>6</td><td>37,000</td></tr> <tr><td>7</td><td>-2,000</td></tr> <tr><td>8</td><td>0</td></tr> <tr><td>9</td><td>0</td></tr> <tr><td>10</td><td>0</td></tr> </tbody> </table>	Chart Count	Pressure [Pa]	0	0	1	0	2	0	3	2,000	4	12,000	5	25,000	6	37,000	7	-2,000	8	0	9	0	10	0
Chart Count	Pressure [Pa]																								
0	0																								
1	0																								
2	0																								
3	2,000																								
4	12,000																								
5	25,000																								
6	37,000																								
7	-2,000																								
8	0																								
9	0																								
10	0																								
Deviation at 5°																									

Upper half	<p style="text-align: center;"><b>Pressure Profile at Exit Side of Bucket</b></p> <p style="text-align: center;">— Pressure Profile at Exit Side of Bucket</p>
Lower half	<p style="text-align: center;"><b>Pressure Profile at Exit Side of Bucket</b></p> <p style="text-align: center;">— Pressure Profile at Exit Side of Bucket</p>
Deviation at 7.5°	
Upper half	<p style="text-align: center;"><b>Pressure Profile at Exit Side of Bucket</b></p> <p style="text-align: center;">— Pressure Profile at Exit Side of Bucket</p>



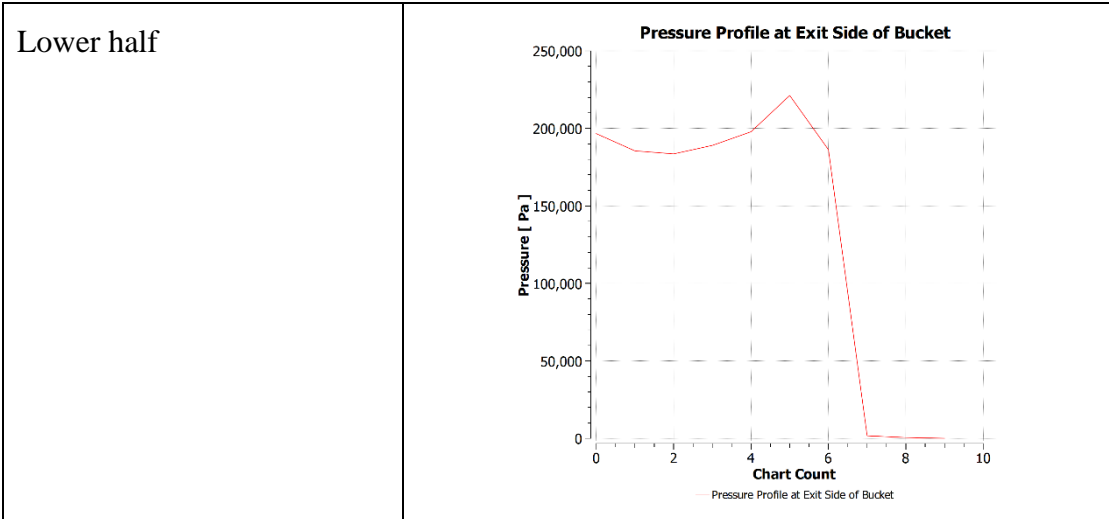
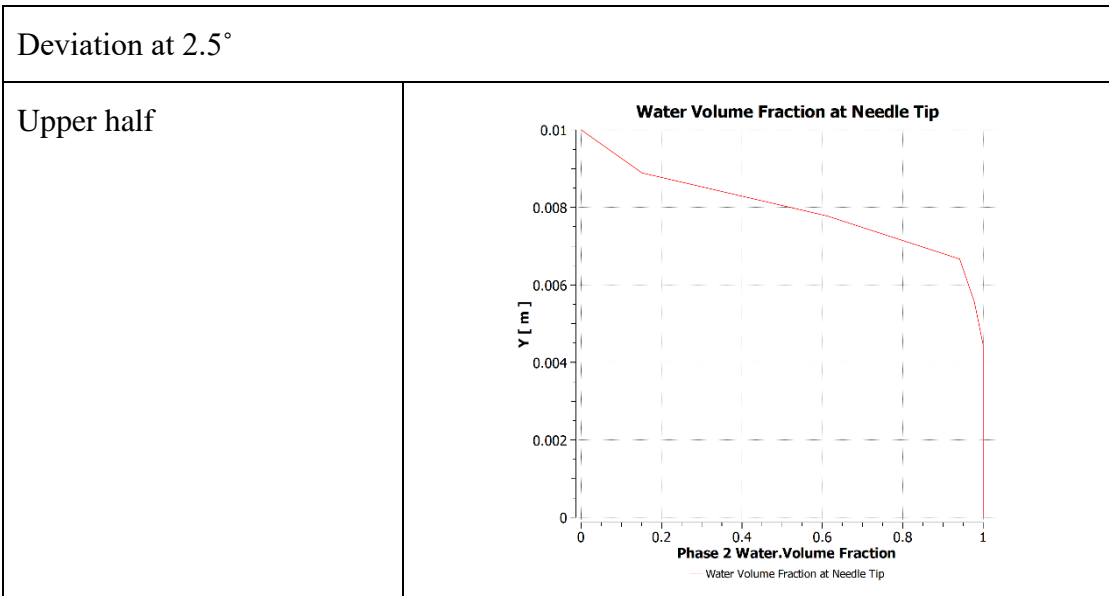
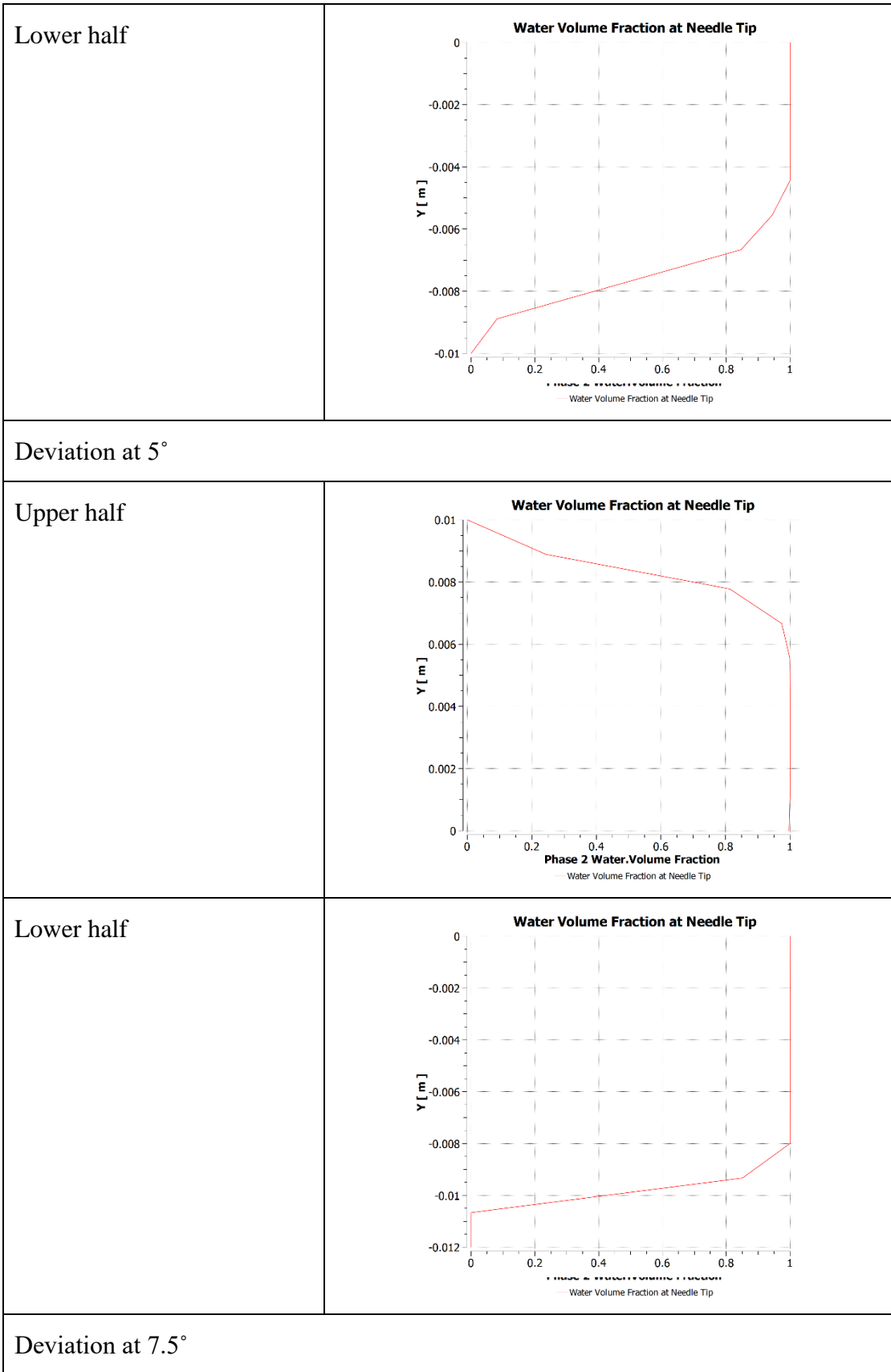


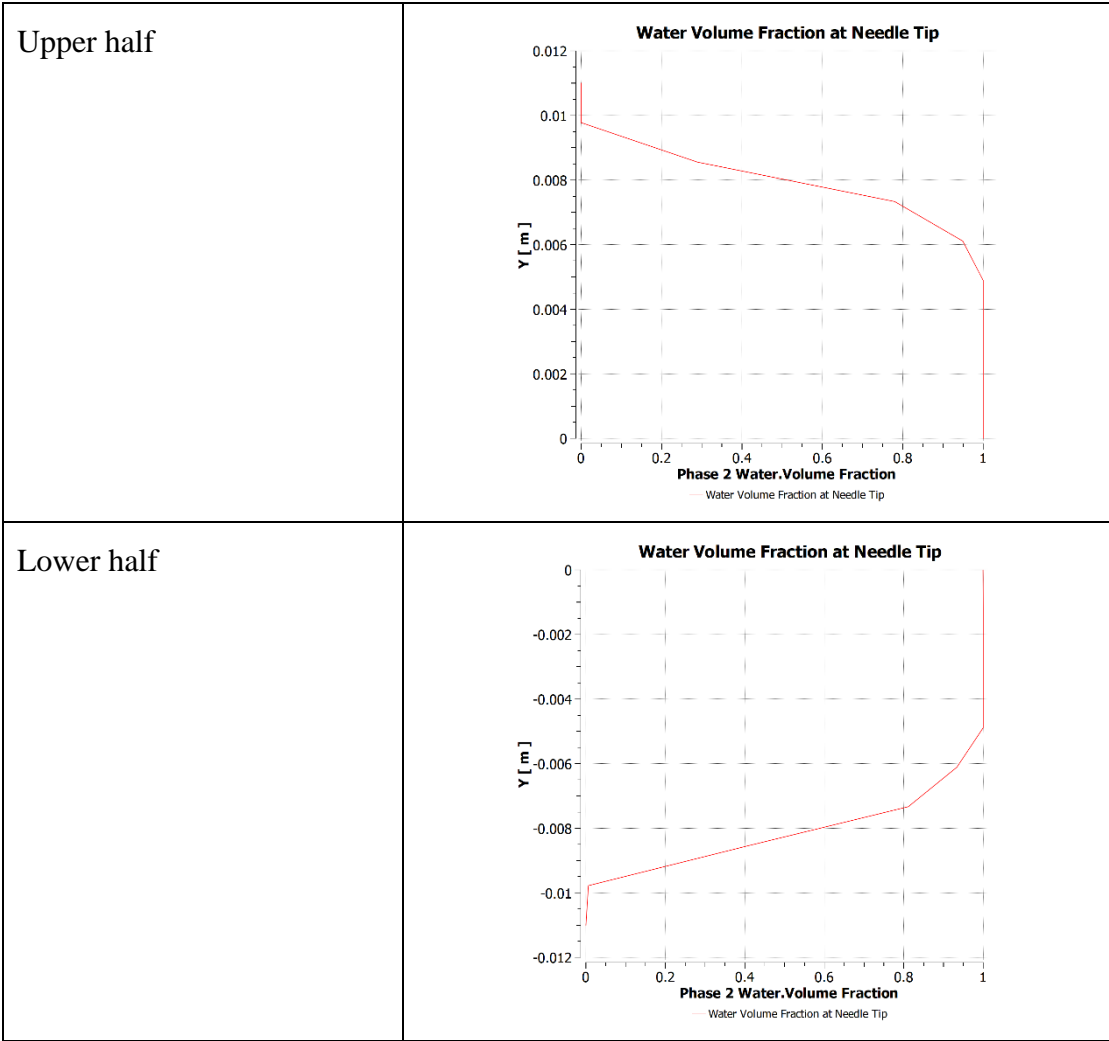
Table 4.15 show the pressure profile at exit side of bucket. The pressure at the beginning of the chart count obtains a similar value i.e. zero whereas the lower half profile of 7.5 degrees shows the maximum value at the beginning of the chart count i.e. 200kPa.

#### 4.4.10 Water Volume Fraction at Needle Tip

Table 4.16: Water volume fraction of different angular deviations at needle tip





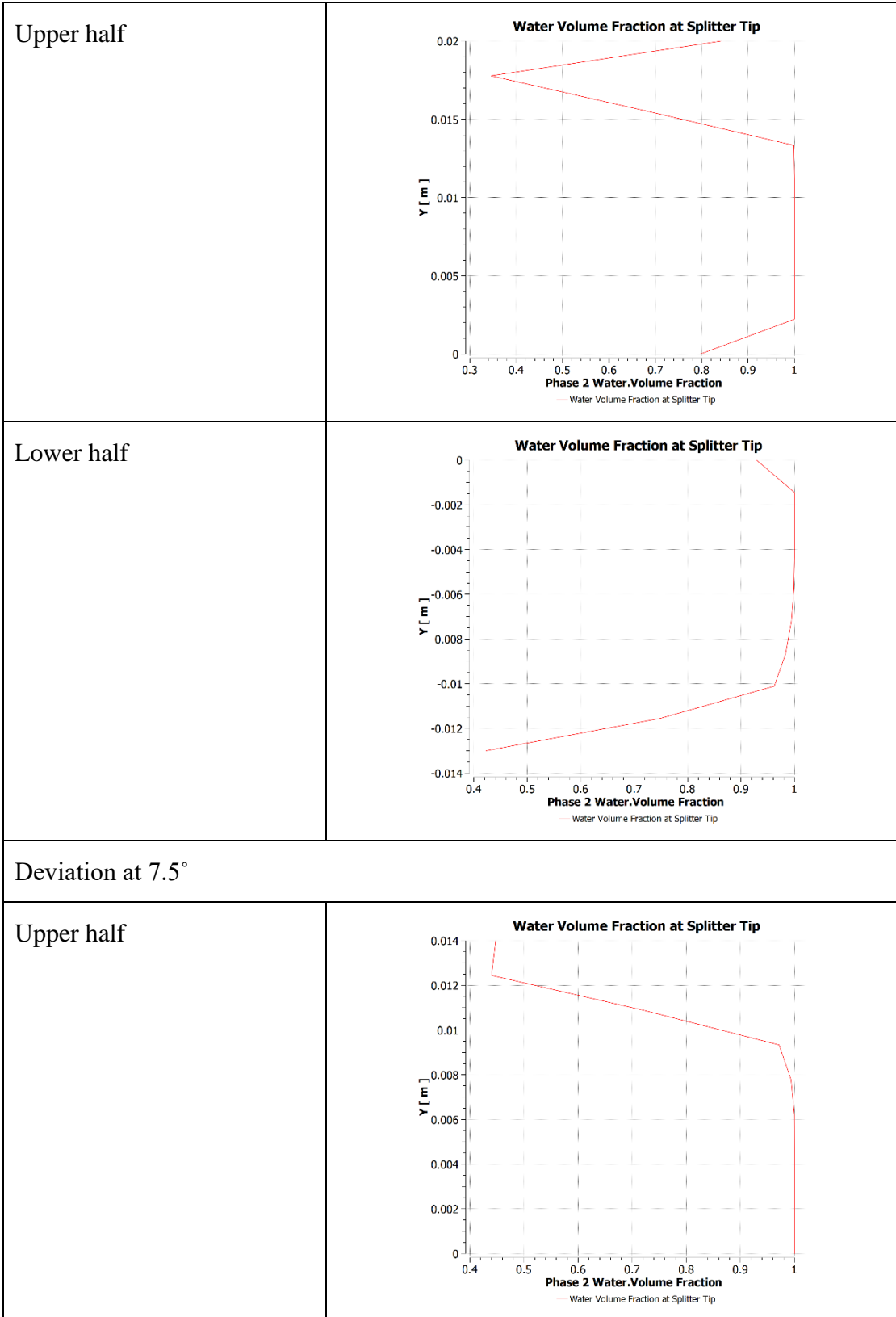


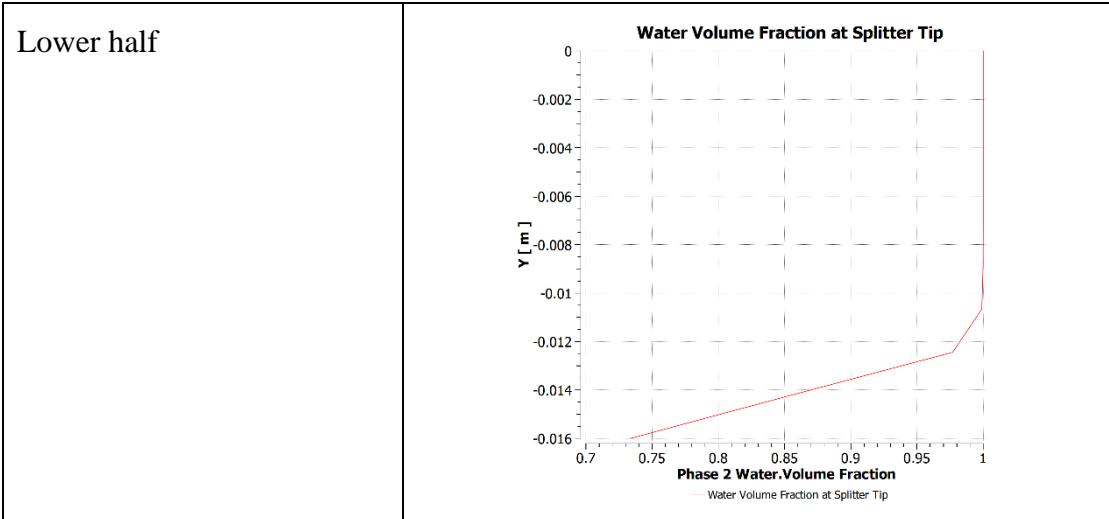
As shown in Table 4.16 the water volume fraction at needle tip of the different angular deviation shows the tentative similar value of water sheet thickness in the lower and upper half. Which shows that the flow simulation is going in the right way.

#### 4.4.11 Water Volume Fraction at Splitter Tip

Table 4.17: Water volume fraction of different angular deviation at splitter tip

Deviation at 2.5°	
Upper half	<p>Water Volume Fraction at Splitter Tip</p> <p>Y [m]</p> <p>Phase 2 Water.Volume Fraction</p> <p>Water Volume Fraction at Splitter Tip</p>
Lower half	<p>Water Volume Fraction at Splitter Tip</p> <p>Y [m]</p> <p>Phase 2 Water.Volume Fraction</p> <p>Water Volume Fraction at Splitter Tip</p>
Deviation at 5°	

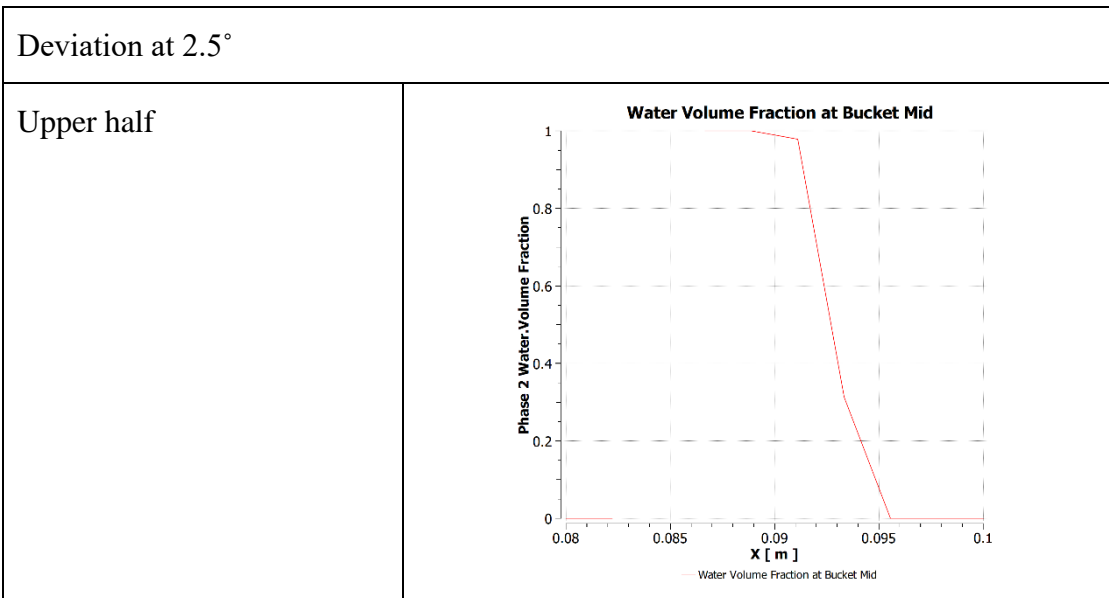




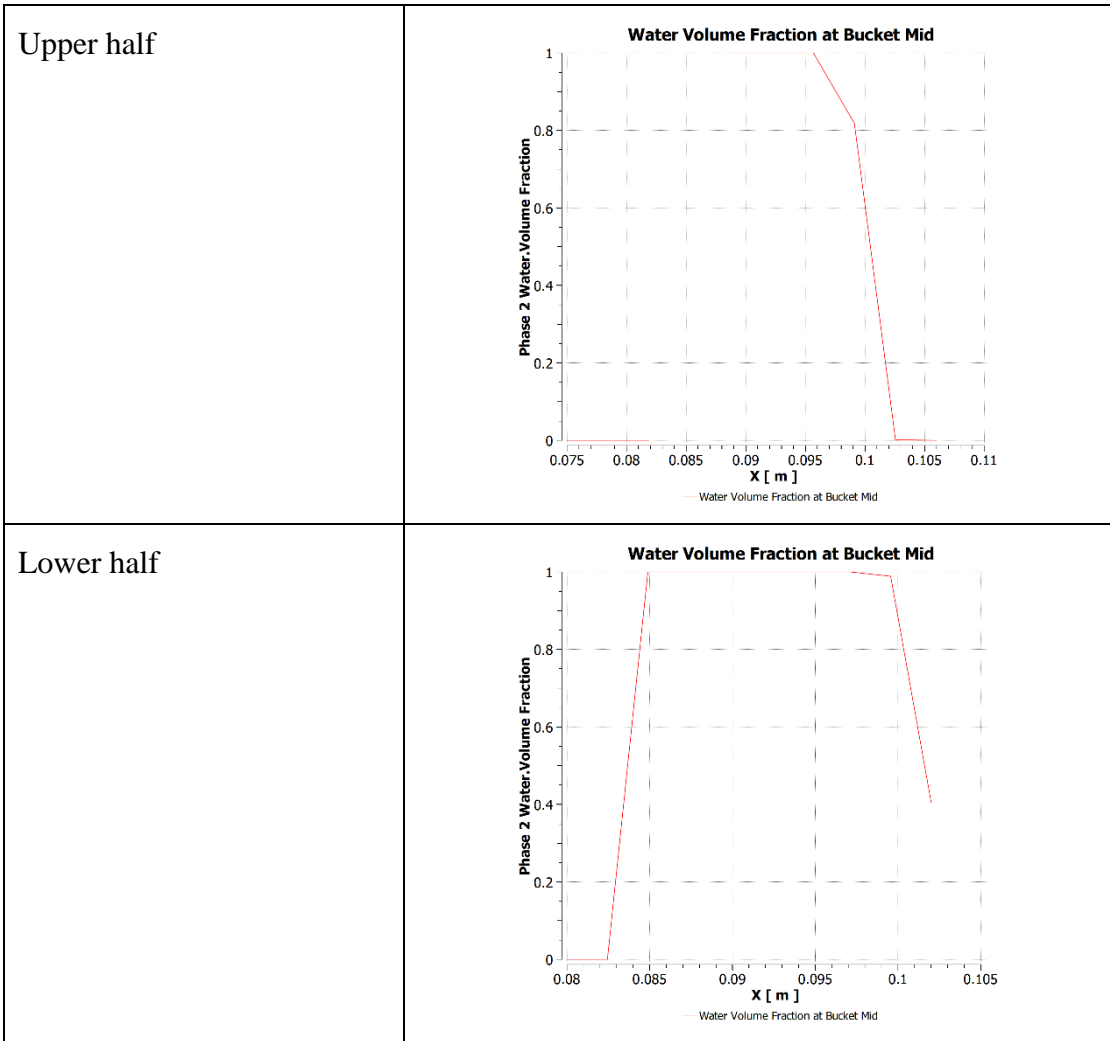
From Table 4.17 the water sheet thickness in the 2.5 degrees upper half and the lower half value get decreases from the value obtained at needle tip whereas the water sheet thickness value increases for the other two cases from the water sheet thickness at needle tip

#### 4.4.12 Water Volume Fraction at Middle of bucket

Table 4.18: Water volume fraction of different angular deviation at Middle of bucket



Lower half	<p style="text-align: center;"><b>Water Volume Fraction at Bucket Mid</b></p> <p style="text-align: center;">Phase 2 Water Volume Fraction</p> <p style="text-align: center;">x [ m ]</p> <p style="text-align: center;">— Water Volume Fraction at Bucket Mid</p>
Deviation at 5°	
Upper half	<p style="text-align: center;"><b>Water Volume Fraction at Bucket Mid</b></p> <p style="text-align: center;">Phase 2 Water Volume Fraction</p> <p style="text-align: center;">x [ m ]</p> <p style="text-align: center;">— Water Volume Fraction at Bucket Mid</p>
Lower half	<p style="text-align: center;"><b>Water Volume Fraction at Bucket Mid</b></p> <p style="text-align: center;">Phase 2 Water Volume Fraction</p> <p style="text-align: center;">x [ m ]</p> <p style="text-align: center;">— Water Volume Fraction at Bucket Mid</p>
Deviation at 7.5°	



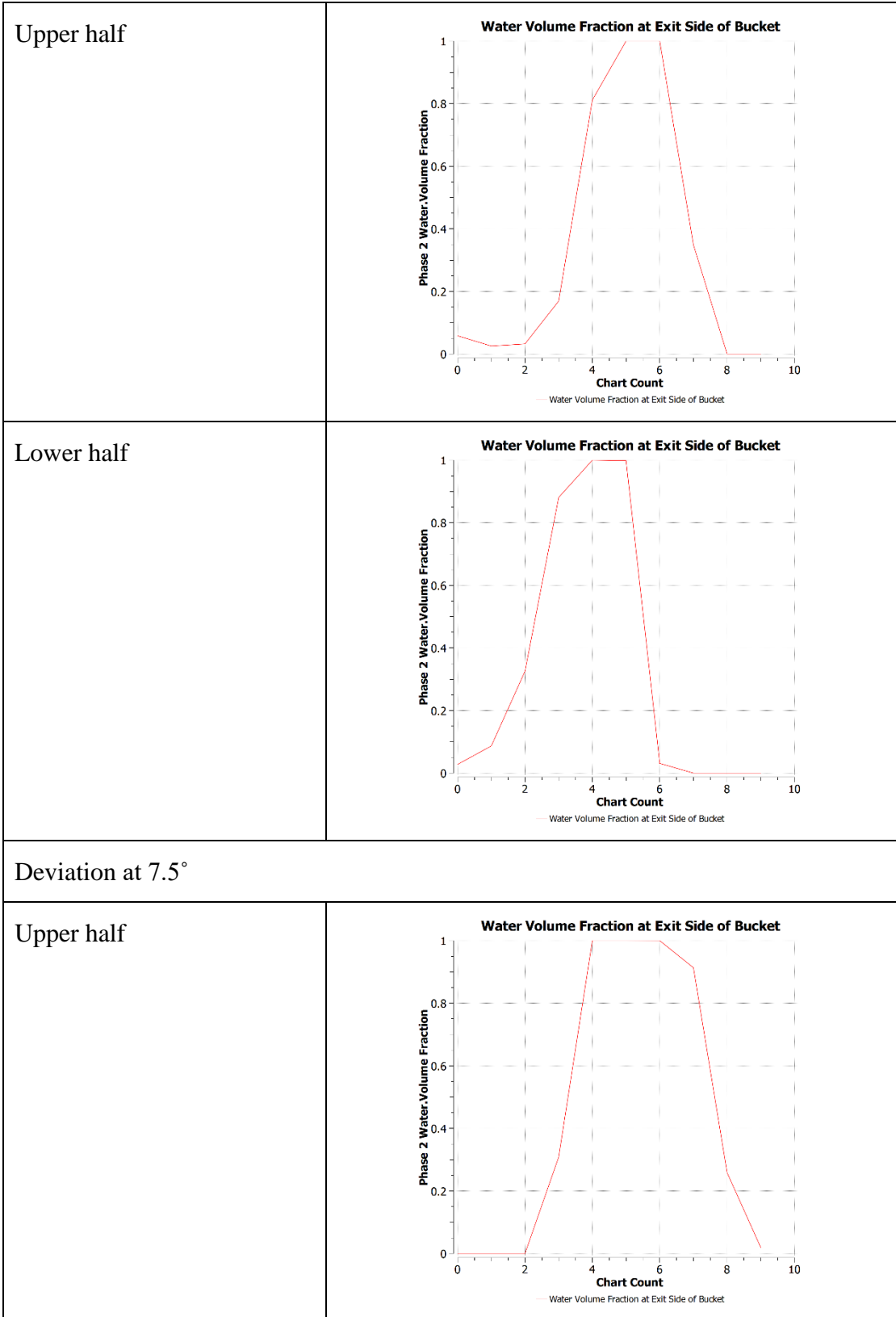
From Table 4.18 the recorded value of the water volume fraction at middle of bucket is seen as the maximum value. Among all the deviation cases at the middle position of water volume fraction 5 degrees shows the highest value.

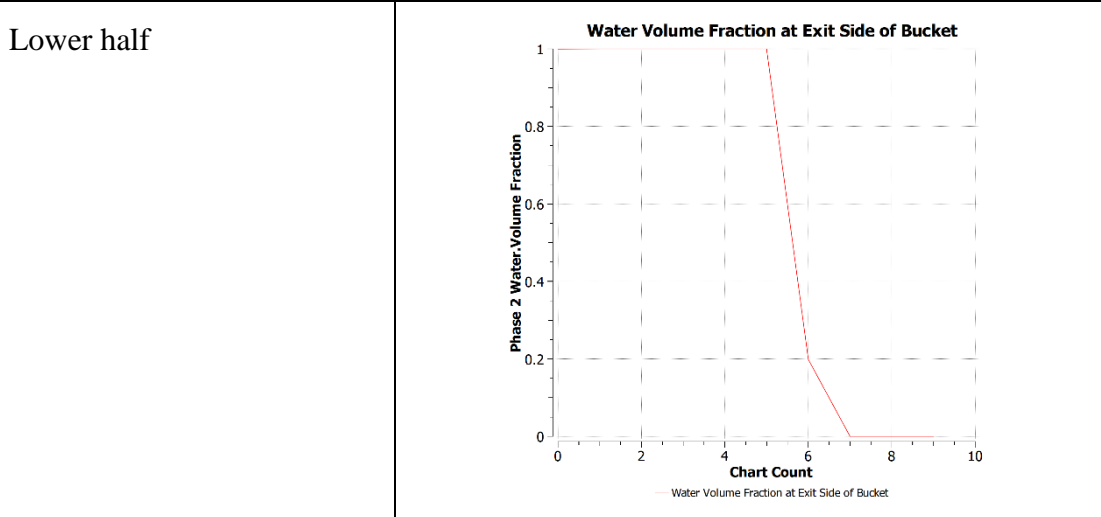


#### 4.4.13 Water Volume Fraction at Exit Side of Bucket

Table 4.19: Water volume fraction of different angular deviations at exit side of bucket

Deviation at 2.5°																									
Upper half	<p><b>Water Volume Fraction at Exit Side of Bucket</b></p> <table border="1"> <caption>Data for Upper half, 2.5° deviation</caption> <thead> <tr> <th>Chart Count</th> <th>Water Volume Fraction</th> </tr> </thead> <tbody> <tr><td>0</td><td>0.00</td></tr> <tr><td>1</td><td>0.00</td></tr> <tr><td>2</td><td>0.00</td></tr> <tr><td>3</td><td>0.00</td></tr> <tr><td>4</td><td>0.00</td></tr> <tr><td>5</td><td>1.00</td></tr> <tr><td>6</td><td>1.00</td></tr> <tr><td>7</td><td>0.35</td></tr> <tr><td>8</td><td>0.00</td></tr> <tr><td>9</td><td>0.00</td></tr> <tr><td>10</td><td>0.00</td></tr> </tbody> </table>	Chart Count	Water Volume Fraction	0	0.00	1	0.00	2	0.00	3	0.00	4	0.00	5	1.00	6	1.00	7	0.35	8	0.00	9	0.00	10	0.00
Chart Count	Water Volume Fraction																								
0	0.00																								
1	0.00																								
2	0.00																								
3	0.00																								
4	0.00																								
5	1.00																								
6	1.00																								
7	0.35																								
8	0.00																								
9	0.00																								
10	0.00																								
Lower half	<p><b>Water Volume Fraction at Exit Side of Bucket</b></p> <table border="1"> <caption>Data for Lower half, 2.5° deviation</caption> <thead> <tr> <th>Chart Count</th> <th>Water Volume Fraction</th> </tr> </thead> <tbody> <tr><td>0</td><td>0.00</td></tr> <tr><td>1</td><td>0.00</td></tr> <tr><td>2</td><td>0.00</td></tr> <tr><td>3</td><td>0.75</td></tr> <tr><td>4</td><td>1.00</td></tr> <tr><td>5</td><td>1.00</td></tr> <tr><td>6</td><td>1.00</td></tr> <tr><td>7</td><td>0.05</td></tr> <tr><td>8</td><td>0.00</td></tr> <tr><td>9</td><td>0.00</td></tr> <tr><td>10</td><td>0.00</td></tr> </tbody> </table>	Chart Count	Water Volume Fraction	0	0.00	1	0.00	2	0.00	3	0.75	4	1.00	5	1.00	6	1.00	7	0.05	8	0.00	9	0.00	10	0.00
Chart Count	Water Volume Fraction																								
0	0.00																								
1	0.00																								
2	0.00																								
3	0.75																								
4	1.00																								
5	1.00																								
6	1.00																								
7	0.05																								
8	0.00																								
9	0.00																								
10	0.00																								
Deviation at 5°																									





From Table 4.19 the water sheet thickness at the exit side gets thicker as the deviation of angle increases.

#### 4.4.14 Calculation of Overpressure and Flow Condition at Bucket Exit

Overpressure coefficient in the Water Sheet

##### 1. Overpressure Coefficient At 2.5° Upper

Bucket thickness = 1.001 mm (from geometry)

Water sheet thickness at exit = 1.5 mm

water-sheet height (h)= 1.001+1.5=2.501mm

$$c_p = 2 * (1 - 0.47)^2 \frac{2.501}{0.55 * 16.54475}$$

$$= 0.1544$$

##### 2. Overpressure Coefficient At 2.5° Lower

Water sheet thickness at exit = 3 mm

Water-sheet height (h) = 1.001+3=4.001mm

$$c_p = 2 * (1 - 0.47)^2 \frac{4.001}{0.55 * 16.54475}$$

$$= 0.247$$

##### 3. Overpressure Coefficient At 5° Upper

Water sheet thickness at exit = 1 mm

water-sheet height (h)= 1.001+1=2.001mm

$$c_p = 2 * (1 - 0.47)^2 \frac{2.001}{0.55 * 16.54475}$$
$$=0.1235$$

#### **4. Overpressure Coefficient At 5° Lower**

Water sheet thickness at exit = 0.95 mm

water-sheet height (h)= 1.001+0.95=1.951mm

$$c_p = 2 * (1 - 0.47)^2 \frac{1.951}{0.55 * 16.54475}$$
$$=0.1204$$

#### **5. Overpressure Coefficient At 7° Upper**

Water sheet thickness at exit = 2 mm

Water-sheet height (h) = 1.001+2=3.001mm

$$c_p = 2 * (1 - 0.47)^2 \frac{3.001}{0.55 * 16.54475}$$
$$=0.1853$$

#### **6. Overpressure Coefficient At 7° Lower**

Water sheet thickness at exit = 4 mm

Water-sheet height (h) = 1.001+4=5.001mm

$$c_p = 2 * (1 - 0.47)^2 \frac{5.001}{0.55 * 16.54475}$$
$$=0.3087$$

In the Table 4.20 shows the calculation of different condition overpressure coefficient in which the 7.5 degree shows the maximum value among all the cases. Due to the changes in the flow direction pressure in-between the bucket and water sheet increases.

Table 4.20: Overpressure coefficient value at different angular deviation

S.N.	Deviation	Overpressure coefficient at Upper half	Overpressure coefficient at Lower half
1.	2.5°	0.1544	0.247
2.	5°	0.1235	0.1204
3.	7.5°	0.1853	0.3087

The above value of the overpressure coefficient shows the pressures variation in between the flow and bucket. The overpressure coefficient of 5 degree angular deviation show the similar value. Calculations were made for the overpressure coefficient produced in the bucket at an eccentric angle. The results were 0.1544, 0.247, 0.1235, 0.1204, 0.1853 and 0.3087 for the top and lower halves of 2.5, 5 and 7.5 degrees respectively. This suggests that eccentric installation increases bucket loading.

#### 4.5 Comparison of Flow Parameters Charts

##### 4.5.1 Velocity Profile at Needle Tip

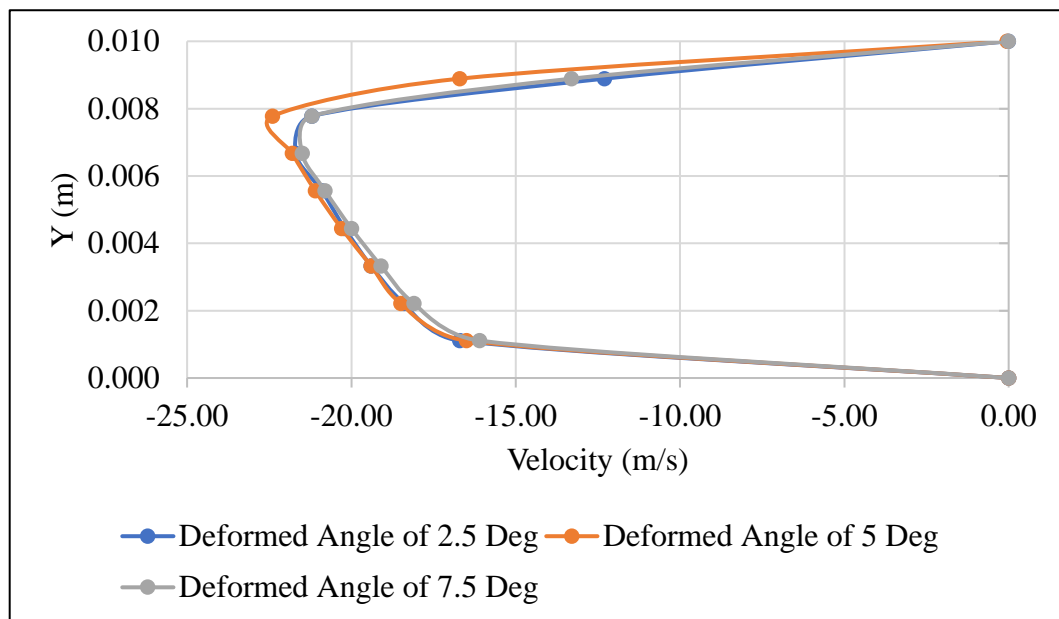


Figure 4.3: Upper half velocity of different angular deviation

Figure 4.3 shows the variation of velocity of the different angles at needle tip, the velocity change of different deformed angles seen that more or less change. The maximum velocity was obtained between the needle wall and to nozzle wall. As we see the deformed angle of 7.5 degrees, which has maximum velocity among the deflection

angle. It can be seen that the velocity at needle tip is zero, which is desired and verified with the centric condition.

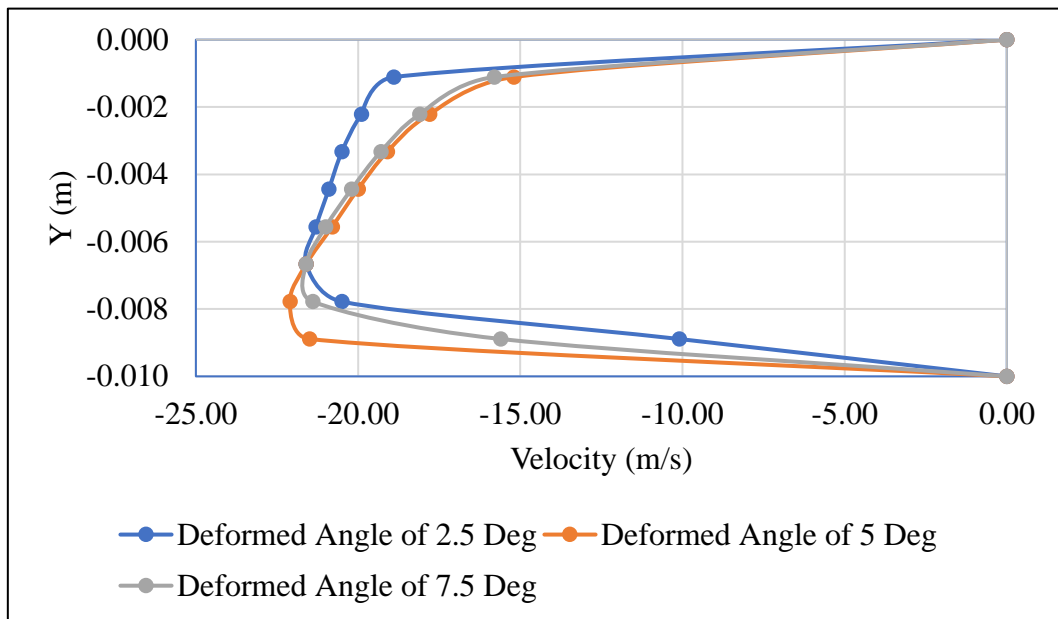


Figure 4.4 Lower half velocity of different angular deviation

Figure 4.4 shows the lower half velocity profile at needle tip, from the above figure it is seen that as the deformation angle increases velocity is slightly seen increased. At the deformation angle of 5 degrees, the maximum velocity is around 22 m/s seen.

#### 4.5.2 Pressure Profile at Needle Tip

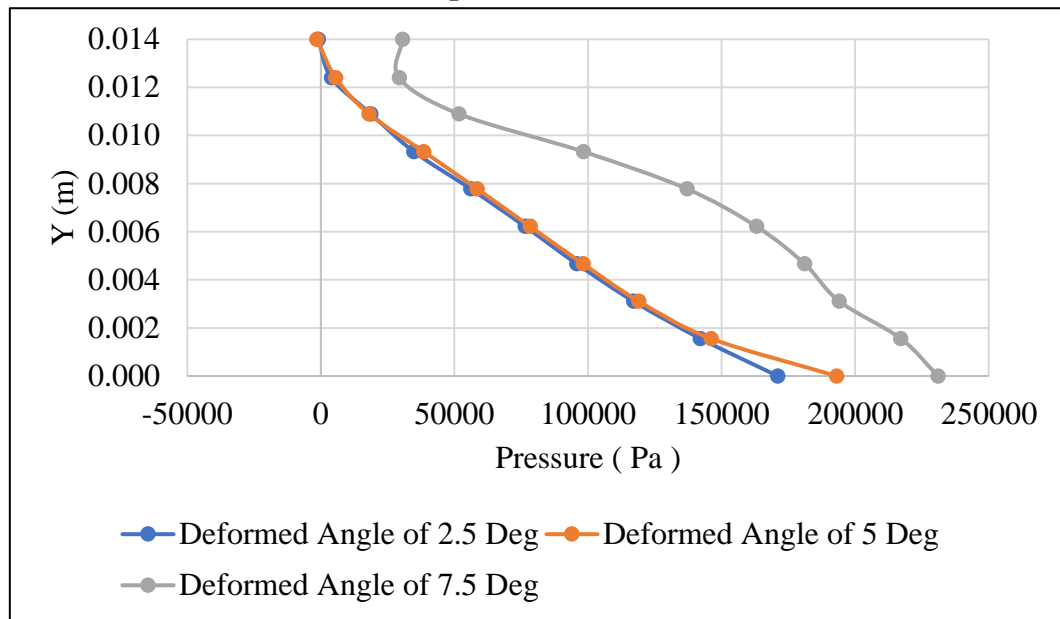


Figure 4.5: Upper half pressure variation of different angular deviation

The visualization of pressure distribution is shown in Figure 4.5 for different deformed angle. The higher pressure at needle tip is seen which validates the velocity profile at needle tip and the maximum pressure condition region obtained.

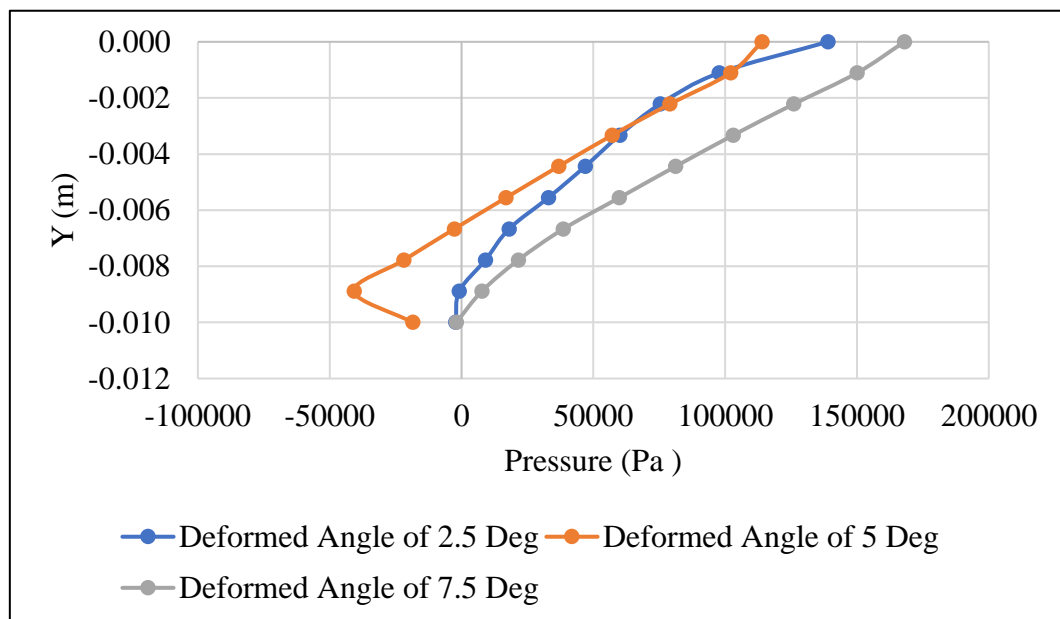


Figure 4.6: Lower half pressure variation of different angular deviation

The visualization of pressure distribution is shown in Figure 4.6 for different deformed angles. The maximum pressure was seen in the needle tip which gradually decreases as the height of water sheet increased.

### 4.5.3 Velocity Profile at Splitter Tip

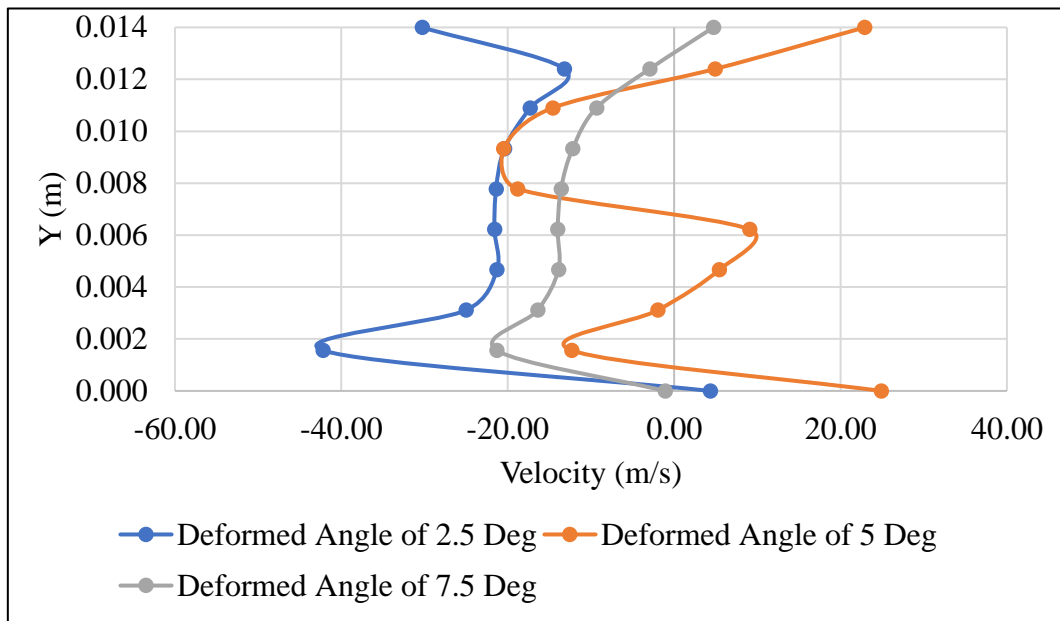


Figure 4.7: Upper half velocity variation of different angular deviation

Figure 4.7 shows the variation of velocity of the different angles at splitter tip, the velocity change of different deformed angles seen that the 2.5 degree has maximum velocity. As the water gets thick the velocity change decreases. The positive velocity at deformed angle of 7.5 degree the seen which occur due to the flow detachment.

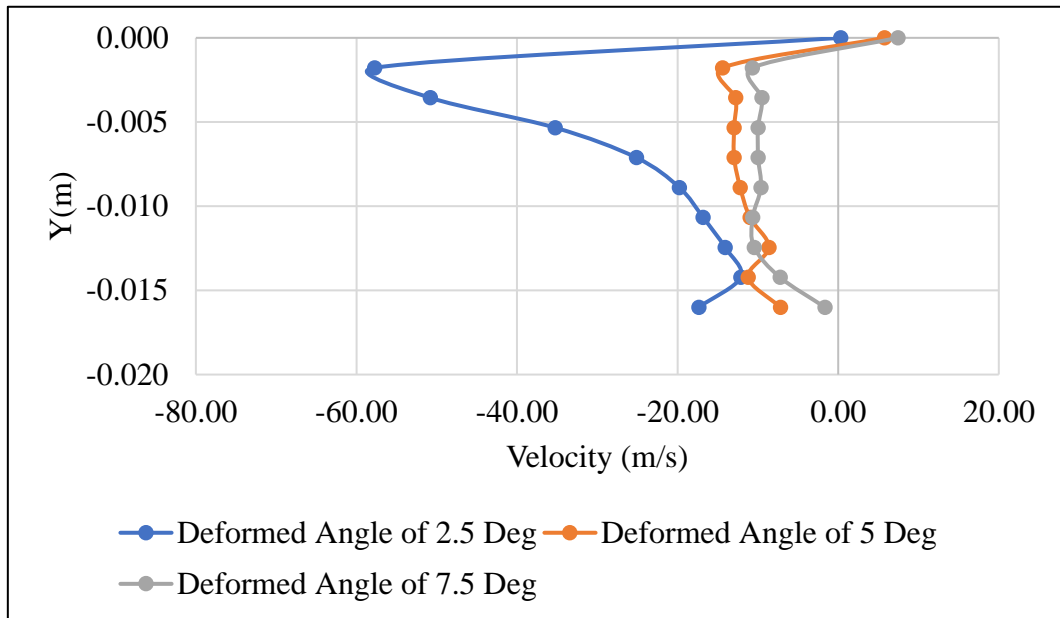


Figure 4.8: Lower half velocity variation of different angular deviation

Figure 4.8 shows the variation of velocity of the different angles at the lower half of the splitter tip, the velocity change of the deformed angle for 2.5 degrees has maximum



velocity, and 5 degrees and 7.5 degrees show a slight change. As the water sheet gets thick the velocity change decreases and tends to be zero for higher angle deflection.

#### 4.5.4 Pressure Profile at Splitter Tip

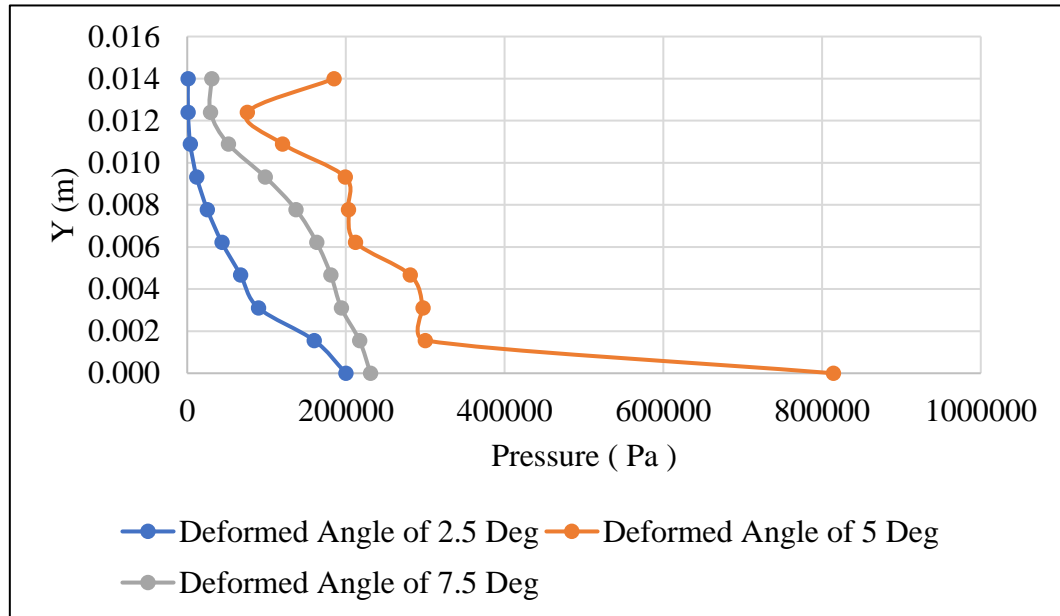


Figure 4.9: Upper half pressure variation of different angular deviation

Figure 4.9 the maximum pressure distribution of the upper half at splitter tip obtained. The pressure distribution of deformed angle 2.5 degrees and 7.5 degrees give a similar trend and more or less the same value while a deformed angle of 5 degrees has maximum alteration and give a higher value i.e 800000 Pa. As the flow gets thick the pressure distribution over height get decreases.

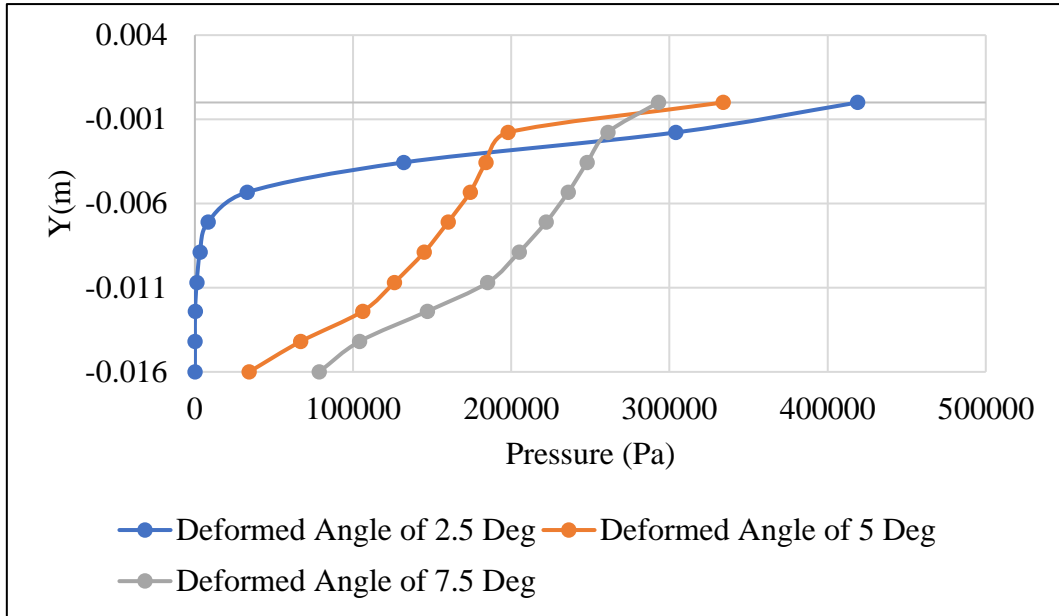


Figure 4.10: Lower half pressure variation of different angular deviation

Figure 4.10 the maximum pressure distribution of the lower half at splitter tip obtained. The pressure distribution of deformed angle 5 degrees and 7.5 degrees give more or less similar value at splitter tip i.e 300000 Pa while deformed angle 2.5 degrees have higher value i.e around 400000 Pa. As the flow gets thick the pressure distribution over height get decreases.

#### 4.5.5 Velocity Profile at Middle of Bucket

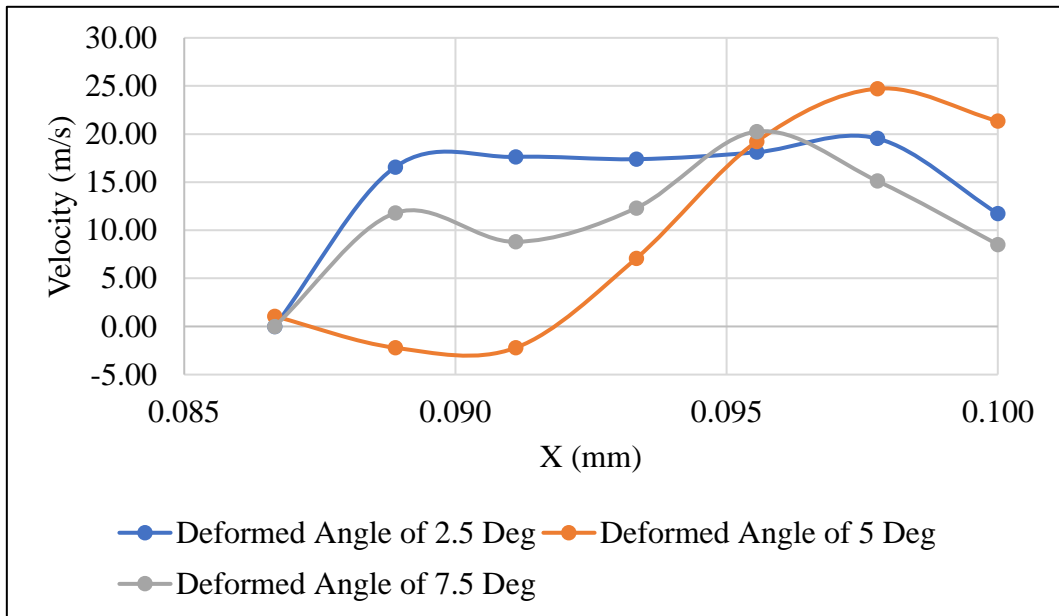


Figure 4.11: Upper half velocity variation of different angular deviation

Figure 4.11 shows the variation of velocity of a different angle of the upper half at middle of bucket, the velocity change at the bucket wall is seen as zero which is desired value. The deformed angle of 5 degrees shows the negative velocity which is due to vortex formation.

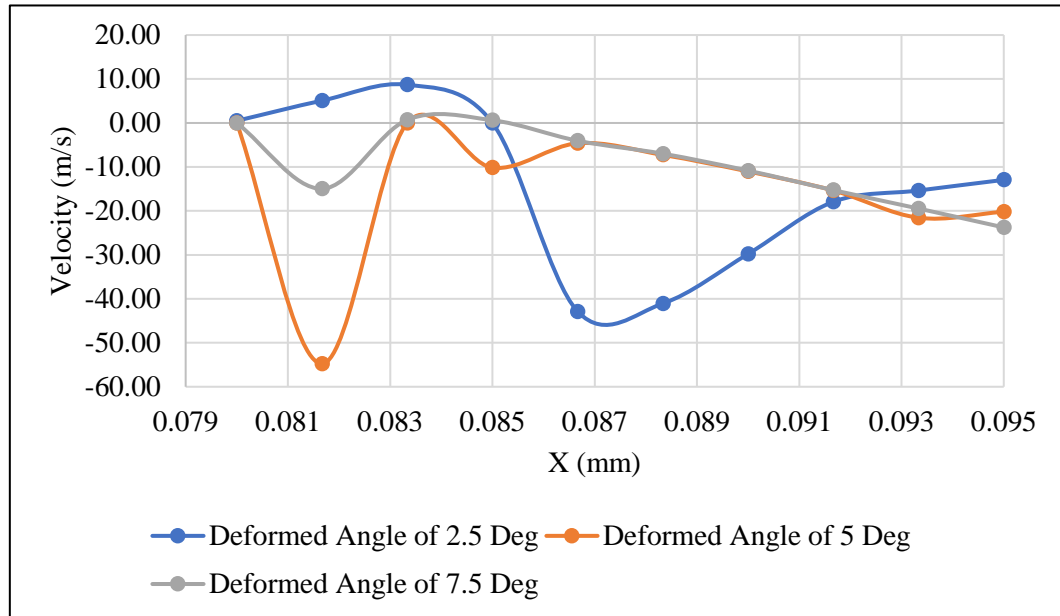


Figure 4.12 Lower half velocity variation of different angular deviation

Figure 4.12 shows the variation of velocity of a different angle of lower half at middle of bucket, the velocity change at the bucket wall is seen as zero which is desired value. The deformed angle of 2.5 degrees shows the positive velocity which is due to circulation formation. The maximum velocity 60m/s found at 5 degrees deformed angle.

#### 4.5.6 Pressure at Middle of Bucket

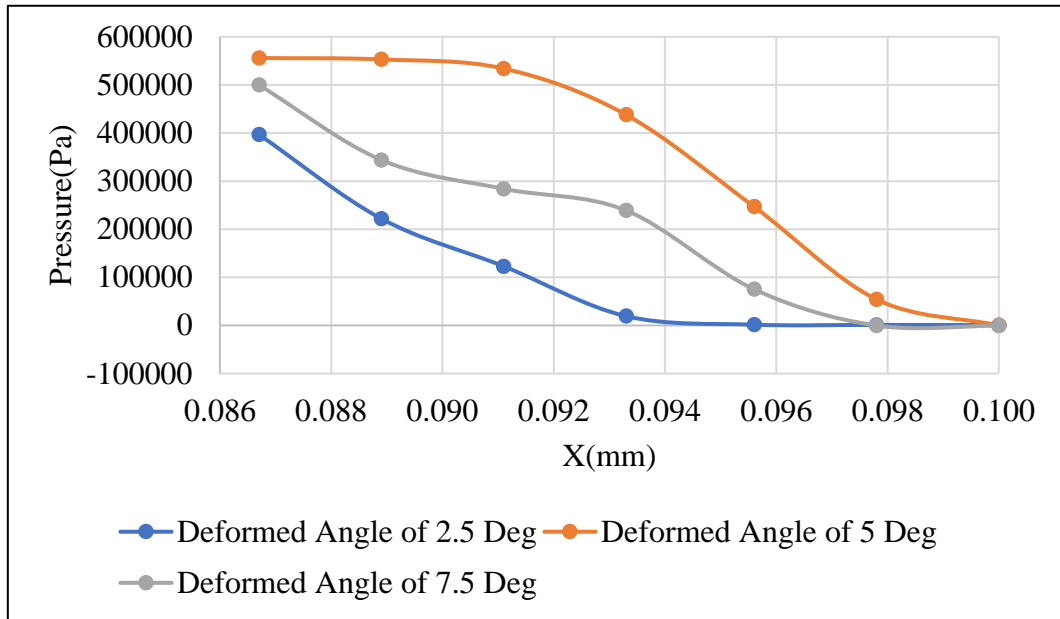


Figure 4.13: Upper half pressure variation of different angular deviation

Figure 4.13 the pressure distribution of the upper half at middle of bucket obtained. The variation in the maximum pressure at different deformed angles found a similar trend at the wall of the bucket.

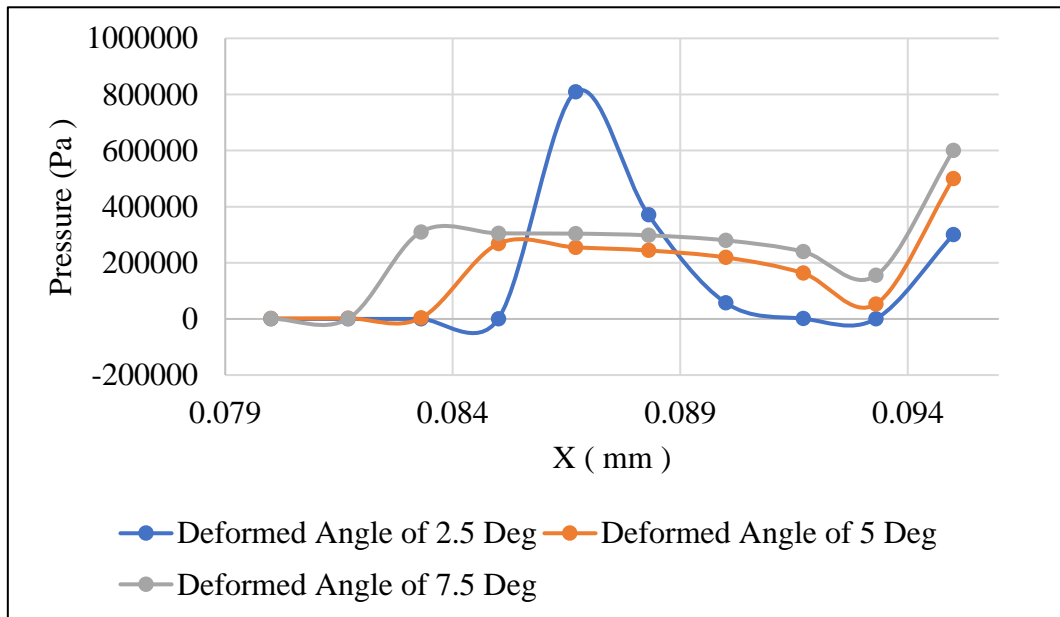


Figure 4.14: Lower half pressure variation of different angular deviation

Figure 4.14 the pressure distribution of the lower half at middle of bucket obtained. The variation in the maximum pressure at different deformed angles found a similar trend at the wall of the bucket.

#### 4.5.7 Velocity Profile at Exit Side of Bucket

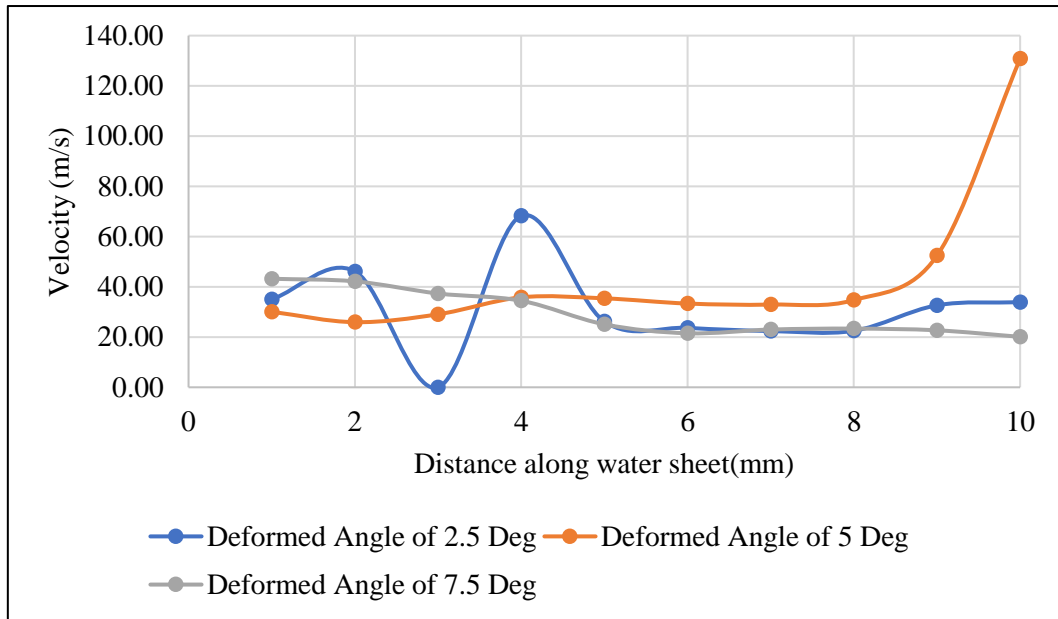


Figure 4.15: Upper half velocity variation of different angular deviation

Figure 4.15 shows the variation of velocity at a different angle of upper half at exit side of bucket. The 2.5 degree angular deviation velocity changes more after flying from the bucket and after moving 5 mm along the water sheet the velocity of 2.5 degrees and 7.5 degrees have the same value. The velocity of the 5-degree deformed angle shows the maximum value after moving away from the bucket at around 130m/s.

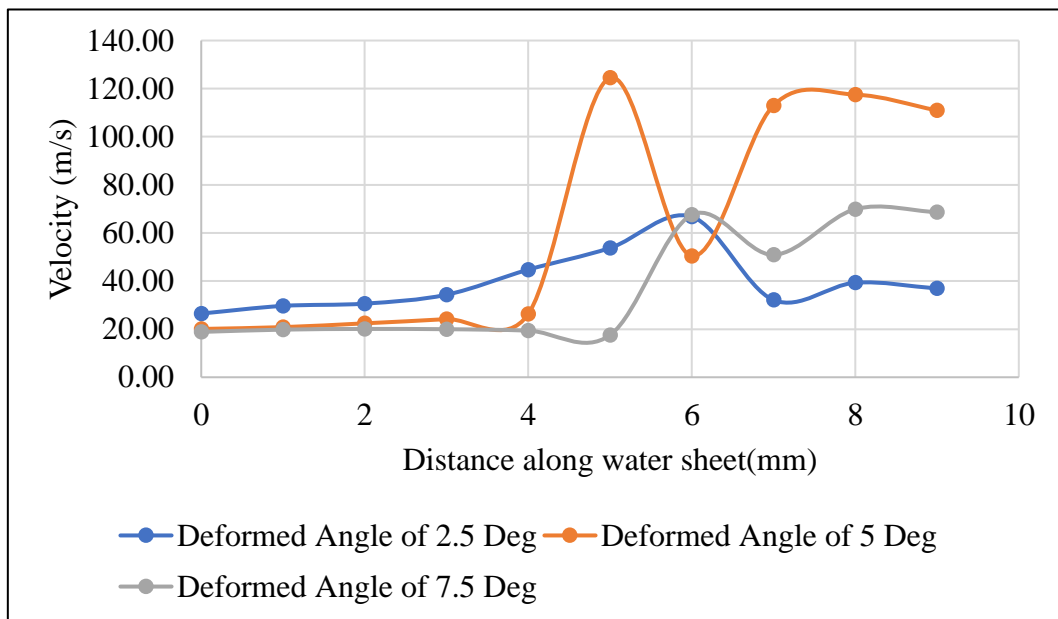


Figure 4.16: Lower half velocity variation of different angular deviation

Figure 4.16 shows the velocity at the exit profile has a similar value but after leaving the bucket the changes in the velocity vary. Maximum changes were seen in the 5 degree deformation angle.

#### 4.5.8 Pressure Profile at Exit Side of Bucket

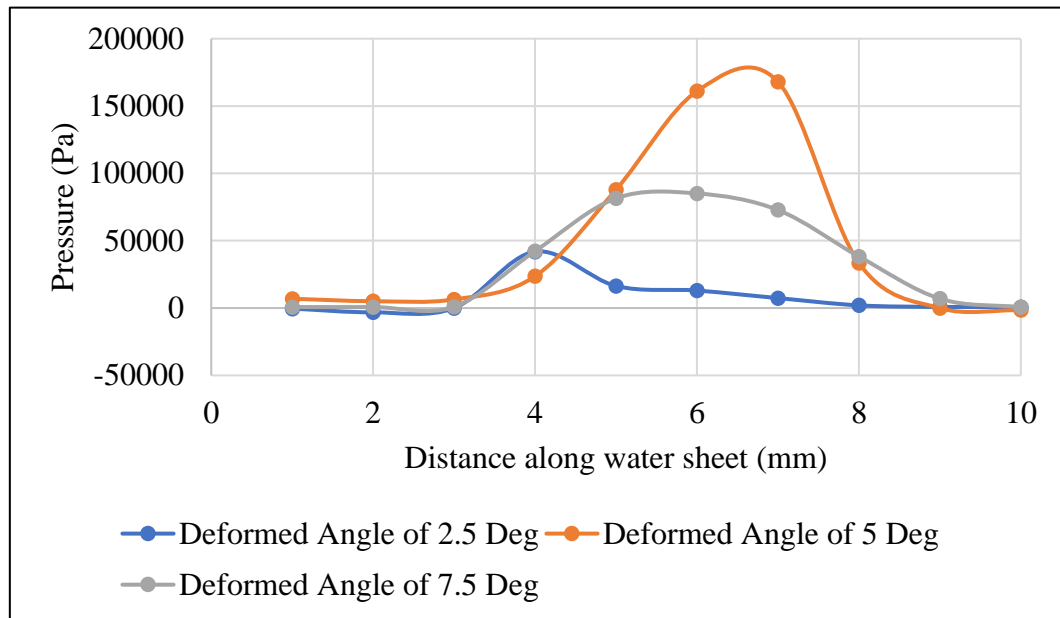


Figure 4.17: Upper half pressure variation of different angular deviation

Figure 4.17 shows the pressure variation at exit side of bucket in which the maximum pressure is represented by the 5 degree deformation angle a value has 175 kPa and the other value of the other two deviations has a more or less similar value.

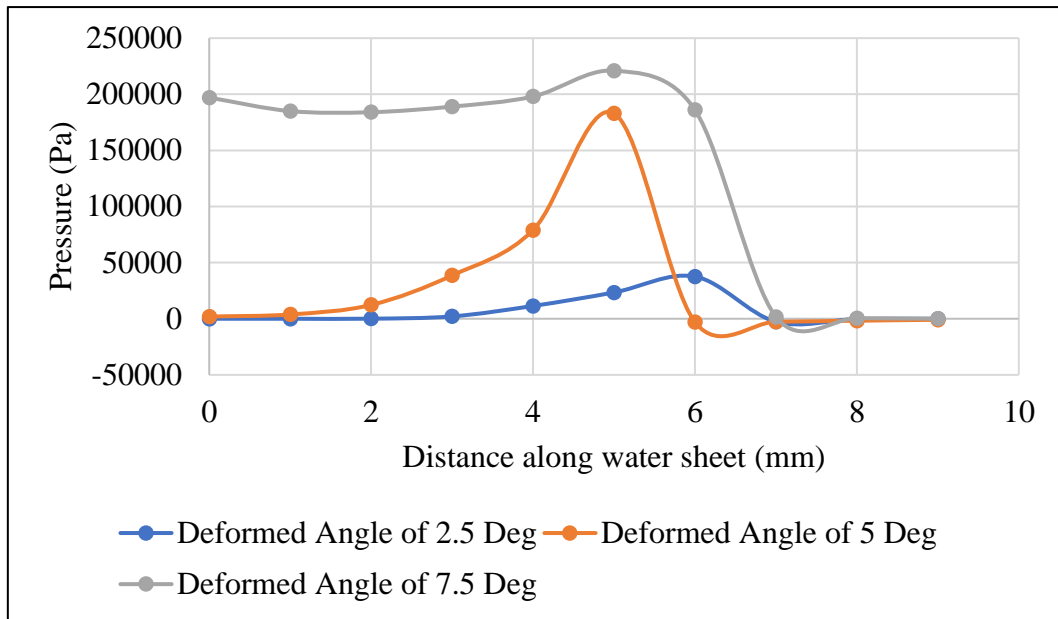


Figure 4.18: Lower half pressure variation of different angular deviation

Figure 4.18 shows that the lower half pressure profile at exit side of bucket in which the deviation angle of 2.5 degrees and 5 degrees at the beginning of flow exit show zero pressure, whereas a 7.5 degree angular deviation shows the 200kPa pressure at the beginning of exit flow. After flying away from the flow from the bucket at some distance the angular deviation of 5 degrees has a nearer value than the angular deviation of 7.5 degrees.

#### 4.5.9 Water Volume Fraction at Needle Tip

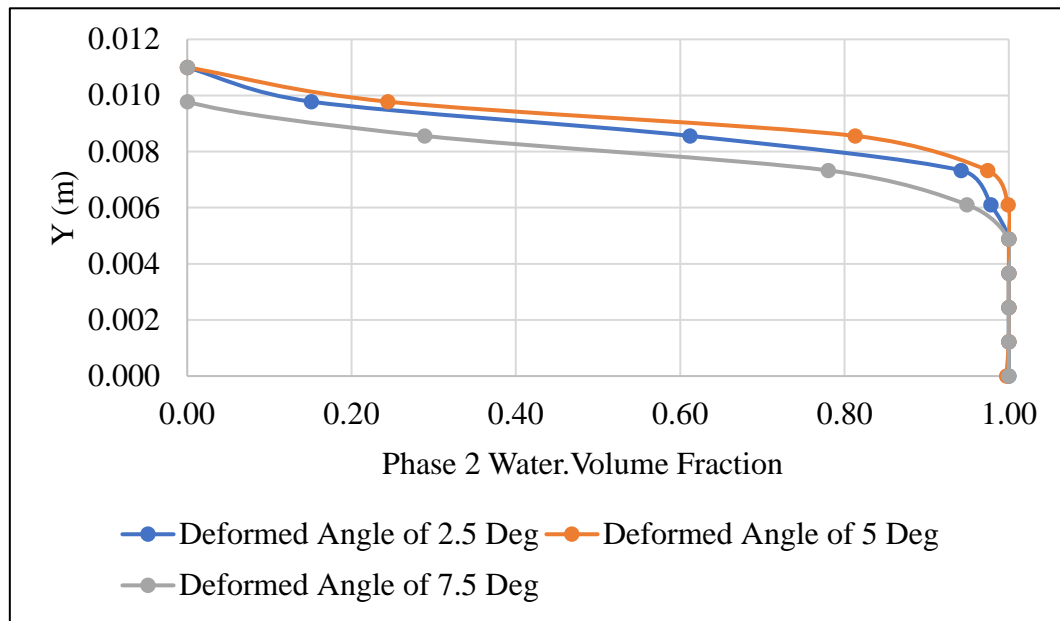


Figure 4.19: Upper half water volume fraction of different angular deviation

Figure 4.19 shows that the water sheet thickness at the upper half of the needle tip has a constant value for all the deformed angles and the value is about 5 mm.

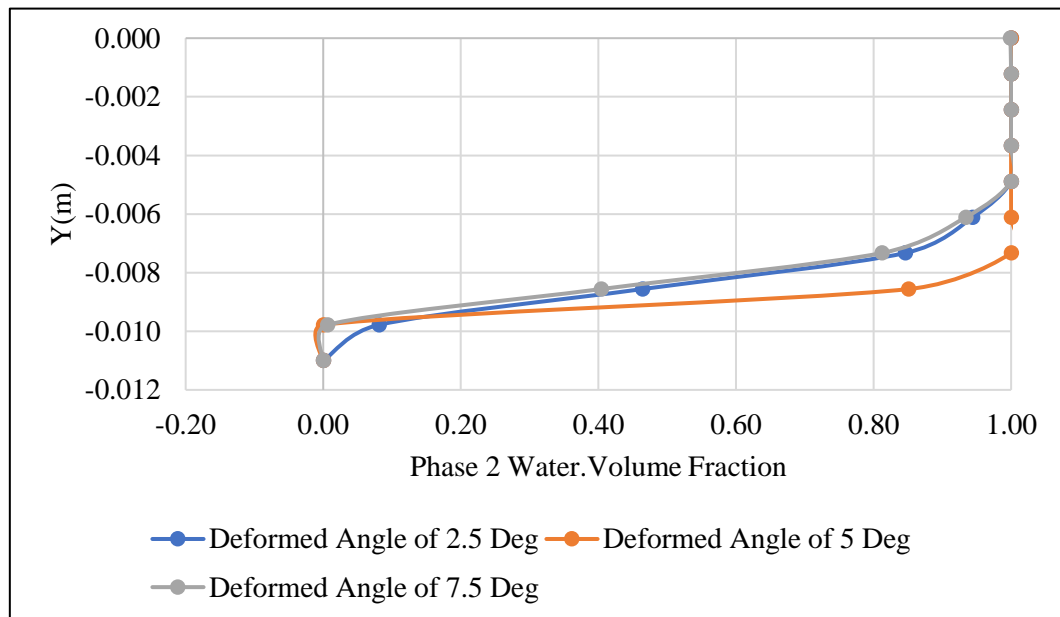


Figure 4.20: Lower half water volume fraction of different angular deviation

Figure 4.20 shows that the water sheet thickness at the lower half of the needle tip has a constant value for the deformed angles at 2.5 and 7.5 degrees and the deformed angle at 5 degrees has thicker than that of the other two values.



#### 4.5.10 Water Volume Fraction at Splitter Tip

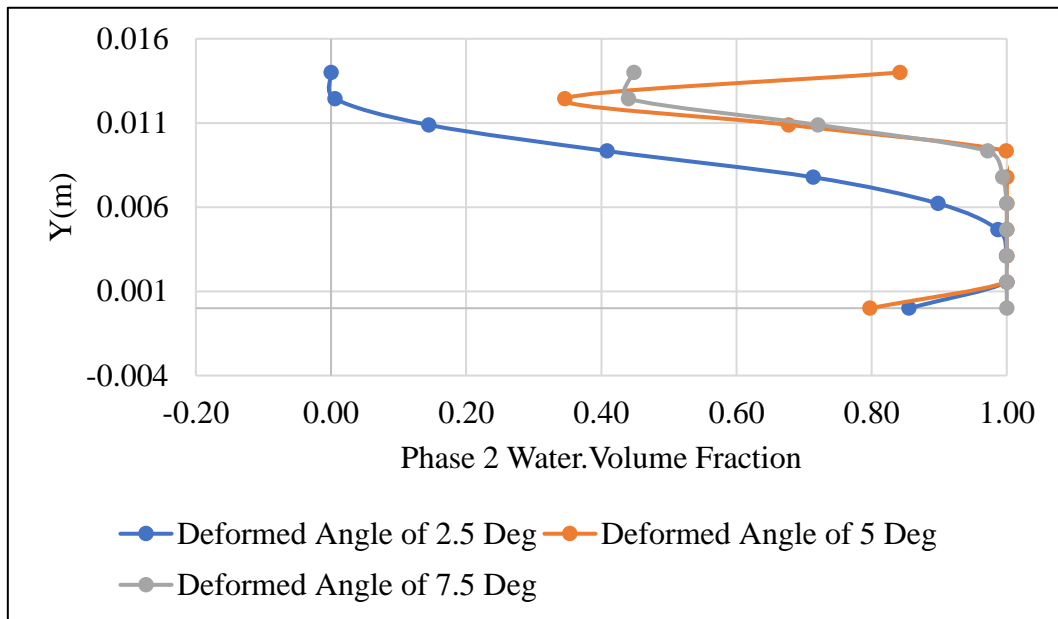


Figure 4.21: Upper half water volume fraction of different angular deviation

Figure 4.21 shows that the water sheet thickness at the upper half of the splitter tip has a constant value for the deformed angle of 5 and 7.5 degrees and the deformed angle of 2.5 degrees has the thin water sheet thickness as compared to the value of the other two angles.

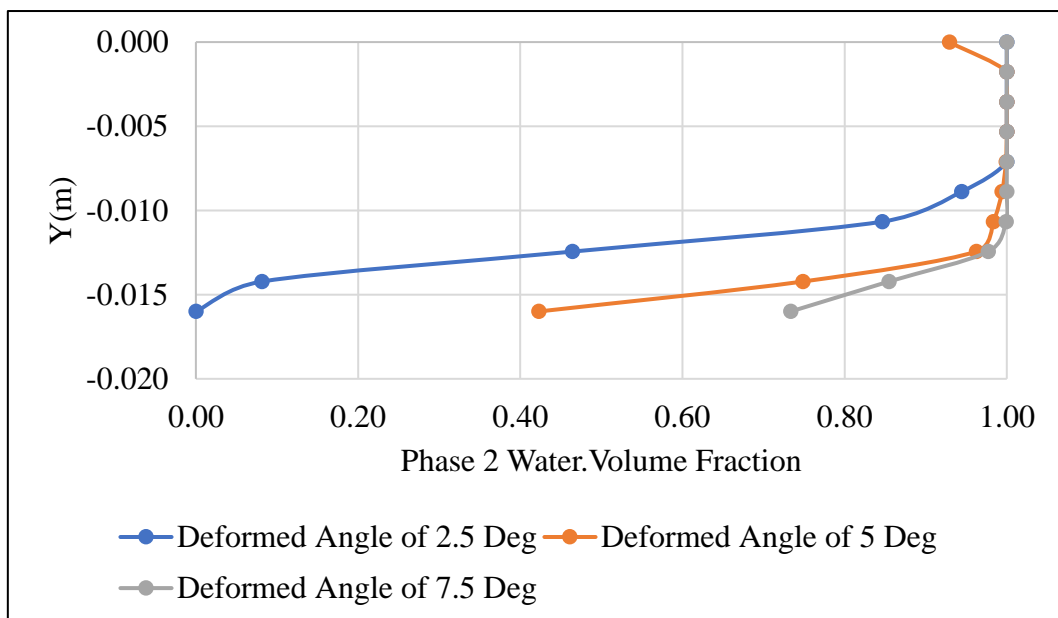


Figure 4.22: Lower half water volume fraction of different angular deviation

Figure 4.22 shows that the water sheet thickness at the lower half of the splitter tip has a constant value for the deformed angle of 5 and 7.5 degrees and the deformed angle of 2.5 degrees has the thin water sheet thickness as compared to the value of the other two angles.

2.5 degrees has the thin water sheet thickness as compared to the value of the other two angles.

#### 4.5.11 Water Volume Fraction at Middle of bucket

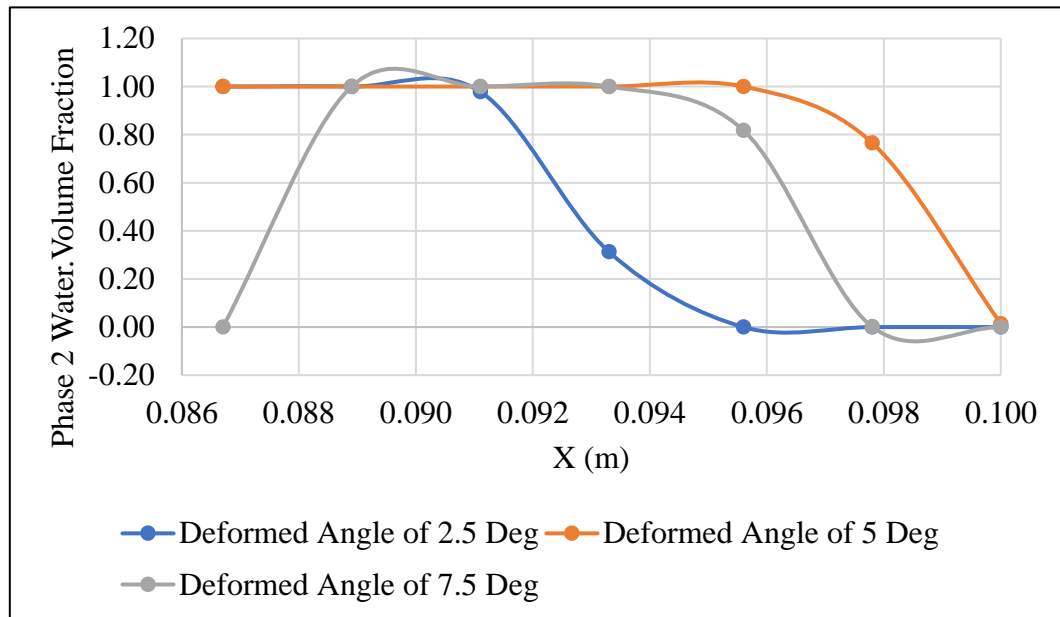


Figure 4.23: Upper half water volume fraction of different angular deviation

Figure 4.23 shows the water sheet thickness at the upper half of middle of bucket which has a maximum water sheet thickness of 4.5mm at a 5 degree angular deviation. Water sheet thickness at 2.5 degrees and 7.5 degree angular deviation has similar values i.e. 2mm. From the above graph it is seen that the thickness increases as the angular deviation increases.

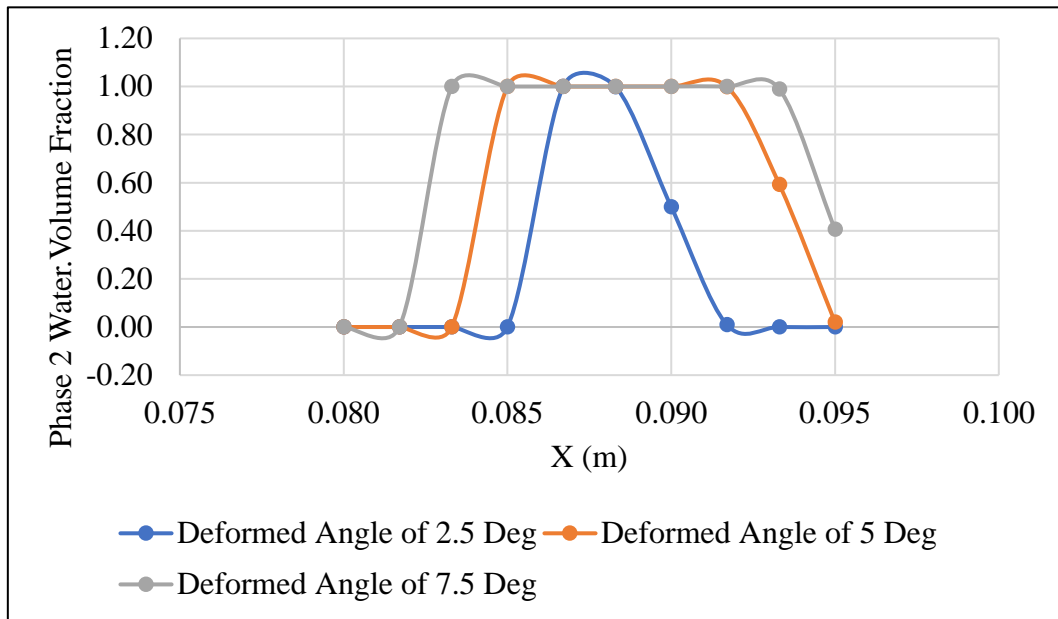


Figure 4.24: Lower half water volume fraction of different angular deviation

Figure 4.24 shows the water sheet thickness at the lower half of middle of bucket which has a maximum water sheet thickness of 12.2 mm at a 7.5 degree angular deviation. Water sheet thickness at 5 degrees has 7.33 mm and at 2.5 degree angular deviation has a minimum value i.e. 1 mm. From the above graph, it is seen that the thickness increases as the angular deviation increases. Which validates the statement that as the height increases the water sheet thickness increases.

#### 4.5.12 Water Volume Fraction at Exit Side of Bucket

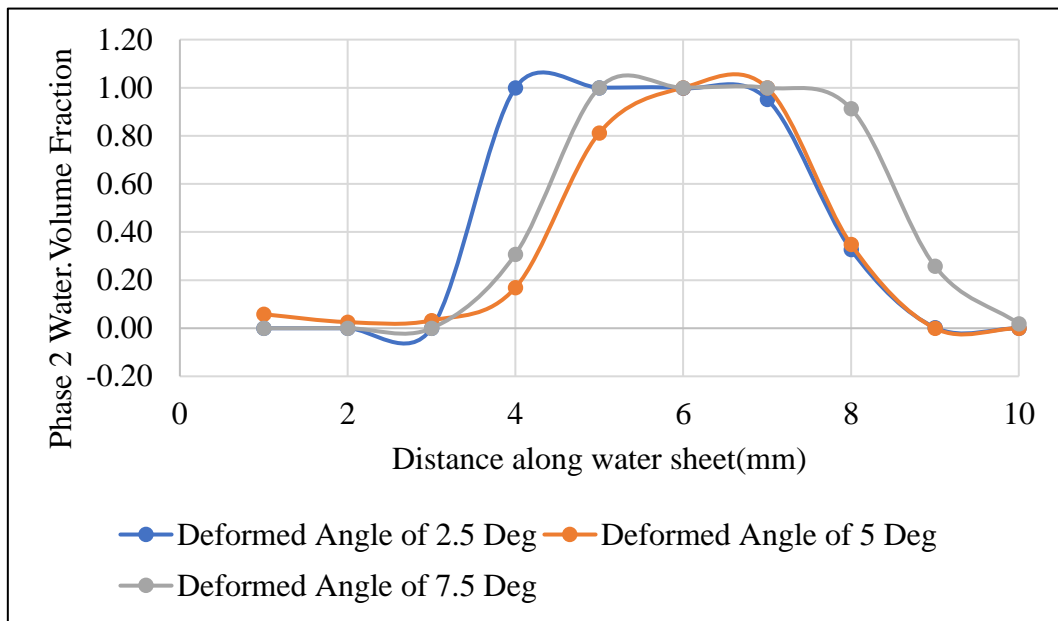


Figure 4.25: Upper half water volume fraction of different angular deviation

Figure 4.25 shows the water sheet thickness at the upper half of the exit side of bucket which has minimum water sheet thickness. At 2.5 degrees and 5 degree angular deviation has a similar value of more or less 1mm. Water sheet thickness has 2mm at a 7.5 degree angular deviation as the minimum value. The water sheet thickness has a tentative value as the bucket thickness which verifies the previous study and shows that the simulation done was right.

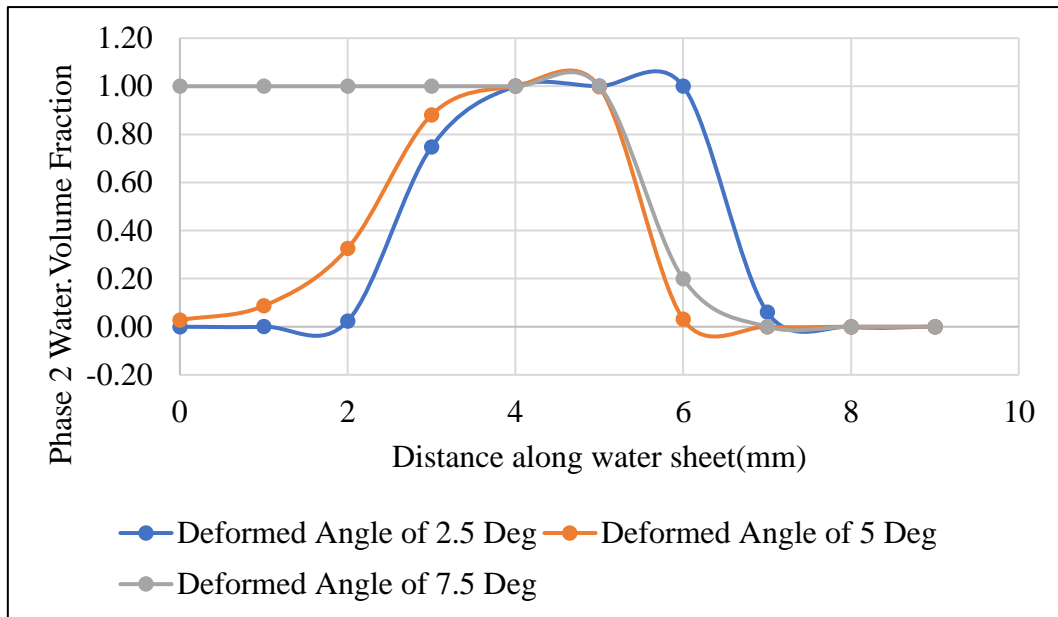


Figure 4.26: Lower half water volume fraction of different angular deviation

Figure 4.26 shows the water sheet thickness at the lower half of the exit side of bucket which has minimum water sheet thickness but has a greater value than the upper half. The water sheet thickness obtained has 2 mm at 2.5 degrees, 4 mm at 5 degrees, and 5 mm at 7.5 degrees angular deviation. The lower half thickness increases as the angular deviation increases.

#### 4.5.13 Deviation vs Overpressure Coefficient

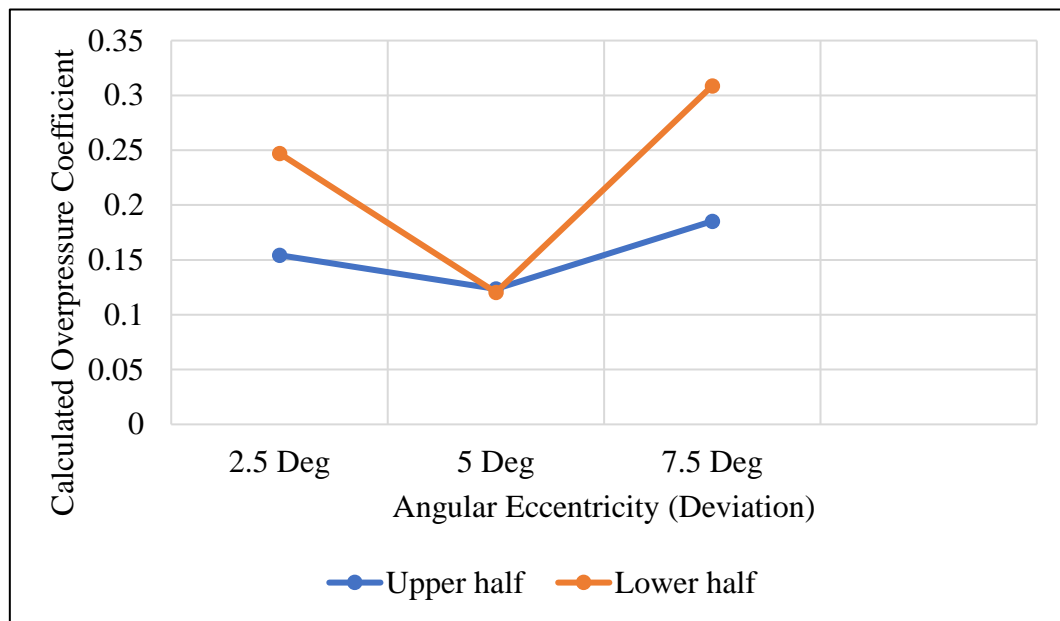


Figure 4.27: Overpressure coefficient at different angular deviation

As shown in Figure 4.27 coefficient of overpressure at the lower half of 7.5 degrees has a maximum value. The figure value at the lower half of 2.5 degrees has 0.25 which decreases as the angular deviation increases but when the deviation further increases the value of the overpressure coefficient at the bucket is increased. In the upper half case, the value of the overpressure seen slightly changes with the deviation angle.

## CHAPTER FIVE: CONCLUSIONS AND RECOMMENDATIONS

### 5.1 Conclusions

The conclusion of this research work is:

1. A field setting research was conducted on a 1 MW Pelton turbine unit, to understand the effect of eccentricity on Pelton turbine performance. The turbine runner was rotated manually after reinstallation following standard installation practices as recommended by the manufacturer. The average eccentricity measured on one complete rotation of the unit was 2.65 mm. Due to this eccentricity, notable axial vibrations were seen with no lateral vibration observed. The effect of this vibration was a rise in the temperature of the thrust bearing by 20 Degree C while the temperature of guide bearings was fairly constant.
2. Numerical modeling of Jet deviation at splitter was conducted for centric installation case of a model 2 kW Pelton turbine unit. For model verification, theoretical calculations of water sheet thickness were calculated and compared against the one obtained from numerical modeling. The error in water sheet thickness was 32.75%. Also, the velocity derived from experimental observation was compared against the one obtained from numerical modeling. The error in velocity computation was 11.5 %. The error is accounted for numerical errors, assumptions in deriving the water sheet thickness equation, and certain installation errors. The acceptable range of error verifies the modeling approach used in the study.
3. Flow modeling was done for the case of the angular eccentricity of the jet-bucket interaction of the Pelton turbine. The angular eccentricity of 2.5, 5, and 7 degrees was considered in the study. By modeling the jet bucket interaction by dividing the control volume into two parts i.e., the upper half of the bucket-jet interaction and the lower half of the bucket-jet interaction, the change in velocity profile, pressure profile, and water sheet thickness across the bucket was studied. For verification of flow modeling in each case, the velocity profile at needle tip is compared with the velocity profile obtained for the centric installation case. For all cases modeled, the velocity profile fairly overlaps with the velocity profile obtained for the centric installation case.

It was seen that with deviations, flow circulation (vortex formation) was also observed in the bucket. The formation of vortex in the bucket, changes in pressure, and velocity profile corresponds to a loss in energy transfer hence reduced efficiency. An increase in water sheet thickness with angular eccentricity corresponds to an increase in the weight of water trapped in the bucket which is different in either half of the bucket. This additional weight and weight difference in either half may be one of the sources of mechanical vibrations in addition to the unbalanced forces. The overpressure coefficient produced in the bucket at eccentric angles 2.5, 5 and 7.5 degree for the upper and lower half was calculated to be 0.1544, 0.247, 0.1235, 0.1204, 0.1853, and 0.3087. This illustrates the overloading of the bucket with more angular deviation.

## **5.2 Recommendations**

1. As eccentric installation is associated with reduced performance of the Pelton turbine, it is recommended that operators and fabricators follow strict protocols for maintaining the centricity of the jet-bucket interaction and preventing angular eccentricity.
2. This study may further be advanced by experimental modeling and three-dimensional numerical modeling of the flow in cases of angular eccentricity.



## REFERENCES

1. Anderson, J. D. (1995a). Basic Philosophy of CFD. In *Computational Fluid Dynamics* (pp. 3–14). Springer Berlin Heidelberg. [https://doi.org/10.1007/978-3-540-85056-4\\_1](https://doi.org/10.1007/978-3-540-85056-4_1)
2. Anderson, J. D. (1995b). Governing Equations of Fluid Dynamics. In *Computational Fluid Dynamics* (First, pp. 15–51). Springer Berlin Heidelberg. [https://doi.org/10.1007/978-3-540-85056-4\\_2](https://doi.org/10.1007/978-3-540-85056-4_2)
3. Anil Sapkota. (2021). *Numerical Modelling of Sand Particle Led Erosion in Reverse Engineered Pelton Turbine Bucket*. 7(1), 37–72. [https://www.researchgate.net/publication/269107473\\_What\\_is\\_governance/link/548173090cf22525dcb61443/download%0Ahttp://www.econ.upf.edu/~reynal/Civil\\_wars\\_12December2010.pdf%0Ahttps://think-asia.org/handle/11540/8282%0Ahttps://www.jstor.org/stable/41857625](https://www.researchgate.net/publication/269107473_What_is_governance/link/548173090cf22525dcb61443/download%0Ahttp://www.econ.upf.edu/~reynal/Civil_wars_12December2010.pdf%0Ahttps://think-asia.org/handle/11540/8282%0Ahttps://www.jstor.org/stable/41857625)
4. ANSYS Inc. (2013). *ANSYS Fluent Theory Guide* (Release 15).
5. Bajracharya, T. R., Acharya, B., Joshi, C. B., Saini, R. P., & Dahlhaug, O. G. (2008). Sand erosion of Pelton turbine nozzles and buckets: A case study of Chilime Hydropower Plant. *Wear*, 264(3–4), 177–184. <https://doi.org/10.1016/j.wear.2007.02.021>
6. Dhungana, S. (2020). Flow analysis in eccentric bucket of Micro Pelton turbine: Multiphase modelling with transient state condition. *Sustainability (Switzerland)*, 4(1), 1–9. <https://pesquisa.bvsalud.org/portal/resource/en/mdl-20203177951%0Ahttp://dx.doi.org/10.1038/s41562-020-0887-9%0Ahttp://dx.doi.org/10.1038/s41562-020-0884-z%0Ahttps://doi.org/10.1080/13669877.2020.1758193%0Ahttp://serisc.org/journals/index.php/IJAST/article>
7. Dixon, S. L., & Hall, C. A. (2010). *Fluid mechanics and thermodynamics of turbomachinery*. Butterworth-Heinemann/Elsevier.
8. Egusquiza, M., Egusquiza, E., Valero, C., Presas, A., Valentín, D., & Bossio, M. (2018). Advanced condition monitoring of Pelton turbines. *Measurement*, 119, 46–55. <https://doi.org/10.1016/J.MEASUREMENT.2018.01.030>

9. Felix, D., Abgottspon, A., Aumelas, V., Maj, G., & Winkler, K. (2016). *Hydro-abrasive erosion of hydraulic turbines caused by sediment – a century of research and development*. <https://doi.org/10.1088/1755-1315/49/12/122001>
10. Kjølle, A. (2001). *Hydropower in Norway: Mechanical Equipment*.
11. Kumar, A., Kumar, A., & Staubli, T. (2019). Analytical modelling and mechanism of hydro-abrasive erosion in pelton buckets. *Wear*, 436–437(March), 203003. <https://doi.org/10.1016/j.wear.2019.203003>
12. Narendra Kumar Mandal. (2021). *Pelton Runner Erosion Due To Cavitation : A Case Study Of Storage Hydropower Plant, Kulekhani First Hydropower Station*. 3(March), 6.
13. NEA. (2021). A year in review fiscal year 2020/21. *Nepal Electricity Authority*, 9–10. [https://nea.org.np/annual\\_report](https://nea.org.np/annual_report)
14. Pachhain, A. K. (2020). *Numerical Modelling of Deterioration of Efficiency of Pelton Turbine due to Bucket Erosion*. 2507(February), 1–9.
15. Panthee, A., Thapa, B., & Neopane, H. P. (2015). Quality control in welding repair of Pelton runner. *Renewable Energy*, 79(1), 96–102. <https://doi.org/10.1016/j.renene.2014.10.042>
16. Poudel, L., Thapa, B., Shrestha, B. P., Thapa, B. S., Shrestha, K. P., & Shrestha, N. K. (2012). Computational and experimental study of effects of sediment shape on erosion of hydraulic turbines. *IOP Conference Series: Earth and Environmental Science*, 15(PART 3), 1–9. <https://doi.org/10.1088/1755-1315/15/3/032054>
17. Rai, A. K., Kumar, A., Yexiang, X., Guo, B., & Staubli, T. (2021). *Analysis and visualization of progressive erosion in Pelton buckets Analysis and visualization of progressive erosion in Pelton buckets*. <https://doi.org/10.1088/1755-1315/774/1/012105>
18. Ratna, T., Babu, A., Sapkota, A., & Rahadi, T. (2021). *Effect of Spear Needle Eccentricity on the Pelton Turbine Jet*. 8914, 302–309.
19. Sangal, S., Singhal, M. K., & Saini, R. P. (2018). Hydro-abrasive erosion in

- hydro turbines: a review. *International Journal of Green Energy*, 15(4), 232–253. <https://doi.org/10.1080/15435075.2018.1431546>
20. Timilsina, A. B. (2019). *Sand Particle Led Erosion in Pelton Turbine Injector*.
21. Versteeg, H. K., & Malalasekera, W. (1995). An introduction to computational fluid dynamics - the finite volume method. In *undefined*.
22. VOITH Workshop, St. Poelten, A. (n.d.). Pelton turbines Harnessing the power of water. *A Voith and Siemens Company*, 1.
23. Zhang, Z. (2016a). Pelton turbines. In *Pelton Turbines*. <https://doi.org/10.1007/978-3-319-31909-4>
24. Zhang, Z. (2016b). Working Principle of Pelton Turbines. In *Pelton Turbines* (pp. 13–28). Springer International Publishing. [https://doi.org/10.1007/978-3-319-31909-4\\_2](https://doi.org/10.1007/978-3-319-31909-4_2)

## PUBLICATION

IOE Graduate Conference (Accepted): Numerical Modelling of Deflection of the bucket splitter of Pelton Turbine



त्रिभुवन विश्वविद्यालय  
Tribhuvan University  
इन्जिनियरिङ अध्ययन संस्थान  
Institute of Engineering

**डीनको कार्यालय**  
**OFFICE OF THE DEAN**

GPO box- 1915, Pulchowk, Lalitpur  
Tel: 977-5-5215331, Fax: 977-5-525830  
dean@ioe.edu.np, www.ioe.edu.np  
गोरखापोषी ब- १९१५, पुल्चोक, ललितपुर  
फोन- ५५२१५३१, फ्याक्स- ५५२५८३०

Date: September 14, 2022

### To Whom It May Concern

This is to confirm that the paper titled "*Numerical Modelling of Deflection of the flow at the bucket splitter of Pelton Turbine*" submitted by **Rupa Pandey** with Conference ID **12185** has been accepted for presentation at the 12<sup>th</sup> IOE Graduate Conference being held in October 19 – 22, 2022 at Thapathali Campus, Kathmandu.

Khem Gyanwali, PhD  
Convener,  
12<sup>th</sup> IOE Graduate Conference



## APPENDIX



